Driven Inelastic Gases

By

Prasad.V.V

A thesis submitted to the Jawaharlal Nehru University
for the degree of Doctor of Philosophy

Department of Theoretical Physics
Raman Research Institute
Bangalore 560 080

February 2016

Typeset in LaTeX 2_ε.

Declaration:

I hereby declare that the work reported in this thesis is entirely original. This thesis is composed independently by me at Raman Research Institute under the supervision of Dr. Sanjib Sabhapandit. I further declare that the subject matter presented in this thesis has not previously formed the basis for the award of any degree, diploma, membership, associateship, fellowship or any other similar title of any university or institution. I also declare that I have run it through the Turnitin plagiarism software.

Dr. Sanjib Sabhapandit

Prasad. V. V.

Theoretical Physics Group
Raman Research Institute
Bangalore 560 080
India

Certificate:

This is to certify that the thesis entitled **"Driven Inelastic Gases"** submitted by Prasad.V.V for the award of the degree of Doctor of Philosophy of Jawaharlal Nehru University is his original work. This has not been published or submitted to any other University for any other Degree or Diploma.

Prof. Ravi Subrahmanyan
(Centre Chairperson)
Director
Raman Research Institute
Bangalore 560 080
India

Dr. Sanjib Sabhapandit
(Thesis Supervisor)

Acknowledgements

First of all, I would like to express my gratitude to my supervisor Dr. Sanjib Sabhapandit for giving me the opportunity to work with him, without whose support and patient guidance, the thesis would not have been accomplished.
I would also like to thank Prof. Abhishek Dhar for his support and advice. He has been a constant source of motivation for me.

I would also like to thank the wonderful teachers at the Indian Institute of Science, particularly Prof. H. R. Krishnamurthy and Prof. Diptiman Sen. The schools of statistical physics held at RRI have helped a lot in expanding my horizon. I take this opportunity to thank all the lecturers of the schools, whom I had the fortune to listen.

I would like to thank all the faculties at the Theoretical Physics group, for their encouragement. I am also indebted to Sam from whom I had learned a lot. Maddy has always been a friend to all of us. I will not forget the laughing sessions we had at TP. I also like to thank Sandipan for his friendship. Manju's welcoming nature made the life at TP, homely and joyful. I thank him for all the help he has done.

Living at RRI has been made pleasant by the efforts of lots of people. Administrative office was always helpful in making us feel the official work almost effortless. I also thank all the library staff for their help. I take this opportunity to thank canteen as well as gardening section of RRI. I also thank Umaji, Sharadaji, Padmaji and Mangalaji for making me not worry about cooking (Khichdi) throughout the week–except on Sundays.

Talks with seniors were helpful in forming my thinking, in and out of science. I thank RK, Nishant,

JK, Madhukar for their encouragement. I thank Wasim, Shabeeb, Rajib and Debasish for their memorable friendship. I also thank the wonderful moments that I had with my juniors: Nazma, Mriganko, Rahul, Shafi, Gayathri, Amruta, Madhuri, Surya, Shivam, Anirudh, Santanu, Deepak, Raj and others.

Playing Football and Volleyball were not only refreshing but educating, which has helped me change the way I looked things around me. I thank all the friends from the field for that. Arifda, Arijitda, Tridibda, Polleyda, all of them were generous in making me learn the beautiful game.

I do not have words to thank some not-so-sane guys, adamant of pulling me out of my comfort zone. Arnab, Anjan, Chaitra, I owe you for whatever you have done and not done. I also thank Suman for imparting his queer Gyan, which needs to be forgotten each time one shuts down the computer. I thank Amrita, Jagdish, Samim, Jyothi, Avinash, Swami and Mahavir for their company.

My parents have been constantly supporting all through my life with whatever dreams I wanted to pursue. I thank them for backing me in my highs and lows. I also thank my sister and her family for their support and encouragement.

List of Publications

I. Articles in journals/Unpublished eprints:

[1] V.V. Prasad, Sanjib Sabhapandit, and Abhishek Dhar.
High-energy tail of the velocity distribution of driven inelastic Maxwell gases.
Europhysics Letters **104**, 54003 (2013).

[2] V.V. Prasad, Sanjib Sabhapandit, and Abhishek Dhar.
Driven Inelastic Maxwell Gases.
Phys. Rev. E **90**, 062130 (2014).

Synopsis

One of the notable features of equilibrium systems is the universality in their statistical properties. An illustration of this universality can be found in the statistics of a classical gas of particles, which interact via elastic collisions (eg. molecular gases). The system when isolated goes to equilibrium. Using methods of kinetic theory, J.C. Maxwell and later Ludwig Boltzmann showed that the velocity distribution of a gas of particles in equilibrium follows the Gaussian with a variance proportional to the temperature of the gas.

A generalisation of the above system can be made by considering the interparticle collision to be inelastic; i.e., as the particles collide, the momentum is conserved, but not the kinetic energy. This makes the system intrinsically non-equilibrium, with the total energy constantly decreasing as the particles collide with each other. Hence, to obtain a steady state, the system needs to be driven from outside. Inelastic gas in a steady state presents us a non-equilibrium analogue of elastic gas at equilibrium. A natural question that one asks is whether there exist any universality in the velocity statistics of driven inelastic gases too? This is the question that we address in the thesis. The system is interesting from the point of view of granular systems too. Granular systems interact via inelastic hard core collisions and it is interesting to understand the statistical properties of these systems.

There have been experimental, analytical, as well as numerical studies, probing the statistical properties of these systems. The experimental systems typically consist of a collection of granular materials such as beads made of glass, stainless steel etc., which are loosely packed. The driving is done by shaking the container which imparts the momentum needed to sustain a steady state. Notably, the observed velocity distribution of the particles showed deviation from the Gaussian

for higher velocities. Particularly, some experiments predicted a stretched exponential behaviour $P(v) \sim \exp(-A|v|^{\alpha})$ for the tails of the distribution with $\alpha \approx 1.5$ for a range of parameters. The analytical study based on kinetic theory for a hard sphere system of inelastic gases driven by diffusive noise, $dv/dt = \eta$ had also observed the same exponent, as a solution for the Boltzmann equation. Contrasting picture came forth from the numerical studies which showed a wide range of $\alpha < 2$ instead of a universal value. This lead us to look at the system closer, using a simple analytic model of inelastic gas.

Chapter 1: Introduction

In this chapter we introduce the paradigm of inelastic gases. We describe the interesting physics that come about due to their inelastic nature, like the cooling of an isolated system, emergence of clustering and so on. We introduce the observables of our interest as well as the existing knowledge about them. We set up the background for our work by reviewing the current understanding of the velocity distributions of driven inelastic gases from experimental, analytical and numerical point of view. In the aim of tackling the differences among the various studies, we resort to a mean field system of inelastic gas where any particle can interact with any other particle with equal probability. Such a system is called a Maxwell gas.

Chapter 2: Inelastic Maxwell gas with discrete time dynamics

We consider an inelastic Maxwell gas with each constituent particle associated with a scalar velocity. The system evolves with discrete time dynamics such that at each time step, the velocities of a randomly chosen pair of particles change as they collide with each other or they are driven independently. We consider two variants of the dynamics. In one, the collision and driving occur simultaneously on a pair. In the other case, either collision or independent driving happens on the chosen pair probabilistically. In both the cases, we find that even though the time evolution of the distribution functions form a set of hierarchical equations, those of the variance and the two-point correlation function of the velocity form a closed set of equations. This does not need any approximations. With the help of these equations we observe that the Maxwell gas driven by a discrete version of diffusive driving does not have a steady state. We also do a direct simulation for a hard sphere system which shows that this is true for them too. As the analytical results which predicted the universality of steady state velocity distribution used this mode of driving in their models, our results indicate that those models cannot correspond to real systems.

This motivates us to consider a new model of driving motivated by wall-particle collisions – used in experiments to drive granular systems – for which the system goes to a steady state. The exact tail of the velocity distribution in the steady state is found to have a Gaussian form.

Chapter 3: Inelastic Maxwell gas with continuous time dynamics

In this chapter, we extend the result we obtained in the case of the discrete model to a continuous time model where the collision and driving occur as point processes with certain rates. From the evolution equation of the velocity distribution function which follow a BBGKY-type hierarchy, we find the exact evolution equations for the variance and the two-point velocity correlation function. The system when driven by the wall-particle collisions is found to reach a steady state. An exact mapping with the discrete time model allows one to find the velocity distribution in this case also. Besides, we find that the driving by wall collisions in a particular limit becomes an Ornstein-Uhlenbeck process, which has been employed in studying driven granular gases by some of the authors.

Chapter 4: Inelastic gas on a one-dimensional ring

In the chapter, we use the closure relation obtained for the Maxwell gas to calculate the exact form of the spatial correlation function of velocities for a quasi-Maxwell gas living on a periodically bounded one-dimensional lattice. Here, each lattice point has associated with it, a scalar velocity. The velocities change due to a nearest neighbour interaction which mimics the two particle collision. The driving is done independently on each lattice point as if by wall collisions. We find the two-point velocity correlation in the steady state as a function of lattice separation. We observe that it decays exponentially with lattice separation. This study can be seen as an initial step to understand the experimental findings where one obtains similar behaviour.

Dr. Sanjib Sabhapandit
Theoretical Physics Group
Raman Research Institute
Bangalore 560 080
India

Prasad.V.V

Contents

1

Introduction

Statistical mechanics aims to understand phenomena at the macroscopic scale by looking at physics at the microscopic level. One of the central problems in the development of equilibrium statistical mechanics was the description of dilute classical gases of molecules. Using Kinetic theory, Maxwell and later Boltzmann developed a statistical description of the macroscopic variables from the collisional dynamics of molecules. It was also found that the single particle velocity distribution follows a universal Gaussian form. An immediate extension of this system can be imagined if one considers a dilute gas of molecules/particles which collide *inelastically*. Such collisions cause the kinetic energy of the system to decay. The system when isolated, loses it's energy indefinitely as time evolves, unlike it's elastic counterpart whose total energy does not vary with time. The thesis is about these *Inelastic* gases. Although a seemingly simple extension of the molecular gases, the inelastic gases present us with a prototypical non-equilibrium system with non-trivial characteristics. They also give us an opportunity to check whether there is any

universality in the velocity distributions of these systems like it's elastic analogue.

Another motivation in studying inelastic gases is to model a system of particles made of granular matter. Granular matter is widely observed in nature, ranging from the sand at the door step, food grains to the clouds of cosmic dust. They also find applications in fields ranging from pharmaceutical industry to construction. A granular system is a set of macroscopic objects, which interact via inelastic hard particle collisions. The inelasticity is attributed to the irreversible transfer of kinetic energy to degrees of freedom like the vibrational ones which cause the energy to dissipate as heat or sound. Another characteristic of granular systems is that the ambient temperature does not play any role, as thermal energy is not sufficient to sustain the kinetic energy of these large bodies. Because of this, one usually treats these systems as athermal. The properties mentioned above make granular systems unique; they exhibit a wide variety of phenomena which are different from those of the usual phases of matter. For example, they show solid like behaviour while packing, and flow like liquid when poured. They also show phenomena like pattern formations and clustering. In spite of their wide presence, the analytical understanding of most of these phenomena is still a challenge. Even industrially, it is important to know their behaviour in various situations of applicability. A preliminary step for this is to understand them in simple scenarios. A simplified granular system that one can consider is a set of granular particles in motion with only binary contacts allowed. Such a system is known by the name of *granular gas*. Example would be a rarified system of marbles in a box in the absence of any external volume force. Now, one can hope to pursue the path of Maxwell and Boltzmann and build description of this simpler model while retaining the essential features of a granular system.

As seen above, inelastic gases can be studied both to understand a dilute system of granular particles (granular gases) and as a prototypical model of non-equilibrium system. Inelastic gases exhibit interesting properties. For example, a gas comprising of inelastic particles in a finite volume, with random initial velocities loses the kinetic energy up on collisions and approaches a state of rest where there is no motion of particles. One also observes clustering of particles leading to spatial inhomogeneities. The resultant spatial distribution of clusters is seen to be statistically similar to that of clusters in inter-stellar materials, which has resulted in studies probing the connection between inelastic behaviour in these systems to the mechanism of star formation [1].

Granular systems that are present in nature typically contain particles of diverse shapes, sizes

and masses. The behaviour of the systems should in general depend on these features also. For example, break down of energy equipartition is observed experimentally in a vibrated binary mixture granular beads [2]. Theoretical studies on multi-species system of inelastic gases were also pursued by several authors [3, 4]. Granular gases of non-spherical particles too have been studied by the community; a recent experiment that has probed granular gases of rod shaped particles, exhibited interesting features like the lack of clustering, absence of equipartition between rotational and translational kinetic energies etc. [5]. Having said all these, even a simpler system of mono species gas of spherical inelastic particles is still rich enough with a lot of intriguing physical properties, but understood very little. We would be addressing these 'uniform gases' which still challenges our understanding, even after decades long studies.

The constituent particles of inelastic gases by definition interact with one another via inelastic collisions between two particles. This is because, collisions between more than two particles at the same time are less probable in a dilute system. Also, there are situations in which one has to consider interactions due to non-contact forces. Examples are granular systems of electrically charged or magnetized particles [6, 7]. In our studies we would consider systems with only inelastic collisions.

In the remaining parts of the chapter we plan to introduce the basic quantities of our interest and the current understanding about them. We will start (Sec. 1.1) with the inelastic collisions and derive the set of rules describing the change in velocities of the colliding particles. Later in Sec. 1.3, we briefly outline the non-trivial dynamic effects that result from the inelasticity. This will include both the isolated as well as driven cases. Later (Sec. 1.4), we will go on to summarize the current understanding of inelastic gases from experimental, numerical as well as analytical point of view. As our studies are predominantly analytical, we emphasize on the previous analytical studies, which is based on kinetic theory. From the master equation for the distribution functions, which involves a BBGKY-type hierarchy, we present the assumptions leading to the Boltzmann equation. Here, we survey the existing solutions for the Boltzmann equation for the simpler case of a homogeneous system. Lastly, we explain (Sec. 1.5) certain issues related to previous works, namely the lack of agreement between the various results. This will help us set the background and significance of the problems addressed in the thesis. We conclude by briefing the specific problems covered in the later chapters.

1.1. Inelastic collisions

Inelastic collisions are those in which the total momentum of the colliding particles remain unchanged but a portion of their kinetic energy is lost irreversibly. For frictional particles, angular momentum also plays a role, which is out of the scope of the present work.

Let us consider two inelastic frictionless particles of same species with velocities respectively, $\boldsymbol{v_1}$ and $\boldsymbol{v_2}$, which are vectors. As the two particles collide their velocities change. This change should conserve the momentum which implies:

$$\boldsymbol{v_1} + \boldsymbol{v_2} = \boldsymbol{v_1^*} + \boldsymbol{v_2^*}. \tag{1.1}$$

Here the '$*$' denotes the velocities before collision, and the ones without '$*$' are those after collision.

The loss in kinetic energy on each collision is captured by single parameter r, called the coefficient of restitution. It is usual to assume r to be a constant which is independent of the velocities of colliding particles. The collision satisfies the Eq. (1.2), which relates the relative velocities before and after collision.

$$(\boldsymbol{v_1} - \boldsymbol{v_2}) \cdot \boldsymbol{\sigma} = -r(\boldsymbol{v_1^*} - \boldsymbol{v_2^*}) \cdot \boldsymbol{\sigma} \tag{1.2}$$

In Eq. (1.2), $\boldsymbol{\sigma}$ is the unit vector from the centre of mass of particle 1 to that of particle 2 when in contact (also called the impact direction). Additionally, one assumes that the velocities in the direction perpendicular to the impact direction are not affected by the collisions. The coefficient of restitution r takes the values ranging from 0 to 1. When r has the minimum value 0, it represents a maximally dissipating system. On the other extreme, $r = 1$ represents the elastic collisions seen in conventional molecular gas. In the intermediate range, the gas evolves via inelastic collisions and are the ones which we are interested in.

The two relations, Eq. (1.1) and Eq. (1.2), provide a one-to-one relation between the precollision velocities and the postcollision velocities:

$$\begin{aligned} \boldsymbol{v_1} &= \boldsymbol{v_1^*} - \frac{(1+r)}{2}[(\boldsymbol{v_1^*} - \boldsymbol{v_2^*}) \cdot \boldsymbol{\sigma}]\boldsymbol{\sigma}, \\ \boldsymbol{v_2} &= \boldsymbol{v_2^*} + \frac{(1+r)}{2}[(\boldsymbol{v_1^*} - \boldsymbol{v_2^*}) \cdot \boldsymbol{\sigma}]\boldsymbol{\sigma}. \end{aligned} \tag{1.3}$$

A simpler equation can be obtained if the velocities are one-dimensional objects and are parallel to the impact direction of the particles, as shown below (Eq. (1.4)).

$$\begin{aligned} v_1 &= \frac{(1-r)}{2} {v_1}^* + \frac{(1+r)}{2} {v_2}^*, \\ v_2 &= \frac{(1+r)}{2} {v_1}^* + \frac{(1-r)}{2} {v_2}^*. \end{aligned} \tag{1.4}$$

1.2. Granular temperature

Due to the macroscopic size of granular particles, the thermal energy $K_B T$ turns out to be much less in scale compared to the average kinetic energy of the particles. For example, a stainless steel ball of 1 mm diameter with typical velocity 1 m/s (as used in [8]) has the kinetic energy 6 orders of magnitude greater than the thermal energy at room temperature. This shows that the temperature T of the system cannot cause any motion of the particles. Due to this fact granular systems are considered athermal. But still, one can define the average kinetic energy of the individual particles to be the 'Granular Temperature', T_g of the system:

$$T_g(t) = \langle \frac{1}{2} m v^2(t) \rangle. \tag{1.5}$$

This construction enables one to ask questions related to the laws of thermodynamics, validity of equipartition theorem [2, 3] etc., for granular systems.

1.3. Dynamical properties of inelastic gases

The advent of experimental and numerical techniques caused an increased interest in exploring dynamical properties of inelastic gases in the 90's. These studies have lead to uncover a number of interesting behaviours. We will now discuss some of these which are relevant to our studies. The dynamical behaviour of inelastic gases can be probed in two different situations: (a) Isolated and (b) Driven.

1.3.1. Isolated inelastic gas: free cooling

An inelastic gas when isolated from external environment evolves very differently compared to an elastic gas. As mentioned before, the lack of supply of energy to balance the dissipation due to inelastic collisions causes the system to lose energy indefinitely (and so it lacks a steady state). This process is called the 'the *cooling* of a granular gas'. Cooling occurs in two regimes. An initial regime where the particles lose their kinetic energy while sustaining the homogeneity in the system. The evolution eventually gives way to an inhomogeneous regime, with the formation of clusters while cooling. The decay of energy as a function of time behaves differently in the two regimes.

In the homogeneous regime, the decay of energy follows the *Haff's law* [9], given by the formula:

$$T_g(t) = \frac{T_g(0)}{(1 + t/t^*)^2} \tag{1.6}$$

This result can be obtained using simple arguments as follows. The change in granular temperature ΔT_g in time Δt is the average loss in kinetic energy per collision, multiplied by the average number of collisions in time Δt. The change in kinetic energy, $\langle \Delta E \rangle$ in the system due to a single collision

$$\begin{aligned} \langle \Delta E \rangle =& \frac{1}{2} m \langle (v_i^2 + v_j^2) - (v_i^{*2} + v_j^{*2}) \rangle \\ =& -\frac{m(1-r^2)}{4} \langle (v_i - v_j)^2 \rangle \end{aligned} \tag{1.7}$$

the second equality follows from Eq. (1.4). Now $\langle (v_i - v_j)^2 \rangle \propto T_g$. The typical number of collisions in time Δt is given by $\Delta t(\Delta v/l)$, with l the mean free path which is inversely proportional to the number density of particles. Also, $\Delta v = \langle (v_i - v_j)^2 \rangle^{1/2} \propto \sqrt{T_g}$. From these, the average change in the granular temperature, ΔT_g per time Δt is obtained as,

$$\frac{\Delta T_g}{\Delta t} \propto -(1-r^2) \frac{\sqrt{T_g}}{l} T_g.$$

In the limit $\Delta t \to 0$,

$$\frac{dT_g}{dt} \propto -(1-r^2) T_g^{3/2}. \tag{1.8}$$

Integrating the above equation (Eq. (1.8)) one obtains the Haff's law (Eq. (1.6)) where $t^* \propto (1-r^2)\sqrt{T_g(0)}$. We mention that this result is true when the coefficient of restitution r does not depend on collision velocities. For viscoelastic particles the coefficient of restitution depends on the relative velocities of the colliding particles, for which the temperature evolution shows $t^{-5/3}$ decay instead of the Haff's cooling behaviour [10].

The homogeneity does not stay too long as clusters start appearing. Goldhirsch and Zanetti [11] showed the dependence of clustering on the coefficient of restitution and the mean free path of the particles. They showed [11] that the clusters are not formed if the system size is less than $l/\sqrt{(1-r^2)}$. Onset of clustering changes the power of the cooling behaviour which starts deviating from the Haff's law. Particularly in one dimension, it has been shown that inelastic gases in its clustering regime, asymptotically goes to a sticky gas like behaviour [12, 13]. Thus in one dimension, using the exact evolution of sticky gas [14, 15], one obtains the asymptotic behaviour of cooling inelastic gas with $T_g \propto t^{-2/3}$. For higher dimensions the correspondence between inelastic and sticky gas is not yet clear [16, 17].

We learned above, that the kinetic energy decreases monotonically for an isolated inelastic gas. For a bounded system the final state is a rest state with no motion. In the unbounded case, the system approaches either a state with the clusters receding from each other, like a fan state in sticky gas [18], or a single cluster which moves in center of mass velocity.

1.3.2. Driven inelastic gas: steady states

To keep an Inelastic gas in motion, one needs to supply energy to the system to compensate for the energy dissipated through collisions. If the dissipated energy is balanced by the supplied energy, the system goes into a steady state. Such a system is interesting, as they present us a realization of a gas in non-equilibrium steady state which allows us to contrast between equilibrium and non-equilibrium steady states.

A natural question one may ask is related to the statistical properties of the particle velocities in the steady state. Particular importance is on the steady state distribution of velocity, because of the following reason. One knows that the velocity distributions of elastic gases in equilibrium has the Maxwellian distribution with the variance as a measure of temperature irrespective of

the way it has been coupled to the environment or the material properties of the constituent particles. Similarly, one may ask whether there is any universality in the distribution functions of a driven inelastic gas also. More specifically, whether the velocity distribution is Maxwellian; If not, is there any other universal distribution?

Even with a long history of analysis, a consistent understanding of the properties inelastic gases is yet to be achieved, including those of steady states. The thesis deals with these kind of questions. We will be analyzing certain models of inelastic gases and try to understand the steady state properties of these models. Though there have been predictions about universality, there were also observations counter to this. The only feature that the previous studies agreed on was the deviation from the Maxwellian distribution. This prompts us to study simple models, keeping the essential nature of inelastic gases, with the aim of getting quantitatively precise answers.

In the later part of this chapter we will set up the problem our study. At first we will describe the current understanding of driven inelastic gases from experimental, numerical and analytical studies done before.

1.4. Driven steady states: previous studies

1.4.1. Experimental studies

Development in experimental and imaging techniques have made it possible to probe the velocity distributions in granular gases. A granular gas as mentioned before, is a dilute system of granular materials, examples of which are systems of beads made from glass, steel etc. enclosed in a container. To keep them in motion, one needs to supply energy from outside. The simplest and widely used method is to drive the system via mechanical means. Here, the kinetic energy lost through inter-particle collisions is compensated by collisions of the particles with the vibrating walls of the container [8, 19–22]. Non-mechanical modes of driving includes using electric or magnetic field respectively to drive granular systems which are charged or magnetized [6, 7].

The experimental studies on driven inelastic gases observed steady state velocity distributions, which predominantly showed deviation from the Maxwellian. Earlier studies which observed the steady state distribution [23, 24] were not definitive due to statistical fluctuations. The

experiments that came later, all of which saw an overpopulated tail [8, 19–22]. But the predicted forms differed among themselves.

Even though there were advances in relating the non-Gaussianity to density fluctuations [19], later studies showed this not to be the case, finding strong non-Gaussianity even in the absence of spatial clustering and density correlations [22]. With regards to the form of the distribution, Olaphsen and Urbach [19] on their study on a horizontal monolayer of particles driven vertically, saw the form of the velocity distribution ranging from exponential to Gaussian with increasing amplitude of driving. Blair and Kudrolli [22] also obtained a number of non-Gaussian functions, depending on the values of the parameters. There were studies which predicted universality too. The analytical results by Van Noije and Ernst [25] had proposed a universal distribution of stretched exponential form $P(v) \sim \exp(-A|v|^{\alpha})$, with $\alpha = 3/2$. Later, Losert *et al.* [20] predicted from their experiments, a stretched exponential form, with the exponent $\alpha \sim 1.5$ for a large range of driving frequencies. Rouyer and Menon [8], in an experiment on metal spheres packed in a quasi 2D-system, also predicted for a large range of parameters of driving frequencies and density, a stretched exponential form for the tail of the distribution with $\alpha \sim 1.5$, in agreement with [25]. Similar results were obtained for non-mechanically driven system by Aranson and Olafsen [6]. This was but, not the end of the debate. There were numerical studies which gave results that did not support the above picture.

1.4.2. Numerical studies

As seen, the experimental results were not able to produce a consistent picture about the velocity distributions. Numerical simulations were done independently, hoping to get a better understanding of the differences in results. Numerical simulations of inelastic gases posed a challenging problem termed inelastic collapse, wherein the inelasticity causes the number of collisions to diverge in a finite time gap [26] in event driven simulations. This is usually taken care of, by introducing a cut off velocity below which the collisions are considered to be elastic. In one of the initial computational studies, Kadanoff and co-workers [27] imagined a one-dimensional system of point-particles in motion, each of which can collide to its nearest neighbours, inelastically. The system is bounded on the two sides by walls, such that one of the wall is elastic,

and the other injects energy to the particle in contact with it by assigning a velocity to the particle taken from the Gaussian distribution. The system showed a clustering of particles near the elastic wall. This and certain other studies [28, 29] revealed the inability of inhomogeneous driving to sustain a homogeneous steady state for inelastic gases. Williams and Mackintosh [30] considered a homogeneous driving, with the particles driven by adding uncorrelated white noise to the velocities.

Moon *et al.* [31], in their event driven molecular dynamics simulation on a 3-dimensional system of inelastic gas driven by a momentum conserving noise, found a velocity distribution function with the tail having the stretched exponential form, with the exponent $\alpha \sim 1.5$ for the coefficient of restitution $r < 1/2$. But for $r > 1/2$ they observed an exponent $\alpha \sim 2$. Van zon and Mackintosh [28, 29] considered a 2-dimensional system of inelastic particles with finite size, which dissipates energy through mutual collisions. Two different driving methods were considered: a periodic system with homogeneous driving as well as a bounded system with the driving caused by the collisions of the particles by the wall. They observed that the steady state distribution of the velocity has indeed a stretched exponential form, but the exponent instead of having a universal value, takes a range of values up to 2 which depends on a single parameter, which is the ratio of the rate of collision to that of the driving. This rules out the predictions of the experimental as well as the previous analytical results (which will be discussed later), which predicted a universal exponent $\alpha = 3/2$.

1.4.3. Analytical studies

1.4.3.1. Kinetic theory : an overview

Kinetic theory played an important role in the establishment of statistical mechanics. In simple terms, kinetic theory hopes to study the macroscopic characteristics of a system of very large number of particles from the equations of motion of the individual ones. The method has been employed by Maxwell and later by Boltzmann to study molecular gases in it's equilibrium. As the kinetic theory deals with a gas of particles which evolves via collisions, it seems to be the most obvious starting point even for the inelastic gases. A discussion of the method for inelastic systems is presented next.

In statistical mechanics, one is usually interested in the macroscopic variables of a system and their relation to the dynamics of the very large number of degrees of freedom at the microscopic level. Consider a system of classical gas consisting of N particles living in 3 dimensions. The state of the system at an instant of time – called the microstate – can be described by specifying its $3N$ number of position $\boldsymbol{r}$ as well as same number of momentum $\boldsymbol{v}$ (considering mass to be unity) degrees of freedom. This can also be depicted as a point in the $6N$ dimensional phase space. There can be many microstates which correspond to a single macrostate specifying the observable quantities. Thus, in order to calculate the behaviour of macroscopic quantities, one is interested in the probability of occurrence of the corresponding microstates. One of the ways to compute this is to consider an ensemble or identical copies of the system with each system associated with a point in phase space. Now the fraction of points in unit volume near any particular coordinate $\{\boldsymbol{x}, \boldsymbol{v}\}$ gives a measure of occurrence of the microstates near that coordinate. This is called the phase space density $\rho(\boldsymbol{x}, \boldsymbol{v}, t)$, and is normalized to unity. The phase space density, ρ can in general have a time dependence as indicated by the argument t. The macroscopic value of an observable $\mathcal{O}(\boldsymbol{x}, \boldsymbol{v})$ can be obtained from ρ as,

$$\langle \mathcal{O} \rangle = \int d\boldsymbol{x} d\boldsymbol{v} \mathcal{O}(\boldsymbol{x}, \boldsymbol{v}) \rho(\boldsymbol{x}, \boldsymbol{v}, t). \tag{1.9}$$

In most of the situation the phase density contains much more information than needed. For example, to calculate the pressure of the gas, it is sufficient to know the 1-particle distribution $f_1(\boldsymbol{x}, \boldsymbol{v}, t)$ which gives the probability measure of having any of the N particles to have a velocity $\boldsymbol{v}$ at $\boldsymbol{x}$ and at time t. The 1-particle distribution function $f_1(\boldsymbol{x}, \boldsymbol{v}, t)$ can be derived from ρ as,

$$\begin{aligned} f_1(\boldsymbol{x}, \boldsymbol{v}, t) =& \left\langle \sum_{i=1}^{N} \delta(\boldsymbol{x} - \boldsymbol{x_i(t)}) \delta(\boldsymbol{v} - \boldsymbol{v_i(t)}) \right\rangle \\ =& N \int \prod_{i=2}^{N} d\boldsymbol{x}_i d\boldsymbol{v}_i \rho(\boldsymbol{x_2} = \boldsymbol{x}, \boldsymbol{v_1} = \boldsymbol{v}, \boldsymbol{x_2}, \boldsymbol{v_2}, ..\boldsymbol{x_N}, \boldsymbol{v_N}, t). \end{aligned} \tag{1.10}$$

Here, it is implied that ρ is independent of permuting particles. Similarly, one can construct

the 2-particle, 3-particle distributions. In general, an 'S'-particle distribution can be obtained as:

$$\begin{aligned} f_S(\boldsymbol{x_1}, \boldsymbol{v_1}, ..., \boldsymbol{x_S}, \boldsymbol{v_S}, t) =& \frac{N!}{(N-S)!} \int \prod_{i=S+1}^{N} d\boldsymbol{x}_i d\boldsymbol{v}_i \rho(\boldsymbol{x_1}, \boldsymbol{v_1}, \boldsymbol{x_2}, \boldsymbol{v_2}, ..\boldsymbol{x}_N, \boldsymbol{v}_N, t) \\ =& \frac{N!}{(N-S)!} P_S(\boldsymbol{x_1}, \boldsymbol{v_1}, \boldsymbol{x_2}, \boldsymbol{v_2}, ..\boldsymbol{x_s}, \boldsymbol{v_s}, t), \end{aligned} \tag{1.11}$$

where P_S is the unconditional probability distribution function (PDF) for S particles. In experiments what one usually measures is P_1, the PDF for single particle. Note that (Eq. (1.11)) 'f_S' and 'P_S' differ from each other only by constant multiplicative factor. In the following, we will use both of them interchangeably, which will be evident from the situations.

Kinetic theory gives us a prescription to calculate the time evolution of the distribution functions described before, given the dynamical rules. The evolution of the 1-particle distribution function of a 3D system of inelastic hard spheres interacting via collisions and driven independently from outside, can be written as:

$$\begin{aligned} [\partial_t + \boldsymbol{v_1} \cdot \partial_{\boldsymbol{x}}] f_1(\boldsymbol{v_1}, \boldsymbol{x_1}, t) = \sigma^2 \int d\boldsymbol{v}_2 \int_{(\boldsymbol{v}_1 - \boldsymbol{v}_2)\cdot\boldsymbol{\sigma} > 0} d\boldsymbol{\sigma} (\boldsymbol{v}_1 - \boldsymbol{v}_2) \cdot \boldsymbol{\sigma} \\ \times \left[\frac{1}{r^2} f_2(\boldsymbol{x}_1, \boldsymbol{v}_1^*, \boldsymbol{x}_1 - \boldsymbol{\sigma}, \boldsymbol{v}_2^*, t) - f_2(\boldsymbol{x}_1, \boldsymbol{v}_1, \boldsymbol{x}_1 - \boldsymbol{\sigma}, \boldsymbol{v}_2, t) \right] + \mathcal{F}. \end{aligned} \tag{1.12}$$

The equation accounts for the change in the distribution function $f_1(\boldsymbol{v_1}, \boldsymbol{x}, t)$, with time due to the collisions, free streaming as well as the external driving. In the absence of collision and driving, the terms on the right hand side (RHS) will vanish, and the only cause of change in the distribution will be the free streaming of particles. In the presence of collisions, that will also contribute to the rate of change of f_1 which is described by the integral on the RHS. The evolution of the distribution due to the external forcing is accounted by the term $\mathcal{F}$ on the RHS.

Let us consider the integral on the RHS of Eq. (1.12). The first term in the integral accounts for the increment in f_1 due to the collisions which leads to one of the colliding particle to have a velocity $\boldsymbol{v}_1$ after collision. Here $(\boldsymbol{v}_1^*, \boldsymbol{v}_2^*)$ are precollision velocities which leads to the postcollision velocities $(\boldsymbol{v}_1, \boldsymbol{v}_2)$. The frequency for such an event for a 3D hard sphere system is given by, $\sigma^2(\boldsymbol{v}_1^* - \boldsymbol{v}_2^*) \cdot \boldsymbol{\sigma}$, when it is positive (when negative, it relates to the receding particles). Similarly the second term in the integral accounts for the reduction in f_1 due to a collision in which one of the colliding particles has velocity $\boldsymbol{v}_1$, which changes after collision. Multiplication of $1/r^2$ in the first term comes from the change of variables from $(\boldsymbol{v_1^*},\ \boldsymbol{v_2^*})$ to $(\boldsymbol{v_1},\ \boldsymbol{v_2})$.

As evident, in order to solve the above equation, one needs the knowledge of the 2-particle distribution function f_2. The function f_2 also can be shown to satisfy an evolution equation, solving which requires the information of f_3 and so on. The evolution thus follows a hierarchy of equations known as BBGKY-hierarchy (Bogoliubov, Born, Green, Kirkwood and Yvon). In order to close this hierarchy one needs to consider approximations.

Boltzmann, while developing his kinetic theory for molecular gases, invoked an assumption known as the molecular chaos hypothesis to keep the dominant terms in the distribution function, enabling closure of the hierarchy. According to the hypothesis, the two colliding particles are assumed to be uncorrelated before collision. This enables one to factorize the 2-particle distribution as a product of two 1-particle distributions. i.e.,

$$f_2(\boldsymbol{r}_1, \boldsymbol{v}_1, \boldsymbol{r}_2, \boldsymbol{v}_2, t) = f_1(\boldsymbol{r}_1, \boldsymbol{v}_1, t) f_1(\boldsymbol{r}_2, \boldsymbol{v}_2, t). \tag{1.13}$$

Replacing f_2 in Eq. (1.12)), by the above product form, one can close the hierarchy. The resulting equation is the well known Boltzmann equation. Though the analysis mentioned here is for a dilute gas of particles evolving via binary collisions, an extension of Boltzmann equation to semi-dense systems has been worked out and is known under the name of Enskog-Boltzmann equation [32]. Kinetic theory studies of both isolated and driven gases usually involve analyzing the Boltzmann equation, where one has apriori circumvented the hierarchy using the molecular chaos approximation [25]. There are other studies also which realise closure of the hierarchy by factorising the distributions at some higher order [33].

Though the previous analysis was for a three dimensional system of hard sphere particles, one can generalize it to any dimension and rate of collision $\propto |(\boldsymbol{v}_1^* - \boldsymbol{v}_2^*) \cdot \boldsymbol{\sigma}|^\nu$, $\nu \geq 0$. When $\nu = 1$, it corresponds to the hard sphere gas. When $\nu = 0$ the collision rates no more depend on the velocities and the equations simplify considerably. This is called a *Maxwell gas*. As any particle can collide with any other particle with equal probability, a Maxwell gas can be seen as mean field model of inelastic gas. Maxwell gases serve as model systems which are simple enough to obtain exact quantitative results, at the same time keeping the most crucial features of these systems.

The analytical studies on inelastic gases in literature deal with trying to solve the Boltzmann equation for the 1-particle distribution f_1 or the PDF for one particle, P_1. Though said easily, this turns out to be very difficult. But there are situations in which definite statements can be made.

We will be studying these situations now. We will also mention the perturbative approaches used to obtain solutions in certain limits.

1.4.3.2. Boltzmann equation: homogeneous solutions

A simplification can be considered if one is interested in the homogeneous states of the system. The equations to be satisfied by the homogeneous states can be obtained by integrating out the spatial degrees from the evolution equations of the distribution function. Doing this on Eq. (1.12) results in an equation:

$$\partial_t f_1(\boldsymbol{v_1}, t) = \sigma^2 \int d\boldsymbol{v}_2 \int_{(\boldsymbol{v}_1^* - \boldsymbol{v}_2^*)\cdot\boldsymbol{\sigma}>0} d\boldsymbol{\sigma}(\boldsymbol{v}_1^* - \boldsymbol{v}_2^*)\cdot\boldsymbol{\sigma}\left[\frac{1}{r^2} f_1(\boldsymbol{v}_1^*, t) f_1(\boldsymbol{v}_2^*, t) - f_1(\boldsymbol{v}_1) f_1(\boldsymbol{v}_2, t)\right] + \mathcal{F} \tag{1.14}$$

Homogeneous solutions occur for both freely cooling as well as forced case. It will be worthwhile to review the existing results in connection with the homogeneous solutions in the two cases.

I. The Homogeneous Cooling State

An isolated inelastic gas does not have a homogeneous, time invariant velocity distribution like a molecular gas in equilibrium. But still, a homogeneous state is possible for a free granular gas, which evolves with time. This state loses its kinetic energy monotonically according to Haff's law, and is called the Homogeneous Cooling State (HCS). Even though HCS exist as a solution for the Boltzmann equation, in experiments they are prone to density inhomogeneities. Still the state is of theoretical importance as it is the zeroth order state up on which perturbation studies can be made [34].

The HCS can be described by an isotropic scaling solution for the velocity distribution. i.e., the distribution function satisfies [35] a scaling form with the time dependence coming only through the "granular temperature" $T_g \propto v_0^2$,

$$f_1(\boldsymbol{v}, t) = \frac{n}{v_0^d(t)} \tilde{f}\left(\frac{v}{v_0(t)}\right), \tag{1.15}$$

where v_0 is the root mean square velocity. The scaling variable is renamed as $v/v_0 \equiv c$. The high energy tail of the scaled velocity distribution of a cooling hard sphere gas was predicted to have an exponential form, $\exp(-A|c|)$ [25, 36]. The prediction was later verified numerically [37]. For

inelastic Maxwell gas with scalar velocity, Baldassarri *et al.* [35] obtained a power law tail for the scaling form, $\tilde{f}(c) \sim 1/c^4$. The tail of the scaling form for higher dimensional velocities has also been found analytically to follow a power law with $\tilde{f}(c) \sim 1/|c|^{d+a}$ where d is the dimension of the velocity and a is a function of the coefficient of restitution r ($a = 3$, and is independent of r in one dimension) [38–40].

II. The homogeneous steady state

As discussed earlier, a continuous driving is needed to keep a system of inelastic gas in a steady state. In order to analytically model an inelastic gas in its steady state, one needs to choose a mode of driving which can compensate for the outflow of energy due to collisions. As revealed by the numerical studies [27, 28], localized driving is not enough to sustain a homogeneous steady state. Williams and Mackintosh introduced a simple way to model the driving, which is by adding a white noise to the velocity of the particles with some rate. With this model of driving, the forcing term in the evolution equation for the 1-particle distribution (Eq. (1.12)), becomes $\mathcal{F} = \partial^2_{v_1} f_1(\boldsymbol{x}_1, \boldsymbol{v}_1, t)$. As a result the model is called the *diffusive driving*. Even though other models of driving have been suggested and analyzed, the diffusive driving has been the most employed one as it is one of the simplest schemes to model the experimental systems where the driving is mostly of stochastic nature.

The question of universality appears in the driven context too, asking whether the distribution depends on parameters like the coefficient of restitution, the type of driving mechanism, initial distribution etc. along with others. One of the approach in this direction is to ask for any scaling form as for the HCS. Theoretically, the driven steady states can be studied for a broad class of systems with $\nu \geq 0$, which includes the hard sphere ($\nu = 1$) as well as the Maxwell ($\nu = 0$) gas.

II (a). Perturbative approach : Sonine Polynomial Expansion

An approach in analyzing the homogeneous states, both isolated and driven involves perturbatively expanding about an isotropic Maxwellian distribution–which is the solution of the Boltzmann equation in the elastic limit. For finite inelasticity the isotropic solution for the Boltzmann equation can be found as a systematic Sonine polynomial expansion.

$$\tilde{f}(c) = \phi(c)\{1 + \sum_{p=1}^{\infty} a_p S_p(c^2)\} \tag{1.16}$$

where $\phi(c) = \pi^{d/2} \exp(-c^2)$ and $S_p(c^2)$ are the Sonine polynomials. The method has been

developed for inelastic hard spheres and aims to calculate [25, 41] dominant coefficients in the expansion. The fourth cumulant, a_2 is calculated [25] as a function of the coefficient of restitution r which can quantify the deviation from the Maxwellian. This method has also been extended to the case of Maxwell gases by Carrillo *et al.* [42].

II (b). The High Energy Tails

The perturbation expansions cannot help us to obtain the high energy tails of the scaling form $\tilde{f}(c)$, as they contain information only near the mean of the distribution. But the tail of the distribution in the steady state of inelastic hard sphere gas, when driven by diffusive noise were found by Van Noije and Ernst [25]. They obtained a stretched exponential tail for $\tilde{f}(c) \sim \exp(-A|c|^{\alpha})$ with the exponent $\alpha = 3/2$. M.H.Ernst and R.Brito [40] extended their method to a Maxwell gas system to find an tail to have an exponent $\alpha = 1$. Generalisation for any $\nu > 0$ was done later by Ernst and R.Brito [43] to obtain $\alpha = (\nu + 2)/2$.

1.5. The background and outline of the present work

As mentioned before, in a seminal paper, Van Noije and Ernst [25] found the high energy tail of the scaled velocity distribution function of a inelastic hard sphere system with a diffusive driving, to have a stretched exponential form with an exponent $3/2$ which is independent of the parameters in the system. This result gained more importance as the various experimental realizations [6, 8, 20] of vibrated granular materials also suggested the same exponent for a wide range of parameters. This also lead to the opinion that the theoretical model introduced by van Noije and Ernst [25] possibly could capture the driven homogeneous granular gas correctly, and in turn it has a universal exponent of $3/2$ for the velocity PDF in the steady state.

But the numerical results that followed, obtained rather a range of exponents for the stretched exponential form of the distribution functions ranging up to 2, up on change of parameters which quantify the relative rates of collisions and driving. This motivated us to look the system closely to see what can be the possible reasons for these variety of results.

One of the prime questions that we wanted to address was the following. Is it possible that the analytical model [25] does not represent the experiments that study driven granular gases?

More specifically, we intended to ask whether the model of diffusive driving the right model. We do this in **chapter 2**. In order to get a quantitative answer, we consider the simplest case of a Maxwell gas, which assumes the uniform collision rates for all the particles. We consider a discrete time dynamics, with collisions and driving occurring probabilistically for any possible pair. To our surprise, we find that even though the distributions follow a hierarchy, one can obtain a closed evolution equation for the variance and the two-point correlation functions. One need not invoke any assumption like the molecular Chaos hypothesis. This enables us to calculate the exact evolution for the system. Importantly, we could see that if the driving is done by the discrete time version of diffusive driving, the system no longer stays in a steady state. We introduce another model of driving which can rectify this problem and keep the system in a steady state. We show that for this model, one can calculate the tail of the 1-particle PDF exactly. The model is also important in terms of the non-equilibrium point of view, because it presents an exact result which is usually rare to obtain in the case of non-equilibrium steady states.

In **chapter 3**, we extend this model to a system with continuous time dynamics, and show that the results obtained in the discrete case are valid in the continuous time model also, and is not due to any specificities of the discrete model. We also see that the continuous time model can serve as a generalisation of models with dissipative driving that has been studied in literature. We find an exact mapping of the equations satisfied by the steady state PDF, between the discrete and the continuous time dynamics. This makes it possible to obtain the exact tail of the PDF for the latter class of systems.

In **chapter 4**, we use the tools developed in the earlier chapters to study a system of inelastic gas on a ring. The model that we study comprises of a one-dimensional lattice system. A scalar variable is associated with each of the lattice points which represents the velocity of a particle. With a nearest neighbour interaction same as the usual binary collision rules (Eq. (1.4)), we find a coupled recursion relation for the variance and the two-point correlation functions of the system. This help us find the exact form of the two-point correlation as a function of lattice separation in the driven steady state.

2

Inelastic Maxwell gas with discrete time dynamics

2.1. Introduction

As noted in the earlier chapter, the experimental measurements of steady state velocity PDF show ([6–8, 19–21]) deviation from the Gaussian. It was also observed that it approaches the Gaussian when the rate of driving is increased [21]. Kinetic theory study of uniformly driven inelastic hard spheres by van Noije and Ernst [25] predicts a stretched exponential tail of the form $\tilde{f}(c) \sim \exp(-A|c|^{\alpha})$ with a universal exponent $\alpha = 3/2$, for the scaled velocity c. For the same hard sphere system, Barrat *et al.* [44] find an exponent $\alpha = 3$ in the limit of vanishing inelasticity (see [45]). Though a set of experiments [6, 8, 20] also proposed a stretched exponential tail with the exponent predicted by van Noije *et al.* [25], numerical studies obtained a wide range

of exponents depending on the relative rate of driving to the collisions. Similarly, a model of granular system in one dimension constituted by Brownian particles interacting via binary inelastic collisions, shows a crossover behaviour from Gaussian to non-Gaussian distribution, as one increases the ratio of the relaxation time of the Brownian dynamics to the mean collision time [46]. These studies with a variety of predictions fails to give a consistent picture. In this chapter we do an analytical study of granular systems using simple models, in order to understand the reasons for these inconsistencies.

As reviewed before (Sec. 1.4.3.1), the kinetic theory methods involve deriving Boltzmann equation for the single-particle distribution function. This is done assuming the molecular chaos hypothesis, which allows the factorisation of two-particle distribution function to a product of two single-particle distribution functions. In order to obtain homogeneous solutions one needs to solve an equation obtained after integrating the spatial degrees of freedom (Eq. (2.1)). With the diffusive driving $\mathcal{F} = D\partial_v^2 f_1(\boldsymbol{v}, t)$, the equation has the form:

$$\begin{aligned}\partial_t f_1(\boldsymbol{v_1}, t) = \sigma^2 \int d\boldsymbol{v}_2 \int_{(\boldsymbol{v}_1^* - \boldsymbol{v}_2^*)\cdot\boldsymbol{\sigma}>0} d\boldsymbol{\sigma}\, [(\boldsymbol{v}_1^* - \boldsymbol{v}_2^*)\cdot\boldsymbol{\sigma}]^\nu \\ \times \left[\frac{1}{r^2} f_1(\boldsymbol{v}_1^*, t) f_1(\boldsymbol{v}_2^*, t) - f_1(\boldsymbol{v}_1) f_1(\boldsymbol{v}_2, t)\right] + \partial_{\boldsymbol{v}_1}^2 f(\boldsymbol{v_1}, t).\end{aligned} \tag{2.1}$$

When $\nu = 1$, the above equation represents a hard sphere system in which the collision rate is proportional to the relative velocity of the pair, given the particles are approaching. A simpler model called inelastic Maxwell gas was introduced by Ben-Naim and Krapivsky [47] where the collision rate is independent of the velocities (i.e., $\nu = 0$) of the colliding particles. The velocity distribution of a 1D Maxwell gas with diffusive driving has been found to have an exponential tail $P(v) \sim \exp(-A|v|)$ [4, 48, 49].

Considered to be the simplest model of inelastic gases, the Maxwell model serves to be a good system to study in detail, which might help us understand the possible reasons for the varied results obtained for the driven inelastic gases. As described in this chapter, our studies show that the external driving by an uncorrelated white noise $dv_j/dt = \eta_j(t)$ (represented by a diffusion term in the Boltzmann equation, Eq. (2.1)), is not a good model to predict the steady state behaviour of experimental systems. It turns out that the input of energy due to the driving cannot be compensated by the dissipative collisions in the system, and causes the energy to increase linearly

with time. Thus the system does not have a steady state. We find that this feature is true not only for Maxwell gases but for any $\nu > 0$, including the hard sphere gas.

The diffusive driving is usually justified considering the centre of mass frame [30, 47], in which the system follows the same Boltzmann equation, thanks to the the Galilean invariant nature of it. In this frame one finds that a steady state is indeed achieved. But this assumption is not convincing from the experimental point of view. A better model can be built by mimicking the driving done in real systems. The driving in these systems usually involves collision of the particles with the vibrating walls. Such a driving is naturally accompanied by a damping term which will be shown to solve this overheating. Similar forcing mechanisms were also studied before [4, 46, 50], but the tails of the distribution were unknown. In this chapter, we show that one can find the tail for the velocity distribution in this $real$ steady state.

In the next section we provide a outline of the chapter for the benefit of readers who are not interested in the details.

2.2. Outline

Since we are interested in the steady state properties, we consider the evolution of the system in discrete time step. A set of N identical particles is considered with each characterised by a scalar velocity, v_i, where $i = 1, 2, \ldots, N$. As in [47], the spatial structure is ignored in the model. With the initial velocities taken from a Gaussian distribution independently, the system evolves in discrete time steps as follows. At each step, a pair of particles are chosen randomly, which undergo inelastic collision as well as, they are subjected to independent external driving.

We look at two different types of dynamics for the system. In one, the chosen pair of particles are subjected to collision and driving simultaneously in each step. The second type comes closer to real systems, in which at each step, the pair undergo collision with probability p and driving with probability $1 - p$. The former causes only linear changes in the velocity, leading to the PDF of the velocity to have the Gaussian form at all times. This is not the case with the latter, for which we find a PDF which is non-trivial.

An interesting observation which comes to use is the following: for both the dynamics described above, we find that even though the evolution equations for the distribution function do not close,

those for the energy e(n) (Eq. (2.6)) and the two-point correlation function $\Sigma(n)$ (Eq. (2.7)) close on it's own, as a coupled recursion equation. This can be used to explicitly calculate the time evolution of the above quantities for this model.

The inelastic binary collision change the velocities of the chosen pair of particles (i, j), from (v_i^*, v_j^*) to (v_i, v_j) according to the rule,

$$\begin{aligned} v_i &= \epsilon v_i^* + (1-\epsilon) v_j^*, \\ v_j &= (1-\epsilon) v_i^* + \epsilon v_j^*. \end{aligned} \tag{2.2}$$

Here $\epsilon \equiv (1-r)/2$ with r being the coefficient of restitution as before. In physical systems the restitution coefficient takes value $r \in [0, 1]$, but the equation is valid for the entire range of $r \in [-1, 1]$ for a model of dissipative system. Alternatively, $\epsilon \in [0, 1]$.

For the above model, considering an external driving mechanism (Sec. 2.3), in which uncorrelated Gaussian white noises are added independently to the velocities of the chosen pair, $v_{i(j)} = v_{i(j)} + \eta_{i(j)}$, as in [47], we observe for both the above dynamics that, after time steps of $O(N)$, the system approaches a 'steady state like state' where energy of the system saturates. The correlations that build up during this time is still $O(1/N)$ and so, negligible for a large system. Thus in this state, the molecular chaos hypothesis holds. This helps to calculate the velocity PDF in this state which has the Gaussian form for the first case, and an exponential tail for the latter. The system starts deviating from this state after time steps of $O(N^2)$. At this stage the correlation remains no longer negligible which, along with the the average energy per particle grows linearly with time step eventually. Hence, with the above driving, the system no longer has a steady state.

The absence of steady state for the above cases motivates us to consider a model in Sec. 2.4, with a dissipative term accompanying the noise. In fact, the dissipative term naturally arises, when the external forcing is caused by collisions of particles with a vibrating wall. The change in the velocity of a particle due to a wall-particle collision can be shown to follow the equation (Sec. 2.4), $v = -r_w v^* + \eta$, where r_w is the coefficient of restitution for collision between particle and the wall. The random variable $\eta = (1 + r_w) V_w$, where V_w is the velocity of the wall at the time of collision.

Like the restitution coefficient of the particle-particle collision r, we consider $r_w \in [-1, 1]$.

With the new driving, one can observe that the system goes to a steady state except when $r_w = -1$. From the steady state values one finds that the correlation vanishes in the large N limit as $O(1/N)$. We consider two different types of dynamics: one in which both collision and driving occur simultaneously (Sec. 2.4.1)and the other, where either collision or driving occur at a time, probabilistically (Sec. 2.4.2). The steady state distribution of velocity in the first case is a Gaussian. For the second case, we obtain an exact equation satisfied by the moment generating function of the steady state velocity distribution in the thermodynamic limit. We find that the distribution function becomes Maxwellian in the limit of vanishing inelasticity. For finite inelasticities and $r_w \neq -1$, we obtain two different class of steady state distributions. i.e., for $r_w = 1$ system happens to be in a singular state with the distribution function having an exponential tail, for all other parameters, $|r_w| < 1$ one finds that the high energy tail has a Gaussian form. Later (Sec. 2.4.2.5) we present a weakly interacting gas. We calculate the velocity distribution in perturbative way, where the steady state velocity distribution is given by infinite sum of Gaussians. Finally (Sec. 2.4.2.6) we show that there exists an exactly solvable case of this model: i.e., when the noise is taken from the Cauchy distribution. In this case the velocity distribution is another Cauchy distribution. In Sec. 2.5, we summarize the chapter mentioning possible extensions.

2.3. Driving by white noise

As noted, inelastic gases need to be driven to keep it moving. In theoretical studies, it is usual to model external forcing by adding uncorrelated noise to the velocities of the particles. In this section we will probe the consequence of such a driving. We address two different ways of realising the driving: first when collision and driving occurring at the same step. Then we study when only one of them occurs probabilistically in a time step. We will find that these two cases lead to significantly different results.

2.3.1. Model with binary collisions and external forcing occurring simultaneously

The model consists of N number of particles with identical masses (taken to be unity), with initial velocity distribution being Gaussian with variance σ_0^2. The system evolves in discrete steps as follows. At each step the velocities of a randomly picked pair of particles (i, j) change according to the rule (Eq. (2.3)) taking into account of collision and driving:

$$\begin{aligned} v_i &= [\epsilon v_i^* + (1-\epsilon)v_j^*] + \eta_i, \\ v_j &= [\epsilon v_j^* + (1-\epsilon)v_i^*] + \eta_j, \end{aligned} \tag{2.3}$$

$v_{i(j)}^*$ and $v_{i(j)}$ are the pre and postcollision velocities of $i(j)^{th}$ particle respectively. The noise terms $\eta_{(i,j)}$ at different time steps are uncorrelated and are taken from Gaussian distribution with variance σ^2,

$$\langle \eta_i \eta_j \rangle = \sigma^2 \delta_{ij}. \tag{2.4}$$

This property of the noise will remain same for all the models considered later unless specified otherwise.

2.3.1.1. Two-particle system

Considering a two-particle the system turns out to be useful. Here, one can easily calculate the time evolution of the total energy to see that the system does not go to a steady state. For this we introduce the new set of variables $U = v_1 + v_2$ and $V = v_1 - v_2$. The time evolution for these two variables with the dynamics Eq. (2.3) is given by:

$$\begin{aligned} U &= U^* + \eta_1 + \eta_2, \\ V &= -(1-2\epsilon)V^* + \eta_1 - \eta_2 \ . \end{aligned} \tag{2.5}$$

As before, the '*' indicate the precollision values. One can easily see that the total energy of the system $\langle (U^2 + V^2)/2 \rangle$ will then never reach a steady state. This is because, as U does a random walk, $\langle U^2 \rangle$ keeps increasing linearly with time (number of steps) even though the relative velocity V goes to a steady state (Ornstein-Uhlenbeck process) keeping $\langle V^2 \rangle$ constant. Note that $\langle \ldots \rangle$ refers to an averaging over both initial conditions and noise realisations.

2.3.1.2. The N-particle system

One can see the absence of steady state for a general N particle system also. Consider $v_i(n)$ to be the velocity of the i^{th} particle at the n^{th} time step. The average energy per particle of the system at the n^{th} time step is given by

$$\mathrm{e}(n) = \frac{1}{2N} \sum_{i=1}^{N} \langle v_i^2(n) \rangle \ , \tag{2.6}$$

while the velocity correlation between any two particles is,

$$\Sigma(n) = \frac{1}{N(N-1)} \sum_{i \neq j} \langle v_i(n) v_j(n) \rangle. \tag{2.7}$$

We now show that it is possible to write exact recursion relations for the time evolution of these two quantities. Consider the change in energy $\Delta E_{ij}(n)$ of the system at the n^{th} time step given that particles with labels i and j collide. This can be calculated as,

$$\Delta E_{ij}(n) = \frac{1}{2} \left[v_i^2(n) + v_j^2(n) - v_i^2(n-1) - v_j^2(n-1) \right]. \tag{2.8}$$

Substituting the collision rules Eq. (2.3) in Eq. (2.8), and averaging over the noise we get

$$\begin{aligned} \langle \Delta E_{ij}(n) \rangle = & -\epsilon(1-\epsilon) \left[\langle v_i^2(n-1) + v_j^2(n-1) \rangle \right] \\ & + 2\epsilon(1-\epsilon) \left\langle v_i(n-1) \, v_j(n-1) \right\rangle + \sigma^2 \ . \end{aligned} \tag{2.9}$$

Averaging over all possible pairs of particles one obtains the average change in the total energy of the system at n^{th} time step:

$$\langle \Delta E(n) \rangle = -4\epsilon(1-\epsilon) \, \mathrm{e}(n-1) + 2\epsilon(1-\epsilon) \, \Sigma(n-1) + \sigma^2 \ . \tag{2.10}$$

Note that $\langle \Delta E(n) \rangle = N[\mathrm{e}(n) - \mathrm{e}(n-1)]$. Substituting this in Eq. (2.10), we get the recurrence relation

$$\mathrm{e}(n) = \left(1 - \frac{4\epsilon(1-\epsilon)}{N} \right) \mathrm{e}(n-1) + \frac{2\epsilon(1-\epsilon)}{N} \, \Sigma(n-1) + \frac{\sigma^2}{N} \ . \tag{2.11}$$

To construct the evolution equation for the correlation function Eq. (2.7), let us consider that the collision at the n^{th} time step involved the pair of particles i, j. Then from Eq. (2.3),

$$\sum_{k=1}^{N} v_k(n) = \sum_{k=1}^{N} v_k(n-1) + \eta_i + \eta_j. \tag{2.12}$$

Taking squares on both sides of Eq. (2.12) and averaging over noise we get

$$\sum_{i=1}^{N} \langle v_i^2(n)\rangle + \sum_{i\neq j} \langle v_i(n)v_j(n)\rangle = \sum_{i=1}^{N} \langle v_i^2(n-1)\rangle + \sum_{i\neq j} \langle v_i(n-1)v_j(n-1)\rangle + 2\sigma^2. \tag{2.13}$$

Averaging over all pairs (i,j) and, using the definitions Eqs. (2.6) and (2.7), we get the recurrence relation for $\Sigma(n)$:

$$\Sigma(n) = \frac{8\epsilon(1-\epsilon)}{N(N-1)}\, \mathrm{e}(n-1) + \left(1 - \frac{4\epsilon(1-\epsilon)}{N(N-1)}\right)\, \Sigma(n-1) \tag{2.14}$$

The set of equations Eq. (2.11) and Eq. (2.14) form a coupled set of recursion relations. In compact form they can be represented as,

$$X_n = \boldsymbol{R}\, X_{n-1} + C, \tag{2.15}$$

where, $X_n = [\ \mathrm{e}(n),\ \Sigma(n)]^T$ and $C = [\ \frac{\sigma^2}{N},\ 0]^T$ are column vectors and

$$\boldsymbol{R} = \begin{bmatrix} 1 - \frac{4\epsilon(1-\epsilon)}{N} & \frac{2\epsilon(1-\epsilon)}{N} \\ \\ \frac{8\epsilon(1-\epsilon)}{N(N-1)} & 1 - \frac{4\epsilon(1-\epsilon)}{N(N-1)} \end{bmatrix}, \tag{2.16}$$

This is a linear equation, the solution of which has the form,

$$X_n = \boldsymbol{R}^n X_0 + \sum_{l=1}^{n-1} \boldsymbol{R}^l C\ , \tag{2.17}$$

As the velocities initially are taken from uncorrelated Gaussian distribution, $X_0 = [\ \sigma_0^2/2,\ 0]^T$. After transforming to the eigenbasis of the matrix $\boldsymbol{R}$, we obtain the following explicit solutions:

$$\begin{aligned} \mathrm{e}(n) =& \frac{1}{2}\left(\frac{\sigma_0^2}{N} + \frac{(N-1)^2\sigma^2}{2N^2\epsilon(1-\epsilon)} + \frac{2n\sigma^2}{N^2}\right) \\ &+ \frac{N-1}{2}\left(1 - \frac{4\epsilon(1-\epsilon)}{N-1}\right)^n \left[\frac{\sigma_0^2}{N} - \frac{(N-1)\sigma^2}{2N^2\epsilon(1-\epsilon)}\right]\ , \end{aligned} \tag{2.18}$$

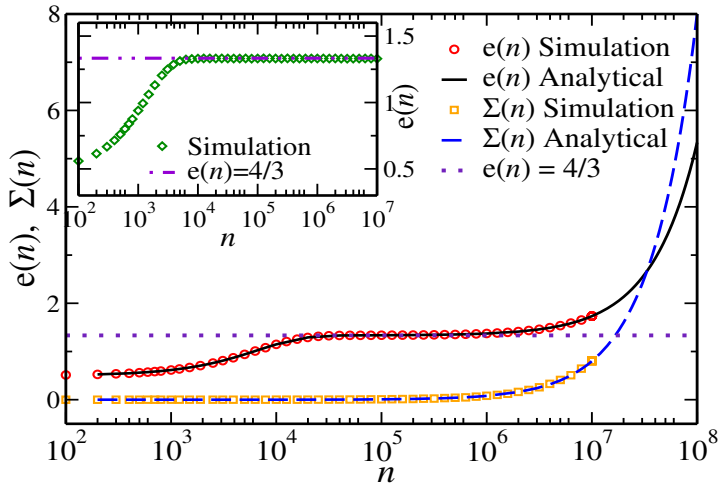

FIGURE 2.1: The evolution of average energy per particle e(n), and velocity correlation $\Sigma(n)$ of a 5000-particle system with discrete Langevin dynamics (Eq. (2.3)) with $\epsilon = 1/4$, $\sigma^2 = 1$. The analytical result for e(n) (Eq. (2.18)), plotted as the solid line (black) is compared with the simulation data given by the circles (red). Similarly, the analytical formula for Σ(n) (Eq. (2.19)), plotted as the dashed line (blue) is compared with the simulation data given by the squares (orange). The intermediate saturation regime with the saturation value (Eq. (2.20)) is represented by the dotted line (indigo). In the inset, the evolution of the energy per particle in the centre of mass frame is shown. The simulation result represented by the diamond symbol (dark green) shows saturation of the energy of the system in this frame. The steady state value is shown by the line with dots and dashes (violet).

$$\begin{aligned}\Sigma(n) = &\left(\frac{\sigma_0^2}{N} - \frac{(N-1)\sigma^2}{2N^2\epsilon(1-\epsilon)} + \frac{2n\sigma^2}{N^2}\right) \\ &- \left(1 - \frac{4\epsilon(1-\epsilon)}{N-1}\right)^n \left[\frac{\sigma_0^2}{N} - \frac{(N-1)\sigma^2}{2N^2\epsilon(1-\epsilon)}\right] \quad .\end{aligned} \tag{2.19}$$

The form of e(n) for an N-particle system as obtained from Eq. (2.18) has been verified by direct simulations and is shown in Fig. 2.1. For large N, we see two different regimes in the evolution of e(n) with time n. At time $n \sim N/[4\epsilon(1-\epsilon)]$ the energy per particle reaches a saturation phase while the correlation is still negligible. We see that for times $N \lesssim n \lesssim N^2$ the energy and correlations are given by:

$$\begin{aligned}\mathrm{e}_{sat} &= \frac{\sigma^2}{4\epsilon(1-\epsilon)} + O(N^{-1}) \ , \\ \Sigma &= O(N^{-1}) \ .\end{aligned} \tag{2.20}$$

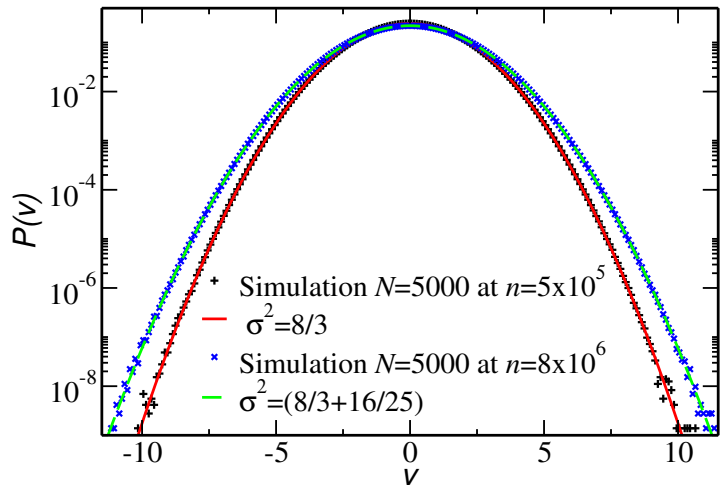

FIGURE 2.2: The velocity distributions at different times for the system with discrete Langevin dynamics (Eq. (2.3)) with $\epsilon = 1/4$, $\sigma^2 = 1$, $N = 5000$. The '+' symbol (black) shows the PDF in the saturation regime. A Gaussian with the variance calculated from Eq. (2.20) neglecting terms of $O(N^{-1})$ is shown by the solid line (red). Similarly, the PDF of the system when the energy starts to increase is shown by the 'X' symbol (blue). The Gaussian with variance calculated from Eq. (2.21) is represented by the dashed line (green). Both the Gaussian are seen to be matching well with the simulations.

For $n >> N^2$, both the energy and the correlation increase linearly with time as

$$\begin{aligned} \mathrm{e}(n) &= \frac{n\sigma^2}{N^2} + \mathrm{e}_{sat} \ , \\ \Sigma(n) &= \frac{2n\sigma^2}{N^2} + O(N^{-1}) \ . \end{aligned} \tag{2.21}$$

One can find out the velocity statistics of the system from the reasoning that follows. The velocity of any given particle at time n can be written as a sum of Gaussian variables (since the initial velocities and noises are taken from Gaussian distributions), where the number of summands is a fluctuating quantity. For large n the effect of the fluctuations is small and therefore, the velocity distribution is Gaussian. The width of the distribution is given by Eq. (2.18). In Fig. 2.2, we plot the analytically obtained velocity distributions in both the saturation regime and the long time regimes along with those obtained from the direct simulations.

2.3.2. Model with binary collisions and external forcing occurring at different rates

In the previous section what we studied is a simple realisation of a driven Maxwell gas with the collision and the white noise driving occurring in the same time-step. We found that the model does not allow a steady state. It is important to show that the result is not due the special nature of the dynamics, but rather general. We do this by considering a more realistic model where the driving and collision does not occur simultaneously but at different times.

The dynamics is as follows. At each time step, a pair of particles is randomly chosen, such that with probability p they collide and with probability $1-p$ they are acted upon by the random noise. Thus at each time step, the new velocities of a randomly picked pair (i, j) are given by:

$$\begin{aligned} v_i &= \alpha[\epsilon v_i^* + (1-\epsilon)v_j^*] + (1-\alpha)[v_i^* + \eta_i], \\ v_j &= \alpha[\epsilon v_j^* + (1-\epsilon)v_i^*] + (1-\alpha)[v_j^* + \eta_j] \, . \end{aligned} \tag{2.22}$$

Here, α is a random number which takes the values 1 and 0 with probabilities p and $1-p$ respectively. Proceeding exactly as before, one can obtain the evolution equation Eq. (2.15) for the energy and correlations, now with

$$\boldsymbol{R} = \begin{bmatrix} 1 - \frac{4p\epsilon(1-\epsilon)}{N} & \frac{2p\epsilon(1-\epsilon)}{N} \\ \\ \frac{8p\epsilon(1-\epsilon)}{N(N-1)} & 1 - \frac{4p\epsilon(1-\epsilon)}{N(N-1)} \end{bmatrix} \tag{2.23}$$

and $C = [(1-p)\sigma^2/N, 0]^T$. The equation is solved to obtain the exact evolution of the $\mathrm{e}(n)$ and $\Sigma(n)$ as before:

$$\begin{aligned} \mathrm{e}(n) = \frac{1}{2}\left(\frac{\sigma_0^2}{N} + \frac{(1-p)\sigma^2(N-1)^2}{2N^2p\epsilon(1-\epsilon)} + \frac{2n(1-p)\sigma^2}{N^2}\right) \\ + \frac{N-1}{2}\left(1 - \frac{4p\epsilon(1-\epsilon)}{N-1}\right)^n \left[\frac{\sigma_0^2}{N} - \frac{(1-p)(N-1)\sigma^2}{2N^2p\epsilon(1-\epsilon)}\right] , \end{aligned} \tag{2.24}$$

$$\begin{aligned} \Sigma(n) = \left(\frac{\sigma_0^2}{N} - \frac{(1-p)\sigma^2(N-1)}{2N^2p\epsilon(1-\epsilon)} + \frac{2n(1-p)\sigma^2}{N^2}\right) \\ - \left(1 - \frac{4p\epsilon(1-\epsilon)}{N-1}\right)^n \left[\frac{\sigma_0^2}{N} - \frac{(1-p)(N-1)\sigma^2}{2N^2p\epsilon(1-\epsilon)}\right] . \end{aligned} \tag{2.25}$$

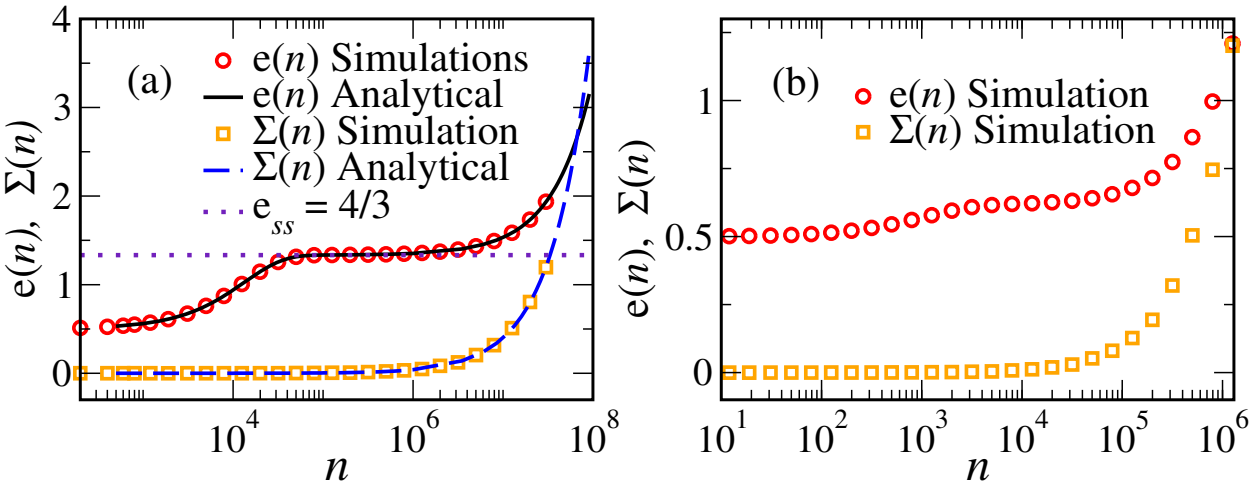

FIGURE 2.3: (a) Evolution of the average energy per particle e(n), and velocity correlation $\Sigma(n)$ of a 5000-particle system with discrete Langevin dynamics (Eq. (2.22)) with p=1/2, $\epsilon = 1/4$, $\sigma^2 = 1$. The analytical result for e(n) (Eq. (2.24)), plotted as the solid line (black) is compared with the simulation data given by the circles (red). Similarly, the analytical formula for Σ(n) (Eq. (2.25)), plotted as the dashed line (blue) is compared with the simulation data given by the squares (orange). The intermediate saturation regime with the saturation value (Eq. (2.26)) is represented by the dotted line (indigo). (b) The evolution of e(n) and Σ(n) for a hard sphere system obtained from simulations are respectively depicted by the circles (red) and squares (orange).

In Fig. 2.3(a), we plot e(n) and $\Sigma(n)$ as functions of n. As before, two regimes in the evolution of energy e(n) are seen. For $N \lesssim n \lesssim N^2$, e($n$) saturates and we have

$$\begin{aligned} \mathrm{e}_{sat} &= \frac{(1-p)\sigma^2}{2p\epsilon(1-\epsilon)} + O(N^{-1}), \\ \Sigma &= O(N^{-1}) \ . \end{aligned} \tag{2.26}$$

For $n >> N^2$ the variance and correlations increase linearly as:

$$\begin{aligned} \mathrm{e}(n) &= \frac{(1-p)\sigma^2 n}{N^2} + \mathrm{e}_{sat} + O(N^{-1}) \ , \\ \Sigma(n) &= \frac{2(1-p)\sigma^2 n}{N^2} + O(N^{-1}) \ . \end{aligned} \tag{2.27}$$

It is interesting to observe (Fig. 2.4) that unlike the Gaussian velocity PDF obtained before (Sec. 2.3.1), in the present case one observes an exponential tail for the PDF at the 'pseudo-steady state' (saturation regime). To see this, let us consider the Moment Generating Function

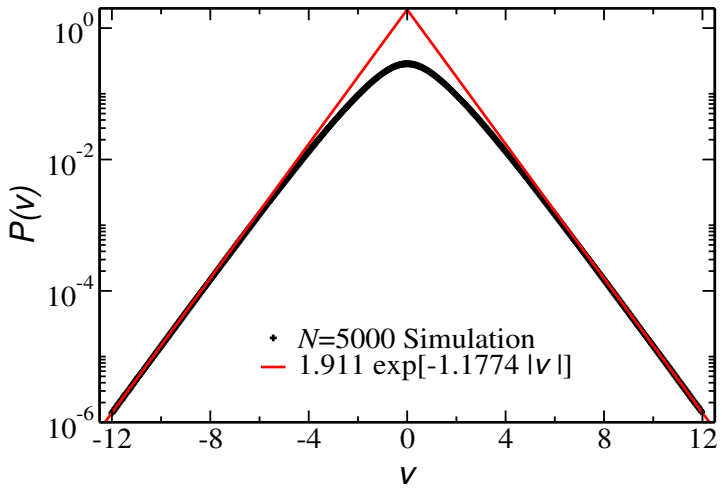

Figure 2.4: Velocity PDF for a 5000 particle system for the parameters $p = 1/2$, $\epsilon = 1/4$ calculated in the 'pseudo' steady state regime is shown.'+' symbol (black) denotes the data points from simulations. The calculated tail of the distribution (Eq. (2.33)) for the particular values is plotted as the solid line (red).

(MGF) of the velocity distribution function defined as:

$$Z(\lambda) = \langle \exp[-\lambda v] \rangle, \tag{2.28}$$

where the averaging is over the PDF. From Eq. (2.26), one finds that in the pseudo-steady state, velocity correlation Σ becomes negligible in the large N limit. Using this, an equation satisfied by the MGF in the pseudo steady state Z_{pss} can be constructed from Eq. (2.22),

$$Z_{pss}(\lambda) = pZ_{pss}([1-\epsilon]\lambda)Z_{pss}(\epsilon\lambda) + (1-p)Z_{pss}(\lambda)\exp[\frac{\lambda^2\sigma^2}{2}]\,, \tag{2.29}$$

where $\exp[\frac{\lambda^2\sigma^2}{2}]$ is the MGF for the Gaussian noise with the variance σ^2. Rearrangement leads to a recursion relation,

$$Z_{pss}(\lambda) = \frac{pZ_{pss}([1-\epsilon]\lambda)Z_{pss}(\epsilon\lambda)}{1-(1-p)\exp[\frac{\lambda^2\sigma^2}{2}]}\,. \tag{2.30}$$

The solution of Eq. (2.30) is

$$Z_{pss}(\lambda) = \prod_{i=0}^{\infty}\prod_{j=0}^{i}\left[\frac{p}{1-(1-p)\exp[\frac{\lambda^2\sigma^2\epsilon^{2j}(1-\epsilon)^{2(i-j)}}{2}]}\right]^{\binom{i}{j}}, \tag{2.31}$$

where we have used the normalization condition $Z(0) = 1$. The pole of $Z_{pss}(\lambda)$ closest to the origin in the complex λ-space determines the behaviour of the velocity distribution near the tail. It happens to be a simple pole λ_0 and is given by,

$$\lambda_0 = \pm \left[\frac{-2ln(1-p)}{\sigma^2} \right]^{\frac{1}{2}} . \tag{2.32}$$

Hence, the distribution has exponential tails given by

$$P_{pss}(v) \sim A(\epsilon) \exp[-|\lambda_0||v|] . \tag{2.33}$$

The pre-factor $A(\epsilon)$ can be obtained by calculating the residue of the function about the pole (Eq. (2.32)) as

$$A(\epsilon) = \frac{p}{\sqrt{-2\sigma^2 ln(1-p)}} \prod_{i=1}^{\infty} \prod_{j=0}^{i} \left[\frac{p}{1-(1-p)\exp[-ln(1-p)\epsilon^{2j}(1-\epsilon)^{2(i-j)}]} \right]^{\binom{i}{j}} . \tag{2.34}$$

For the parameter values $p = 1/2$ and $\epsilon = 1/4$, the slope is $\lambda_0 = 1.1774$ with $A(\epsilon) = 1.9113$. The form of the probability distribution Eq. (2.33) and the results from the simulations for the above set of parameter values is shown in the Fig. 2.4.

2.3.2.1. Dynamics in the centre of mass frame

As mentioned before, the driving by addition of white noise to the velocities was introduced by Williams and Mackintosh [30] for inelastic gases. The observables of interest for them were the velocities in the centre of mass frame. In simulation, this is done by subtracting the centre of mass velocities from the individual ones, before sampling the velocities of the particles. It is instructive to study the behaviour of these rescaled observables in our model too. What we show is that in the centre of mass frame, both the energy and correlation evolve to steady state values.

Consider the definition of velocity correlation function in Eq. (2.7) in the centre of mass frame (we suppress the n dependence of the observables for convenience.)

$$\overline{\Sigma} = \frac{1}{N(N-1)} \sum_{i \neq j} \langle (v_i - v_{cm})(v_j - v_{cm}) \rangle ,$$

where the centre of mass velocity is defined as $v_{cm} = (1/N) \sum_i v_i$. Expanding the RHS of Eq. (2.35) gives

$$\overline{\Sigma} = \Sigma - \langle v_{cm}^2 \rangle . \tag{2.35}$$

From the definition of v_{cm} it follows that $\langle v_{cm}^2 \rangle = (2\mathrm{e} - \Sigma)/N + \Sigma$, hence we get $\overline{\Sigma} = (\Sigma - 2\mathrm{e})/N$. At any finite time this vanishes for large N. For large n both Σ and e increase linearly with n while the difference $\Sigma - 2\mathrm{e} = O(1)$ (see Eqs. (2.20), (2.27)) and so, again $\overline{\Sigma} \to 0$ as $N \to \infty$. Similarly the energy per particle in the centre of mass frame $\overline{\mathrm{e}} = \mathrm{e} - \langle v_{cm}^2 \rangle/2$ which, in the limit of $N \to \infty$, goes to $\mathrm{e} - \Sigma/2 = O(1)$. From Eqs. (2.20), and (2.27), we get the constant $\overline{\mathrm{e}} = \sigma^2/[4\epsilon(1-\epsilon)]$ or $\overline{\mathrm{e}} = (1-p)\sigma^2/[4p\epsilon(1-\epsilon)]$ depending on the dynamics. In the inset of Fig. 2.1, the evolution of the energy in the center of mass frame $\overline{\mathrm{e}}$, is plotted for the dynamics with collision and forcing done simultaneously (Eq. (2.3)), showing the predicted saturation.

Thus the change to the centre of mass frame cause the correlations to vanish. As dynamics is invariant with the change in frame, the steady state obtained is the same as the intermediate saturation regime, which is the steady state solution for the dynamics when the correlations are negligible. The velocity distribution in this case is also the same as in the intermediate saturation regime [47].

2.3.2.2. Hard sphere system

One can ask whether the above results are true for hard sphere system also. Unlike the earlier model, it is difficult to proceed analytically for a hard sphere system. Hence we do a direct simulation of the system. We consider N unit mass particles with scalar velocity. During each time step, with probability p, a pair of particles are chosen to collide and with probability $(1-p)$, a pair is driven by adding uncorrelated Gaussian noise to their velocities. Unlike before, for the hard sphere gas, the colliding pair is chosen with probability proportional to the magnitude of their relative velocity. The simulation results for the evolution of energy and the correlation function are shown in Fig. 2.3(b). One easily observes that the plot is qualitatively similar to that of Maxwell gas.

2.3.2.3. Discussion

We have found that the inelastic Maxwell gas driven by the discrete time version of diffusive forcing cannot have a steady state. This is because, while the inter-particle collisions conserve total momentum of the system, driving causes the total momentum to do a random walk, causing

the energy to grow linearly with time. Though our calculations are for Maxwell gases, simulations done on hard sphere gases with the diffusive driving also show the same behaviour This is indeed expected, because the diffusion of the total momentum exist even for hard sphere gases. More generally, this effect is valid for any system with interactions which conserve momentum.

The time scale over which the correlations start appearing, taking the system away from the pseudo steady state, has a quadratic dependence on the total number of particles in the system. This enables one to use the diffusive forcing to obtain a steady state for a system in the thermodynamic limit. This is because, in this limit the above timescale is pushed towards infinity, which in turn causes the system to be in this 'pseudo' steady state for a longer time.

The above justifications for the the driving scheme are unsatisfactory as we are interested in modelling physical systems, which are finite systems and have steady states even in the laboratory frame. A solution can be found from the experimental systems itself. In most of the experiments, the driving usually involves heating from the walls, where collisions of the particles with the walls impart the necessary kinetic energy to keep the motion. A better way to model the driving is to mimic the wall collisions, as we will see next.

2.4. Random driving with "wall" dissipation

Let us consider a collision event happening between a particle with velocity v^* and a moving wall with velocity V_w^* . The velocities of the particle and the wall after collision becomes v, and V_w respectively. The collision satisfies the equation:

$$(v - V_w) = -r_w(v^* - V_w^*), \tag{2.36}$$

where r_w is the coefficient of restitution of the collision between the particle and the wall. As a mathematical model for dissipative gas, one can consider the negative values r_w and has the range, $r_w \in [-1, 1]$. The mass of the wall being infinitely larger than that of the particle, one can as well assume that the velocity of the wall is almost the same even after the collision. Replacing V_w^* by V_w and rearranging, Eq. (2.36) becomes $v = -r_w v^* + (1 + r_w)V_w$. The velocity of the wall at the collision events are random, and one can replace $(1 + r_w)V_w$ by the random variable η as defined in Eq. (2.4) and obtain:

$$v = -r_w v^* + \eta. \tag{2.37}$$

The driving thus has an additional dissipative term along with the noise. Similar models where a dissipative term accompanies the noise, have been pursued before [4, 46]. These were continuous time models with the rate of change of velocity due to driving, equated to a random noise accompanied by a viscous drag (Ornstein-Uhlenbeck [OU] driving). The OU-driving causes the system to reach a steady state. In the earlier studies [4, 46], the form of the velocity PDF was calculated as a perturbation round the mean, which does not give information in the high energy regime. Here we show that one can proceed further. As done in the previous case, we consider the two situations, first with the collision and energy injection in the same step (Sec. 2.4.1) and then the case where one of them is probabilistically chosen at each step (Sec. 2.4.2).

2.4.1. Model with binary collisions and external forcing occurring simultaneously

Consider that at each time step a randomly picked pair of particles labelled i and j evolves according to the rule:

$$\begin{aligned} v_i &= [\epsilon v_i^* + (1-\epsilon) v_j^*] + [-r_w v_i^* + \eta_i], \\ v_j &= [\epsilon v_j^* + (1-\epsilon) v_i^*] + [-r_w v_j^* + \eta_j]\ . \end{aligned} \tag{2.38}$$

For the N-particle system, the evolution equations for $\mathrm{e}(n)$ and $\Sigma(n)$ can be obtained as before which follow the matrix evolution equation Eq. (2.15) with a different form for the matrix,

$$\boldsymbol{R} = \begin{bmatrix} 1 - \frac{[4\epsilon(1-\epsilon)+4\epsilon r_w - 2r_w^2]}{N} & \frac{2[\epsilon(1-\epsilon) - r_w(1-\epsilon)]}{N} \\ \\ \frac{8[\epsilon(1-\epsilon) - r_w(1-\epsilon)]}{N(N-1)} & 1 - \frac{\left[4\epsilon(1-\epsilon)+4r_w(\epsilon+N-2) - 2r_w^2\right]}{N(N-1)} \end{bmatrix}, \tag{2.39}$$

and $C = (\sigma^2/N, 0)^T$.

Knowing the eigenvalues the matrix $\boldsymbol{R}$ would be enough to tell whether a system which evolves via Eq. (2.15) goes to a steady state or not. The system reaches a steady state, if the eigenvalues

of $\boldsymbol{R}$, say $\lambda_{1,2}$ are such that, $-1 < \lambda_{1,2} < 1$. Using Perron-Frobenius theorem (details of the analysis given in the next section), one can show that when $r_w \neq \{-1, 0\}$, this property is satisfied by the eigenvalues of $\boldsymbol{R}$, and the system will go to a steady state. In Fig. 2.5, we plot the energy per particle computed using the above equation and compare with simulation results.

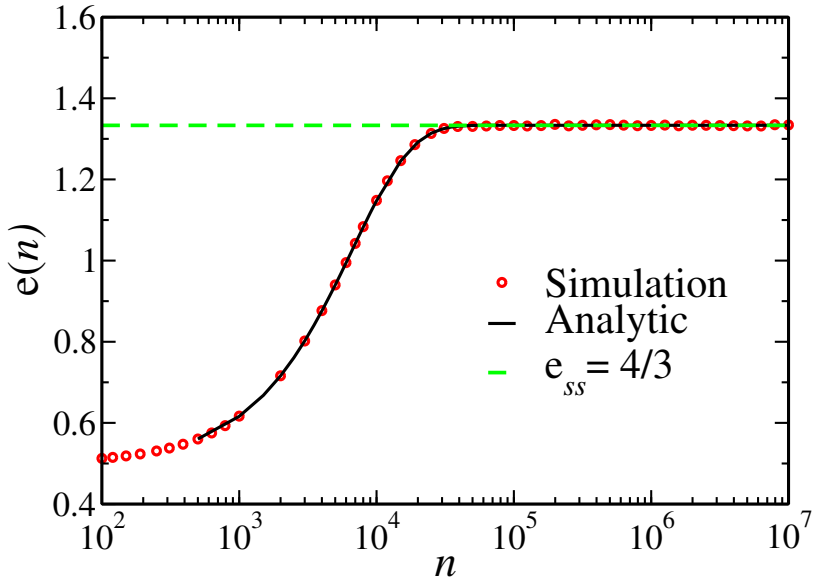

FIGURE 2.5: Energy evolution (e(n)) of a 5000-particle system for the model with the dissipative noise added linearly (Eq. (2.38)) for the parameter values ϵ=1/4, $r_w = 1/2$, $\sigma^2 = 1$. The simulation result is shown in the graph by the circles (red). The analytic evolution of e(n) is shown as the solid line (black). The steady state e_{ss} calculated in Eq. (2.40), is shown as the dashed line (green).

The energy and correlation values in the steady state are obtained as

$$\begin{aligned} e_{ss} &= \frac{\sigma^2[4\epsilon(1-\epsilon) + 2r_w(2[N-1] - r_w - 2[1-\epsilon])]}{4r_w[4\epsilon(1-\epsilon) - 4r_w(1-\epsilon)](N-r_w) + 4r_w^2(2-r_w)[2(N-1)-r_w]}, \\ \Sigma_{ss} &= \frac{2\sigma^2[4\epsilon(1-\epsilon) - 4r_w(1-\epsilon)]}{4r_w[4\epsilon(1-\epsilon) - 4r_w(1-\epsilon)][N-r_w] + 4r_w^2[2-r_w][2(N-1)-r_w]}. \end{aligned} \tag{2.40}$$

For large N, this simplifies to,

$$\begin{aligned} e_{ss} &= \sigma^2/[4\epsilon(1-\epsilon) + 2r_w(2\epsilon - r_w)] + O(N^{-1}) \quad \text{and} \\ \Sigma_{ss} &= O(N^{-1}). \end{aligned} \tag{2.41}$$

As in Sec. 2.3.1, it can be argued that the velocity distribution is Gaussian at large time-steps, for any number of particles. In particular for large N, the velocity correlation $\Sigma_{ss} \to 0$ and it is

easy to show that the MGF (Eq. (2.28)) in the steady state satisfies the equation,

$$Z_{ss}(\lambda) = Z_{ss}((\epsilon - r_w)\lambda) Z_{ss}((1-\epsilon)\lambda) \exp\left[\frac{\lambda^2\sigma^2}{2}\right] \tag{2.42}$$

The solution of Eq. (2.42) is easily found to be $Z_{ss}(\lambda) = e^{\langle v^2\rangle \lambda^2/2}$ with

$$\langle v^2 \rangle = 2 \lim_{N\to\infty} e_{ss}. \tag{2.43}$$

This implies that the steady state velocity distribution is a Gaussian with this variance. This is verified in Fig. 2.6. We note from Eq. (2.38) that the special case when $\epsilon = r_w$, the system follows the trivial dynamics of a set of independent particles.

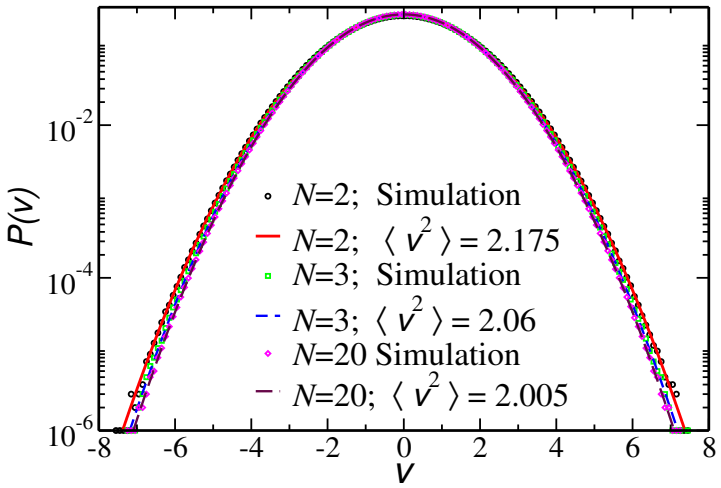

Figure 2.6: Steady state PDF for velocity for the model (Eq. (2.38)) for the parameter values $\epsilon = 0.3$, $r_w = 0.4$ and $\sigma^2 = 1$. The simulation results for number of particles $2, 3, 20$ are represented by the symbols, circle (black), square (green) and diamond (magenta) respectively. The Gaussians with the variance obtained from the cumulant expansion as explained in the Sec. 2.3.1, are shown as bold line (black), dashed line (blue), dashed and dotted line (indigo) in the same order. We can see that as N increases, the variance for the PDF asymptotically goes to 2, obtained from Eq. (2.43) for the given parameter values.

2.4.2. Model with binary collisions and external forcing occurring at different rates

We saw in the previous section (Sec. 2.4.1), the scenario where the mutual collisions and driving by wall collisions occur simultaneously. We found that the exact coupled evolution help us find

the steady state values, e_{ss} and Σ_{ss}. In the large N limit, e_{ss} reaches a finite value, but the correlations vanish as $O(1/N)$. We also saw that because of the linearity in the dynamics, the steady state velocity distribution has the Gaussian form. In the large N limit the variance is given by Eq. (2.43). We now consider a dynamics where at each time step, two particles picked randomly, either collide with each other with probability p or collide with the wall independently with probability $1-p$. The new velocities of the randomly chosen pair (i, j) for the new dynamics are given by,

$$\begin{aligned} v_i &= \alpha[\epsilon v_i^* + (1-\epsilon)v_j^*] + (1-\alpha)[-r_w v_i^* + \eta_i], \\ v_j &= \alpha[\epsilon v_j^* + (1-\epsilon)v_i^*] + (1-\alpha)[-r_w v_j^* + \eta_j], \end{aligned} \tag{2.44}$$

where α is a random number defined as before. Following the procedure in the earlier sections, we get the recursion relation Eq. (2.15) for energy and correlations with

$$\mathbf{R} = \begin{bmatrix} 1 - \frac{\left[4p\epsilon(1-\epsilon)+2(1-p)(1-r_w^2)\right]}{N} & \frac{2p\epsilon(1-\epsilon)}{N} \\ \\ \frac{8p\epsilon(1-\epsilon)}{N(N-1)} & 1 - \frac{\left[4p\epsilon(1-\epsilon)-2(1-p)(1-r_w)^2+4(N-1)(1-p)(1+r_w)\right]}{N(N-1)} \end{bmatrix} \tag{2.45}$$

and $C = [(1-p)\sigma^2/N, 0]^T$.

When $r_w = -1$ the eigenvalues of $\boldsymbol{R}$ become 1 and $1 - p(1-r^2)/(N-1)$, which clearly shows the absence of steady state. This should not be surprising because when $r_w = -1$, the Eq. (2.44) becomes Eq. (2.22), which is the model with collision and the diffusive driving occurring independently. The exact evolution has also been calculated (Eq. (2.24)) for the case showing the lack of steady state.

Further when $r_w \neq -1$, both the eigenvalues have their magnitudes less than unity which can be proved as follows. As the matrix $\boldsymbol{R}$ is a positive matrix, according to Perron-Frobenius theorem, it has a real positive eigenvalue (called Perron-Frobenius eigenvalue) such that the absolute value of other eigenvalue is strictly less than this, which is easy to show for a 2×2 matrix. As the complex eigenvalues of a real matrix always occur in conjugate pairs, the other eigenvalue of $\boldsymbol{R}$ should also be real. The Perron-Frobenius eigenvalue has another property which

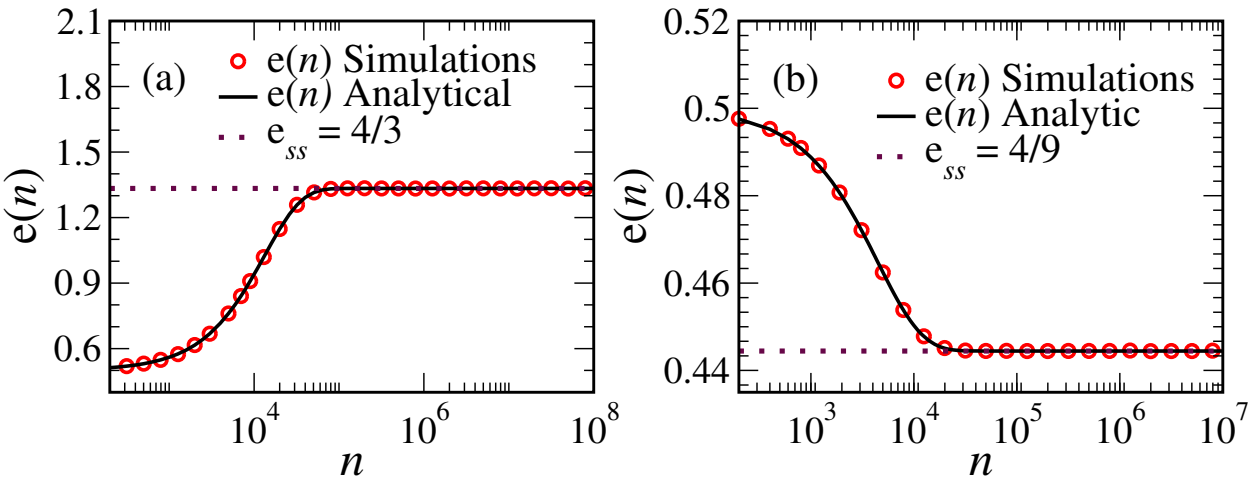

FIGURE 2.7: Existence of steady state for $r_w \neq -1$: Simulation (black circles) and analytical (red solid line) results for the evolution of e(n) calculated for the system with the dynamics Eq. (2.44) for $N = 5000$ with (a) $p = 1/2$, $\epsilon = 1/4$, $r_w = +1$, and $\sigma = 1$, (b) $p = 1/2$, $\epsilon = 1/4$, $r_w = 1/2$, and $\sigma = 1$. The steady state value is portrayed by the (magenta) dotted line

says that it is bounded from above (below) by the maximum (minimum) of the row sums of the matrix. From the explicit form of the above matrix it is immediately evident that both the row sums are less than unity for $-1 < r_w \leq 1$. Thus, both the eigenvalues are less than unity, in absolute value. Hence the system reaches a steady state (see Fig. 2.7). The steady state values of the energy (e_{ss}) and the correlation (Σ_{ss}) are explicitly calculated and are given by Eq. (2.46).

$$\begin{aligned} e_{ss} &= \frac{(\sigma^2/2)\left[2\epsilon(1-\epsilon) + \gamma(1-r_w^2) + 2(N-2)\gamma(1+r_w)\right]}{4\epsilon(1-\epsilon)(1-r_w^2) + \gamma(1-r_w^2)^2 + (N-2)(1+r_w)[4\epsilon(1-\epsilon) + 2\gamma(1-r_w^2)]}\,, \\ \Sigma_{ss} &= \frac{2\sigma^2\epsilon(1-\epsilon)}{4\epsilon(1-\epsilon)(1-r_w^2) + \gamma(1-r_w^2)^2 + (N-2)(1+r_w)[4\epsilon(1-\epsilon) + 2\gamma(1-r_w^2)]}\,, \end{aligned} \tag{2.46}$$

where, $\gamma = (1-p)/p$, which is the ratio of the injection to collision rates. For large N, Eq. (2.46) becomes,

$$e_{ss} = \frac{\gamma\sigma^2}{4\epsilon(1-\epsilon) + 2\gamma(1-r_w^2)} + O(N^{-1}) \tag{2.47}$$

and $\Sigma_{ss} = O(N^{-1})$. Consequently, one can neglect the steady state correlations Σ_{ss} for a large enough system.

Obtaining the velocity PDF in the steady state in this case is difficult unlike the previous dynamics where we found it to be Gaussian. In the interest of extracting the characteristics of

the PDF, we now derive the evolution equation for the MGF (Eq. (2.28)) to be satisfied by the dynamics.

2.4.2.1. The equation for the MGF

In the steady state, the correlations vanish, for $N \to \infty$. In this limit one can show that the Moment Generating Function (MGF) of the steady state velocity PDF, $Z(\lambda) = \langle \exp(-\lambda v) \rangle$ satisfies the equation:

$$Z(\lambda) = pZ(\epsilon\lambda)Z([1-\epsilon]\lambda) + (1-p)Z(r_w\lambda)f(\lambda), \tag{2.48}$$

This can be obtained using the definition of the MGF and Eq. (2.44), and considering the fact that in steady state the MGF does not vary with time. Also, for even velocity distribution $Z(-\lambda) = Z(\lambda)$ and $f(\lambda) = \exp(\lambda^2\sigma^2/2)$ for the Gaussian noise. Note that the MGF, $Z(\lambda) = 1 + \mathrm{e}\lambda^2 + \cdots$ in the limit $\lambda \to 0$.

2.4.2.2. Velocity distribution: near elastic Limit

The exact solution of Eq. (2.48) is rather difficult to obtain. But the equation can be used to calculate the velocity distribution function in the near-elastic limit. In order to obtain a steady state in this limit, one needs to inject energy in correspondingly small amplitude. In other words, one needs to consider along with $\epsilon \to 0$, the limits $r_w = (1-\theta) \to 1$ and $\sigma \to 0$, while keeping σ^2/ϵ and θ/ϵ fixed.

Taylor expanding the Eq. (2.48) up to first order in ϵ and θ, we obtain,

$$Z(\lambda) = pZ(0)[Z(\lambda) - \epsilon\lambda Z'(\lambda)] + (1-p)(1 + \frac{\lambda^2\sigma^2}{2})[Z(\lambda) - \theta\lambda Z'(\lambda)]. \tag{2.49}$$

Here $Z'(\lambda) = dZ(\lambda)/d\lambda$. Taking the limits as prescribed and rearranging, one gets

$$\frac{dZ}{d\lambda} = \lambda\Delta^2 Z(\lambda), \quad \text{where } \Delta^2 = \frac{\gamma\sigma^2/\epsilon}{2\big[1 + \gamma\theta/\epsilon\big]}. \tag{2.50}$$

Looking at Eq. (2.47), one finds that in the above limit $\langle v^2 \rangle \to \Delta^2$. Using the normalisation condition $Z(0) = 1$, the solution of Eq. (2.50) is easily obtained as, $Z(\lambda) = \exp(\lambda^2\Delta^2/2)$, which implies the Gaussian velocity distribution

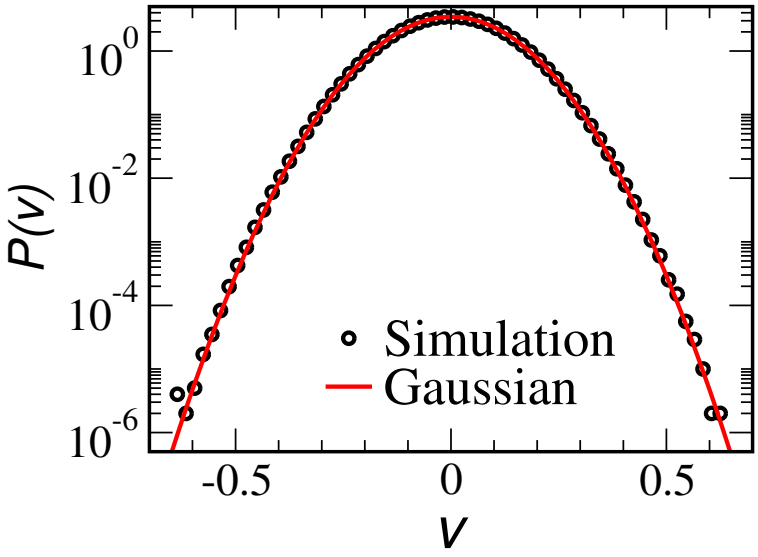

Figure 2.8: Simulation (black circles) and analytical (red solid line) results for steady state velocity PDF in the near-elastic and weak energy injection limit for $N = 100$ with $p = 0.5$, $\epsilon = 0.005$, $r_w = 0.99$, and $\sigma = 0.02$.

$$P(v) = \frac{1}{\sqrt{2\pi\Delta^2}} \exp\left(-\frac{v^2}{2\Delta^2}\right). \tag{2.51}$$

In Figure 2.8, a comparison of the above result with the direct simulation is shown.

2.4.2.3. The high energy Tail

We are not able to find the exact solution for the evolution equation (Eq. (2.48)) in general. But using the equation, one can obtain the behaviour of the tail of the distribution. Consider the situation $r_w = +1$. The Eq. (2.48) in this case becomes:

$$Z(\lambda) = \left[1 - (1-p)\ f(\lambda)\right]^{-1} p\, Z(\epsilon\lambda) Z([1-\epsilon]\lambda)\ . \tag{2.52}$$

One can recognize that this equation is same as the one for the MGF (Eq. (2.30)) in the 'pseudo steady state' obtained for the Maxwell gas with white noise forcing (Eq. (2.22)), which is also the present model with $r_w = -1$. As before (Sec. 2.3.2), the tail of the distribution is determined by the pole closest to the origin $\lambda_0 = \pm\sqrt{-2\ln(1-p)}/\sigma$, coming from the factor $[1-(1-p)\ f(\lambda)]^{-1}$ in Eq. (2.52). This again gives rise to exponential tail $P(v) \sim A(\epsilon) \exp(-|\lambda_0||v|)$. The coefficient, $A(\epsilon)$ is the same as calculated in Eq. (2.34). The comparison with numerical studies shows excellent agreement as shown in the Fig. 2.9.

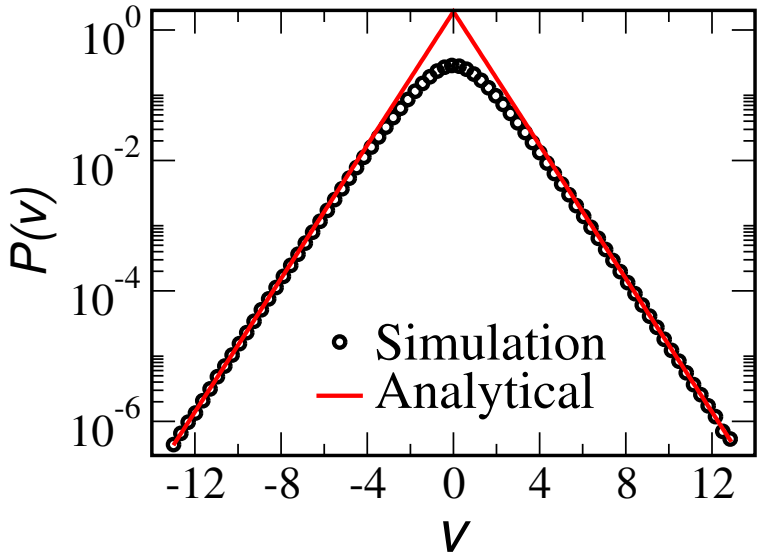

FIGURE 2.9: Simulation (black circles) and analytical (red solid line) results for steady state velocity distribution for $r_w = +1$. The other parameters are $N = 100$, $p = 0.5$, $\epsilon = 1/4$, and $\sigma = 1$.

As we have noticed, Eq. (2.48) is symmetric with respect to $r_w \leftrightarrow -r_w$. But this equation has been derived under the assumption of a steady state. Therefore for the case $r_w = -1$, it is valid *only* in the pseudo-steady state in which case one finds an exponential tail [4, 47–49], as described in Sec. 2.3.2.

For other values of r_w with $|r_w| < 1$, it is hard to obtain the accurate form of the high energy tails from direct simulations. But one can obtain $Z(\lambda)$ by numerically solving Eq. (2.48). Inverting $Z(\lambda)$, we obtain the probability distribution function $P(v)$. For convenience we use the characteristic function $Z_c(k) = Z(ik)$. We consider a special case of parameter values $\epsilon = 1/2$, $r_w = 1/2$ for which, Eq. (2.48) takes a simpler form,

$$Z_c(k) = pZ_c^2(k/2) + (1-p)Z_c(k/2)\exp(-k^2\sigma^2/2). \tag{2.53}$$

The equation (Eq. (2.53)) has the advantage that, in order to compute Z_c for any argument k, one only needs to know it's value at $k/2$. This 'linear' structure is very simple compared to 'tree structure' for a general set of parameter values. The above set of parameter values thus enables one to efficiently calculate $Z_c(k)$, starting with the initial condition $Z_c(k) = 1 - \mathrm{e}k^2$ for $k \ll 1$. The inverse Fourier transform of the obtained $Z_c(k)$, is then computed numerically to obtain the PDF, $P(v)$. This is shown in Fig. 2.10(c), along with that from the direct simulation. The numerically obtained $P(v)$ helps us to probe statistics of very large velocities unlike the direct

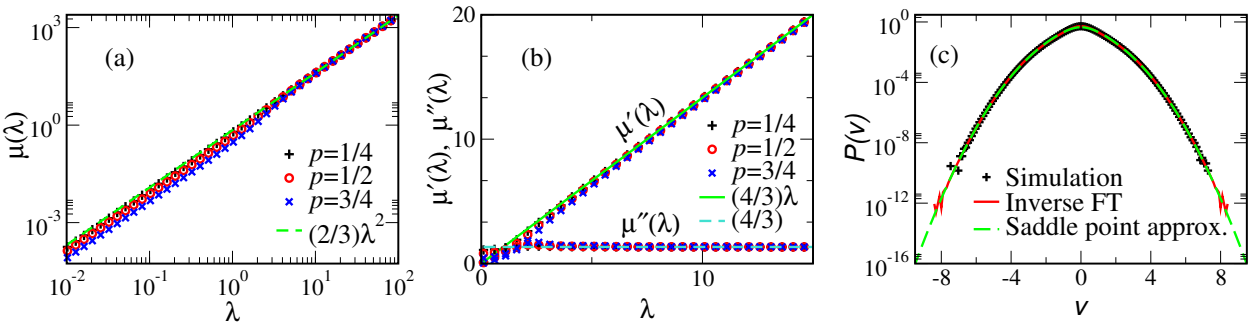

FIGURE 2.10: (a) $\mu(\lambda)$ for $\epsilon = 1/2$, and $r_w = 1/2$ for three different p. These curves asymptotically approach the function $(2/3)\lambda^2$, shown by the (green) dashed line. (b) The first and second derivatives of $\mu(\lambda)$ and their asymptotic values (green solid line and cyan dashed line respectively). The same symbols and colors are used for the same p values for both $\mu'(\lambda)$ and $\mu''(\lambda)$. (c) The velocity distribution for the dynamics Eq. (2.44) for $p = 1/2$, $\epsilon = 1/2$ and $r_w = 1/2$ from simulation (black "+") compared with results calculated from the exact inverse Fourier transform of $Z_c(k)$ (red solid line) as well as from the saddle point approximation (green dashed line), given by Eq. (2.59).

simulations. The tail thus obtained is observed to have a form $P(v) \sim \exp(-A \mid v \mid^{\alpha})$, with α gradually increasing (but < 2) as we go towards higher and higher the velocities.

The picture emerging from the numerical studies turns out to be useful in calculating the tail for a general set of parameter values. We know that $Z(\lambda)$ with the form $P(v) \sim \exp(-A \mid v \mid^{\alpha})$ is analytic if $\alpha > 1$. So if $Z(\lambda)$ is known, one could calculate the large deviation tail of the velocity distribution by the method of saddle point approximation as,

$$P(v) \approx \frac{\exp\left[\mu(\lambda^*) + \lambda^* v\right]}{\sqrt{2\pi|\mu''(\lambda^*)|}}\ , \tag{2.54}$$

where $\mu(\lambda) = \ln Z(\lambda)$ and $\lambda^*(v)$ is the saddle point which is implicitly given by the equation $\mu'(\lambda^*) = -v$. Now, if near the saddle point $\mu(\lambda) \sim b|\lambda|^{\beta}$, one finds $\lambda^* = -\text{sign}(v)\left[|v|/(b\beta)\right]^{1/(\beta-1)}$ and the velocity distribution would have a form

$$P(v) \sim \exp(-A \mid v \mid^{\alpha}) \tag{2.55}$$

with the constants A and α depending on b and β as,

$$\alpha = \frac{\beta}{(\beta-1)} \text{ and } A = b(\beta-1)(b\beta)^{-\alpha}. \tag{2.56}$$

Therefore, if we substitute the ansatz $Z(\lambda) \sim \exp(b|\lambda|^{\beta})$ with $\beta > 1$ in Eq. (2.48), we get

$$\exp(b|\lambda|^{\beta}) \sim \left[p\exp(b|\lambda|^{\beta}[\epsilon^{\beta} + (1-\epsilon)^{\beta}]) + (1-p)\exp(b|\lambda|^{\beta} r_w^{\beta} + \lambda^2\sigma^2/2)\right]. \tag{2.57}$$

Since $\epsilon^\beta + (1-\epsilon)^\beta < 1$ for $\epsilon \in (0,1)$ and $\beta > 1$, the first term on the RHS of Eq. (2.57) becomes negligible compared to the LHS for large $|\lambda| \sim |v|^{1/(\beta-1)}$. Thus, comparing the exponent of the LHS to that of the second term on the RHS, we get $\beta = 2$ and $b = (\sigma^2/2)(1-r_w^2)^{-1}$. This implies the Gaussian tail

$$P(v) \approx \sqrt{\frac{1-r_w^2}{2\pi\sigma^2}}\, \exp\left[-\frac{v^2}{2\sigma^2}(1-r_w^2)\right]. \tag{2.58}$$

Therefore, one finds that the high energy tail is determined, not by the inelastic collisions amongst the particles, but the collisions of the particles with the "wall".

In order to verify the above result, we calculate numerically $Z(\lambda)$ from Eq. (2.48) for the parameter values $\epsilon = 1/2$, $r_w = 1/2$, and $\sigma = 1$, for which $b = 2/3$. It is clear from Fig. 2.8(a) that $\mu(\lambda) \sim b\lambda^2$ for large λ. From $\mu(\lambda)$, one can numerically compute $\mu'(\lambda)$ and $\mu''(\lambda)$. Now, each value of λ corresponds to a velocity $v = -\mu'(\lambda)$, whose PDF, under the saddle point approximation, is numerically obtained using

$$P(v = -\mu'(\lambda)) \approx \frac{1}{\sqrt{2\pi\mu''(\lambda)}} \exp\big[\mu(\lambda) - \lambda\mu'(\lambda)\big]. \tag{2.59}$$

Figure 2.8(c) compares this with the simulation result as well as with the distribution obtained from the exact numerical inverse Fourier transform of $Z_c(k)$.

2.4.2.4. The moments

The form of the steady state distribution can also be verified from the behaviour of the moments. Note that the velocity distribution being even, all the odd moments vanish and one needs to consider only the even moments to characterize the steady state. Assuming Eq. (3.31) for all v, one can compute the moments, which gives,

$$\langle v^{2n}\rangle = (\sigma^2/2)^n (1-r_w^2)^{-n} (2n)!/n!. \tag{2.60}$$

The result is certainly not valid for small n, as easily illustrated by comparing the $n = 1$ case with 2e from Eq. (2.47). But for large n, one expects to agree with this result which can be verified by looking whether the ratio between two successive even moments $\langle v^{2n}\rangle/\langle v^{2n-2}\rangle \sim 2\sigma^2(1-r_w^2)^{-1}n$ for large n.

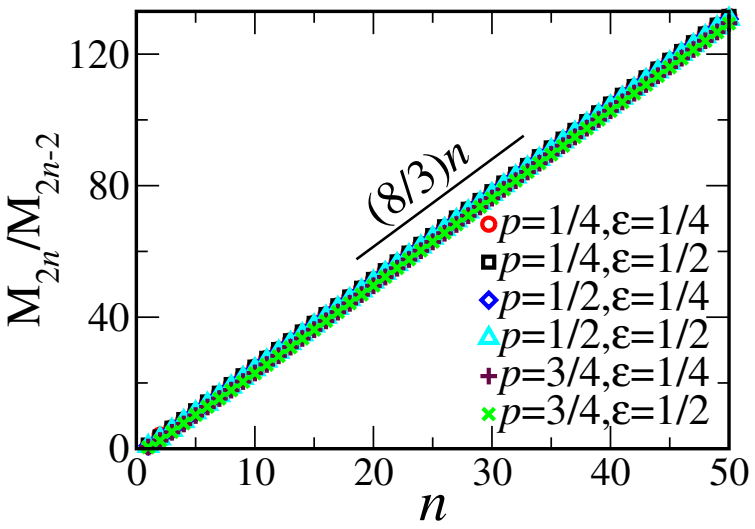

Figure 2.11: The ratios of successive even moments M_{2n}/M_{2n-2} calculated from Eq. (2.62) for $r_w = 1/2$ and $\sigma = 1$.

The moments for any n satisfy the relation given below (Eq. (2.61)), as can be obtained easily from the dynamics (Eq. (2.44)).

$$\langle v^{2n}\rangle = p\langle(\epsilon v_i + (1-\epsilon)v_j)^{2n}\rangle + (1-p)\langle(r_w v_i + \eta_i)^{2n}\rangle. \tag{2.61}$$

Expanding binomially and averaging each term in the expansion, one obtains the $2n$-th moment in terms of the lower ones as shown below.

$$\left[1-\epsilon^{2n}-(1-\epsilon)^{2n}+\gamma\left(1-r_w^{2n}\right)\right]M_{2n} = \sum_{m=1}^{n-1}\binom{2n}{2m}\epsilon^{2m}(1-\epsilon)^{2n-2m}M_{2m}M_{2n-2m} + \gamma\sum_{m=0}^{n-1}\binom{2n}{2m}r_w^{2m}M_{2m}\frac{(2n-2m)!}{(n-m)!}\left(\frac{\sigma^2}{2}\right)^{n-m} \tag{2.62}$$

with $M_0 = 1$. We also use the expression, $\langle\eta^{2n}\rangle = \left(\sigma^2/2\right)^n (2n!/n!)$ as η is a Gaussian noise with the variance σ^2. Using Eq. (2.62) we compute the moments recursively. Figure 2.11 confirms that $M_{2n}/M_{2n-2} \to 2\sigma^2(1-r_w^2)^{-1}n$ for large n.

2.4.2.5. Weakly interacting limit

An interesting situation in which one can perturbatively compute the PDF will be described next. This is when the system is very dilute so that any particle very rarely sense another particle and

each is driven independently. The perturbative expansion is done in terms of p, the probability for inelastic collisions, which is the small parameter in the weakly interacting limit.

The equation (Eq. (2.48)) for $Z(\lambda)$ in the steady state can also be written as:

$$Z(\lambda) = Z(r_w\lambda)f(\lambda) + p\left[Z(\epsilon\lambda)Z((1-\epsilon)\lambda) - Z(r_w\lambda)f(\lambda)\right]. \tag{2.63}$$

We can use this relation for $Z(\lambda)$ recursively, leading to an infinite sum of the following form (up to first order in p):

$$Z(\lambda) = g_\infty(\lambda)Z(0) + p\sum_{q=0}^{\infty}\left[Z(\epsilon r_w^q\lambda)Z((1-\epsilon)r_w^q\lambda) - Z(r_w^{q+1}\lambda)f(r_w^q\lambda)\right]g_q(\lambda) \tag{2.64}$$

where,

$$g_\infty(\lambda) = \prod_{q=0}^{\infty} f(r_w^q\lambda) \tag{2.65}$$

$$g_q(\lambda) = \begin{cases} \prod_{s=0}^{q-1} f(r_w^s\lambda) \text{ for } q > 0 \\ 1 \text{ for } q = 0 \end{cases} \tag{2.66}$$

Considering $Z(0) = 1$ from the normalisation of the PDF and taking terms upto $O(p)$ implies:

$$\begin{aligned} Z(\lambda) &= g_\infty(\lambda) + p\sum_{q=0}^{\infty}\left[\prod_{q'=0}^{\infty} f(r_w^{q'+q}\epsilon\lambda)\prod_{q''=0}^{\infty} f(r_w^{q''+q}(1-\epsilon)\lambda) - \prod_{q'=0}^{\infty} f(r_w^{q'+q+1}\lambda)f(r_w^q\lambda)\right]g_q(\lambda) \\ &= g_\infty(\lambda) + p\sum_{q=0}^{\infty}\left[g_\infty(\epsilon r_w^q\lambda)g_\infty((1-\epsilon)r_w^q\lambda) - g_\infty(r_w^{q+1}\lambda)f(r_w^q\lambda)\right]g_q(\lambda). \end{aligned} \tag{2.67}$$

Now let us take the specific example with normalised Gaussian distribution with variance σ^2 which implies $f(\lambda) = \exp[\frac{\lambda^2\sigma^2}{2}]$. Substituting this in the expression (Eq. (2.65)), we get:

$$g_\infty(\lambda) = \prod_{q=0}^{\infty}\exp\left[\frac{\lambda^2\sigma^2 r_w^q}{2}\right] = \exp\left[\frac{\lambda^2\sigma^2}{2(1-r_w^2)}\right],$$

$$\begin{aligned} g_\infty(\epsilon r_w^q\lambda) &= \exp\left[\frac{\lambda^2\sigma^2\epsilon^2 r_w^{2q}}{2(1-r_w^2)}\right], \\ g_\infty((1-\epsilon)r_w^q\lambda) &= \exp\left[\frac{\lambda^2\sigma^2(1-\epsilon)^2 r_w^{2q}}{2(1-r_w^2)}\right], \\ g_\infty(r_w^{q+1}\lambda) &= \exp\left[\frac{\lambda^2\sigma^2(1-\epsilon)^2 r_w^{2q}}{2(1-r_w^2)}\right], \end{aligned} \tag{2.68}$$

and

$$g_q(\lambda) = \prod_{s=0}^{q-1} \exp\left[\frac{\lambda^2\sigma^2 r_w^{2s}}{2}\right] = \exp\left[\frac{\lambda^2\sigma^2}{2}\left(\frac{1-r_w^{2q}}{1-r_w^2}\right)\right] \quad \forall\ q.$$

substituting the above relations in to Eq. (2.67) we get:

$$Z(\lambda) = \exp\left[\frac{\lambda^2\sigma^2}{2(1-r_w^2)}\right] + p\sum_{q=0}^{\infty}\left\{\exp\left[\frac{\lambda^2\sigma^2((2\epsilon^2-2\epsilon)r_w^{2q}+1)}{2(1-r_w^2)}\right] - \exp\left[\frac{\lambda^2\sigma^2}{2(1-r_w^2)}\right]\right\}. \tag{2.69}$$

The velocity PDF can now be obtained by inverting, Eq. (2.69):

$$P(v) = \sqrt{\frac{(1-r_w^2)}{2\pi\sigma^2}}\exp\left[\frac{-v^2(1-r_w^2)}{2\sigma^2}\right] + p\sum_{q=0}^{\infty}\left\{\sqrt{\frac{(1-r_w^2)}{2\pi\sigma^2((2\epsilon^2-2\epsilon)r_w^{2q}+1)}}\exp\left[\frac{-v^2}{2\sigma^2}\frac{(1-r_w^2)}{((2\epsilon^2-2\epsilon)r_w^{2q}+1)}\right] - \sqrt{\frac{(1-r_w^2)}{2\pi\sigma^2}}\exp\left[\frac{-v^2(1-r_w^2)}{2\sigma^2}\right]\right\}. \tag{2.70}$$

This function has been plotted (Fig. 2.12) for the parameter value $p \sim 0.1$ and is compared with simulation.

We can see that the distribution is made up of an infinite sum of Gaussians as given by the expression in Eq. (2.70). As we go near to the tail of the distribution to higher and higher velocities, the contributions from all the $q \neq 0$ terms vanish asymptotically. Thus the distribution tends to a Gaussian, given by the first term in the series solution (Eq. (2.70)) for the PDF, as we go to larger and larger velocities. This observation is true for any set of values for the parameters, with the constraint that p is very small.

2.4.2.6. Exact steady state when driven with Cauchy noise

Interestingly, an exact solution for the PDF of velocity in the steady state is possible for this model (Eq. (2.44)). This happens if we take the noise distribution to be Cauchy distribution given by the form:

$$f(ik) = \exp\left(-a \mid k \mid\right) \tag{2.71}$$

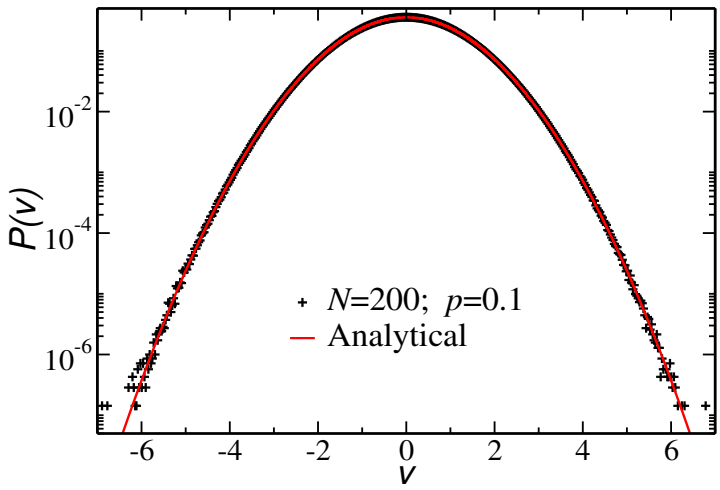

FIGURE 2.12: PDF of velocity in steady state for 200 particle system in the weakly interacting limit of the model Eq. (2.44) with $\epsilon = 1/4$, $r_w = 1/2$. The analytical result obtained by perturbative expansion with $p = 0.1$ plotted as a solid line (red) is compared with the simulation results represented by '+' symbol (black).

As this does not have a well defined variance, we cannot see the total energy of the system evolving to a steady state value in the simulation. Instead, we can see the velocity distributions eventually reaching to a time invariant one, which is itself another Cauchy distribution. We can see this analytically. The evolution equation for $Z_c(k) = Z(ik)$ (see Eq. (2.48)) in this case becomes,

$$Z_c(k) = pZ_c(\epsilon k)Z_c((1-\epsilon)k) + (1-p)Z_c(r_w k)\exp(-a \mid k \mid), \tag{2.72}$$

where $\exp(-a \mid k \mid)$ is the characteristic function for the Cauchy distribution with mean 0. As an ansatz, considering that $Z_c(k) = \exp(-b \mid k \mid)$ satisfies the Eq. (2.72), implies,

$$\exp(-b \mid k \mid) \;=\; p\exp(-b \mid k \mid (\epsilon + 1 - \epsilon)) + (1-p)\exp(-(br_w + a) \mid k \mid), \tag{2.73}$$

which on rearrangement becomes,

$$(1-p)\exp(-b \mid k \mid) \;=\; (1-p)\exp(-(br_w + a) \mid k \mid). \tag{2.74}$$

This implies that the steady state PDF is Cauchy distributed, $\exp(-b \mid k \mid)$ with $b = a/(1-r_w)$. In real space, this is represented by

$$P(v) = \frac{b}{\pi}\frac{1}{b^2 + v^2}, \tag{2.75}$$

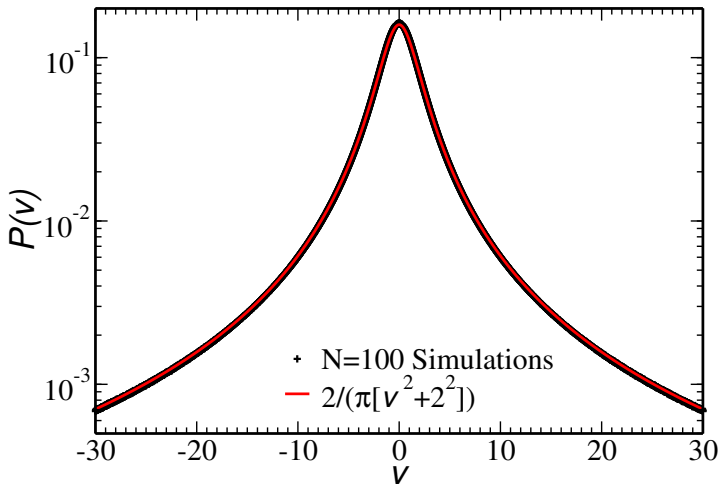

Figure 2.13: The plot shows the steady state PDF of velocity for the model Eq. (2.44) with the parameter values $p = 1/2,\ \epsilon = 1/4,\ r_w = 1/2$ with the driving noise taken from a Cauchy distribution with the parameter $a = 1$. The '+' symbol (black) represents the simulation data. The analytical prediction is plotted as the solid line (red).

with b given above. Note that this result is independent of the rate parameter p and the coefficient of restitution r of the inter-particle collisions. It only depends on the coefficient of restitution for the wall-particle collision r_w and the noise parameter a. The plot (Fig. 2.13) shows the simulation done with the parameters $p = 1/2,\ \epsilon = 1/4,$ and $r_w = 1/2$ with the noise parameter $a = 1$ for the Cauchy distribution. The predicted distribution has $b = 2$.

2.5. Discussion and outlook

In order to understand the observed inconsistencies in the steady state velocity distributions of inelastic gases, we considered a discrete time model of inelastic Maxwell gas, evolving via mutual collision and driving. We observed that even though the BBGKY-type hierarchy of equations describing the evolution of the distribution functions, does not close, the evolution equations of the variance and two-point velocity correlation close, forming a coupled recursion relation between the two. This does not require any assumptions like the molecular chaos hypothesis.

The exact coupled relations enable us to calculate the evolution of energy and two-point correlations exactly. Using this, we find that the conventionally used white-noise (diffusive)

driving does not serve to be a good model to study driven steady states as there is no steady state for the system under the driving. This happens due to the fact that the collisions are not able to compensate for the increase in energy due to driving, and causes the energy of the system to increase linearly with time-steps. Though our studies are for the Maxwell model we find that this is generically the case with hard sphere gases also.

An alternate model of driving mimicking the driving caused by wall collisions, settles the issue of heating. With the help of the recursion relation for the moments of the PDF of particle velocities, the high-energy tail of the PDF is found to have a Gaussian form in the steady state. We also observe that our model has another non-trivial steady state if the noise in the driving is taken from a Cauchy distribution, with the velocity PDF being a Cauchy distribution which has a different parameter value.

The results obtained in this chapter is valid for the Maxwell gas with discrete time evolution. One can extend this to a continuous time model in which the collisions and driving occur with certain rates. This will ensure whether the results obtained for the discrete model is general and not specific to the particular dynamics. We will do this in the next chapter.

3

Inelastic Maxwell gas with continuous time dynamics

3.1. Introduction

Motivated by the universality in equilibrium gases, analytical as well as experimental studies proposed certain universal form for the velocity distribution in driven steady states of inelastic gases. But the numerical and some of the experimental studies were not in agreement with this observation, summoning a closer look at these systems.

In the second chapter, we studied a mean field model of inelastic gas called Maxwell gas evolving in discrete steps. For the model, we found an exact closure in the evolution equations of variance and two-point correlation function of the velocity of the constituent particles. This enabled us to understand the time dependent properties of these quantities. An interesting observation

followed: the Maxwell gas with diffusive driving does not keep the system in a steady state. We also found numerically that this is the case for hard sphere gases too. As the universal tail was observed for the analytical model of a hard sphere system with diffusive driving [25], it should not correspond to a physical steady state.

One can ask whether the above observation is particular to the discrete model or it is generic. This is not very explicit from our analysis, as the method differs from the kinetic theory calculations usually done for continuous time systems [4, 25, 33]. In this chapter, we address this question by studying a Maxwell model evolving in continuous time, where collisions and driving happen with certain rates. Using a method based on kinetic theory, we see that the above observations are true in the continuous time model also.

The continuous time model introduced here, has another significance in connection with real systems. In the experimental studies of driven granular systems, the driving is caused by the collisions of the particles with the vibrating walls of the container. Like inter-particle collisions, the wall-particle collisions also occur as discrete events in time, with finite change in particle velocities. In contrast, the typical analytical models employ continuous driving schemes like diffusive [25] or Ornstein-Uhlenbeck process [4, 33, 46]. We propose that the model that is introduced here is a better scheme of driving in the sense that the driving is taken to be a point process in time with a rate associated with it.

A brief outline follows next which is meant for a reader who is not interested to go through the details.

3.2. Outline

In this chapter we ask the question, whether the results obtained for the Maxwell gas with discrete time dynamics remain valid for the one evolving in continuous time. We show for the latter that one can derive closed set of equations for the variance and the two-point correlation directly from the hierarchy of equations for the distribution functions. The exact equations make it possible to know whether a system goes to steady state or not, when driven. Further, we find that an exact mapping exists between the discrete and the continuum models which enables us to obtain the high-energy tail of the velocity distribution for the continuous time model.

The system of our interest consists of N particles of unit mass with scalar velocity. Following a continuous time dynamics the system evolves as follows: each pair of particles collide with each other with rate $g\tau_c^{-1}$, and each particle is driven independently with rate $g\tau_w^{-1}$ as it collides with the vibrating wall. The term g can in general depend on time. For the Maxwell model it is usual to assume g to be proportional to the typical velocity of the particles. $g = 1$ corresponds to a time independent rate.

Considering the rules of collision and driving same as in the discrete model, we derive the evolution equation for the 1-particle distribution function $f_1(u_1, t)$. This is found to depend on the 2-particle distribution function $f_2(u_1, u_2, t)$ which in turn depends on the 3-particle distribution function $f_3(u_1, u_2, u_3, t)$ and so on. This results in hierarchical set of relations. We find that a closed set of equations can be constructed from this hierarchy, in terms of the variance $\Sigma_1(t)$ and the two-point correlation function $\Sigma_2(t)$, which are derived from the set of distribution functions. The closed coupled equations can be represented as a matrix evolution. Computation of the time evolution of $\Sigma_1(t)$ and $\Sigma_2(t)$ can be done exactly in the case of $g = 1$. When $g = \Sigma_1^{1/2}(t)$, one can do this only numerically due to non-linear nature of evolution.

However, the steady state characteristics are independent of the values of g. From the eigenvalues of the evolution matrix, we find that the system goes to a steady state when the coefficient of restitution of the wall-particle collision, $r_w \neq -1$. From the steady state values obtained analytically, we find that the correlations vanish in the thermodynamic limit. This helps one to construct an equation for the moment generating function for the velocity PDF in the steady state. The exact mapping of the equation with that of the discrete counterpart, shows that the continuous time system also have the same high energy tail as the former.

We find that the Ornstein-Uhlenbeck driving is a special case of this model. This makes it possible to obtain the exact tail behaviour of the velocity distribution of an inelastic Maxwell gas in a steady state when driven by an Ornstein-Uhlenbeck process. Thus our work compliments the previous studies [4, 33, 46], where the PDF of the velocity is calculated as a series expansion around a Gaussian distribution with the variance proportional to the average energy of the system which captures the behaviour in the typical energy scale. From the exact evolution equation one can predict the existence of steady states in different parameter regimes of the system. Particularly, we show the absence of a steady state for a continuous time system driven by purely

diffusive driving, which is a special case of the Ornstein-Uhlenbeck process.

The structure of the chapter is as follows. First, we review (Sec. 3.3) some of the aspects and important results of the model with discrete time dynamics which will facilitate the analysis of the continuous time model. For a slightly different driving scheme, we calculate for the model the exact evolution equation of the variance and the two-point correlation function as well as their steady state values. Using this we construct the equation for the MGF of the steady state velocity PDF. Later we introduce (Sec. 3.4) the continuous time Maxwell model. From the hierarchy of distribution functions we derive the closed set of equations again in terms of the variance and the correlation function. In Sec. 3.4.1, we illustrate how the choice of g determines the time dependent characteristics by considering a system of cooling Maxwell gas in a box. In Sec. 3.4.2, we probe the steady state properties. We construct the equation for the MGF in the steady state and describe the exact mapping of this with that of the discrete model. Finally we present (Sec. 3.5) a special limit at which the mechanism of driving becomes an Ornstein-Uhlenbeck driving. We end the chapter with concluding remarks (Sec. 3.6).

3.3. Maxwell gas with discrete time dynamics

In the previous chapter, we studied a system with N particles of unit mass, which evolves in discrete time steps. Each particle has a scalar velocity v_i with $i = 1, 2..N$ associated with it. During each time step, a pair of particles chosen randomly [out of $N(N-1)/2$ pairs], either collide inelastically with probability p or they are driven with probability $(1-p)$. In order to illustrate the mapping with the continuous time model (Sec. 3.4), we consider a slight variant of this model. Instead of driving independently a randomly chosen pair, one can assume that with probability $(1-p)$ only a single particle is driven. This change does not alter any qualitative behaviour of the system. The probability p is assumed to be constant over time, as in [47]. This is unlike the Maxwell model with the rate of collisions proportional to the root mean square velocity at the time [38]. But the steady state properties are unchanged even if the collision rates/probabilities are taken to be constant over time, while making the analysis relatively simpler.

The change in velocities of the pair (i, j) due to collision satisfies the equation,

$$\begin{aligned} v_i &= \epsilon v_i^* + (1-\epsilon) v_j^*, \\ v_j &= (1-\epsilon) v_i^* + \epsilon v_j^*, \end{aligned} \tag{3.1}$$

where $\epsilon = (1-r)/2$, with r the restitution coefficient. As before, (v_i^*, v_j^*) and (v_i, v_j) are the pre and postcollision velocities respectively. The driving is due to particle's (labelled 'i') collision with the wall which changes its velocity to,

$$v_i = -r_w v_i^* + \eta, \tag{3.2}$$

with r_w the coefficient of restitution of the wall-particle collision, and η a Gaussian noise with variance σ^2 and mean zero. Note that for a mathematical model of driven dissipative system the above equations are well-defined over a range $\{r, r_w\} \in [-1, 1]$.

For the above dynamics, an exact recursion relation gives the evolution of the variance $\Sigma_1(n)$ and the two-point correlation $\Sigma_2(n)$ (denoted as $\Sigma(n)$ in the previous chapter), which are defined respectively as,

$$\begin{aligned} \Sigma_1(n) =& (1/N) \sum_{i=1}^{N} \langle v_i^2(n) \rangle, \\ \Sigma_2(n) =& 1/[N(N-1)] \sum_{i \neq j} \langle v_i(n) v_j(n) \rangle. \end{aligned} \tag{3.3}$$

In abstract form, this is represented as,

$$X_n = \mathbf{R}_d X_{n-1} + C_d \tag{3.4}$$

where

$$X_n = \begin{bmatrix} \Sigma_1(n) \\ \\ \Sigma_2(n) \end{bmatrix}, \qquad C_d = \begin{bmatrix} (1-p)\frac{\sigma^2}{N} \\ \\ 0 \end{bmatrix},$$

and

$$\mathbf{R}_d = \begin{bmatrix} 1 - \frac{\left[4p\epsilon(1-\epsilon) + (1-p)(1-r_w^2)\right]}{N} & \frac{4p\epsilon(1-\epsilon)}{N} \\ \\ \frac{4p\epsilon(1-\epsilon)}{N(N-1)} & 1 - \frac{[4p\epsilon(1-\epsilon) + 2(N-1)(1-p)(1+r_w)]}{N(N-1)} \end{bmatrix}. \tag{3.5}$$

Consider the case $r_w = -1$. As before, one finds that one of the eigenvalues of $\mathbf{R}_d$ is unity. Consequently, the variance and the two-point correlation eventually increase linearly with number of time-steps n. Therefore, the system does not have a steady state for $r_w = -1$. For $-1 < r_w \leq 1$, Perron-Frobenius theorem guarantees that both the eigenvalues of $\mathbf{R}_d$ are less than unity and the system reaches a steady state. The steady state values of the variance and the two-point correlation function, can be calculated as

$$\Sigma_1^{\rm ss} = \frac{\sigma^2\big[4\epsilon(1-\epsilon) + 4\gamma(1+r_w)(N-1)\big]}{4\epsilon(1-\epsilon)(1-r_w^2) + 2(1+r_w)(N-1)\big[4\epsilon(1-\epsilon) + 2\gamma(1-r_w^2)\big]}\ , \tag{3.6a}$$

$$\Sigma_2^{\rm ss} = \frac{\sigma^2 4\epsilon(1-\epsilon)}{4\epsilon(1-\epsilon)(1-r_w^2) + 2(1+r_w)(N-1)\big[4\epsilon(1-\epsilon) + 2\gamma(1-r_w^2)\big]}\ , \tag{3.6b}$$

where $\gamma = (1-p)/(2p)$. In the limit $N \to \infty$, the steady-state variance, $\Sigma_1^{\rm ss}$ becomes independent of N,

$$\Sigma_1^{\rm ss} = \frac{2\gamma\sigma^2}{4\epsilon(1-\epsilon) + 2\gamma(1-r_w^2)}, \tag{3.7}$$

while the two-point correlation function $\Sigma_2^{\rm ss}$ vanishes as $O(N^{-1})$. Hence in large N limit, the equation satisfied by the steady-state single-particle probability distribution closes. The MGF ($Z(\lambda) = \langle \exp(-\lambda v)\rangle$) of the steady state velocities can be shown to satisfy the equation

$$Z(\lambda) = qZ(\epsilon\lambda)Z([1-\epsilon]\lambda) + (1-q)Z(r_w\lambda)f(\lambda), \tag{3.8}$$

where $q = 2p/(1+p)$and $f(\lambda) = \exp(\lambda^2\sigma^2/2)$. As before, we have used the property, $Z(-\lambda) = Z(\lambda)$ for an even distribution. We will see that the Eq. (3.8) provides a mapping with the continuous system.

3.4. Maxwell gas with continuous time dynamics

Looking into real systems, what we observe is that the inter-particle collisions happen as discrete events in continuous time. A natural way to model this is by considering the collisions as uncorrelated point processes in time. If the driving is caused by collision of a particle with the wall, this also should be treated in a similar way. Let us consider a Maxwell gas of N unit mass particles with scalar velocity evolving with such a dynamics. Now each pair of particles collide at a rate $g\tau_c^{-1}$ according to the collision rule specified before Eq. (3.1). Similarly the driving is

done on each particle with a rate $g\tau_w^{-1}$ with the rule Eq. (3.2). Here g takes care of any time dependence on the rates. A class of Maxwell model considers the collision rates proportional to the typical velocity [38]. This is achieved in our model by setting $g = \Sigma_1^{1/2}$. Also, one can analyse the simpler situation of time independent rates with $g = 1$. As will be seen, the two different dynamics only change the time dependent characteristics (see Sec. 3.4.1).

Let $u_i(t)$ denote the velocity of the i-th particle at time t. One can define a set of velocity distribution functions for the system,

$$f_1(v_1, t) \equiv \sum_{i=1}^{N} \langle \delta(v_1 - u_i(t)) \rangle, \tag{3.9a}$$

$$f_2(v_1, v_2, t) \equiv \sum_{i=1}^{N} \sum_{j \neq i}^{N} \langle \delta(v_1 - u_i(t)) \delta(v_2 - u_j(t)) \rangle, \tag{3.9b}$$

$$f_3(v_1, v_2, v_3, t) \equiv \sum_{i=1}^{N} \sum_{j \neq i}^{N} \sum_{k \neq i,j}^{N} \langle \delta(v_1 - u_i(t)) \delta(v_2 - u_j(t)) \times \delta(v_3 - u_k(t)) \rangle, \tag{3.9c}$$

and so on. The evolution equations of the above distributions form a hierarchy with $f_1(v_1, t)$ depending on $f_2(v_1, v_2, t)$, which in turn depends on $f_3(v_1, v_2, v_3, t)$ and so on. The first two of these equations are given by,

$$\begin{aligned} \frac{\partial}{\partial t} f_1(v_1, t) &= g\tau_c^{-1} \left[\int dv_2 \overline{T}(v_1, v_2) f_2(v_1, v_2, t) \right] \\ &\quad + g\tau_w^{-1} \left[\int dv_1^* f_1(v_1^*, t) \langle \delta \left(v_1 - [-r_w v_1^* + \eta_1] \right) \rangle_{\eta_1} - f_1(v_1, t) \right], \end{aligned} \tag{3.10a}$$

$$\begin{aligned} \frac{\partial}{\partial t} f_2(v_1, v_2, t) &= g\tau_c^{-1} \left[\overline{T}(v_1, v_2) f_2(v_1, v_2, t) + \int dv_3 \left[\overline{T}(v_1, v_3) + \overline{T}(v_2, v_3) \right] f_3(v_1, v_2, v_3, t) \right] \\ &\quad + g\tau_w^{-1} \left[\int dv_1^* f_2(v_1^*, v_2, t) \langle \delta \left(v_1 - [-r_w v_1^* + \eta_1] \right) \rangle_{\eta_1} \right. \\ &\quad \left. + \int dv_2^* f_2(v_1, v_2^*, t) \langle \delta \left(v_2 - [-r_w v_2^* + \eta_2] \right) \rangle_{\eta_2} - 2 f_2(v_1, v_2, t) \right]. \end{aligned} \tag{3.10b}$$

The evolution equations account for the change in the distributions due to the two kinds of events. The first square bracket on the RHS of Eqs. (3.10a) and (3.10b) gives the contribution from the mutual collision between the particles. Here $\overline{T}(v_1, v_2)$ is an operator defined as, $\overline{T}(v_1, v_2) S(v_1, v_2) = r^{-1} S(v_1^*, v_2^*) - S(v_1, v_2)$, and acts only on the two variables designated by its arguments. The second square brackets on the RHS are the contribution from driving, where the

angular brackets refer to the averaging over the noise distribution. To break the hierarchy arising in similar equations, various approximation schemes have been used in the past [33, 51]. But we show that it is possible to obtain a closed set of coupled equations for the variance and the two-point correlation function without employing any such approximation. The solution of these coupled equations can be used to determine the situations at which one can close the hierarchy for the single-particle distribution function in the $N \to \infty$ limit.

The variance and the two-point correlation function can be obtained from the distribution functions as

$$\Sigma_1(t) = \frac{1}{N}\int dv_1 v_1^2 f_1(v_1, t), \tag{3.11a}$$

$$\Sigma_2(t) = \frac{1}{N(N-1)}\int dv_1 dv_2 v_1 v_2 f_2(v_1, v_2, t). \tag{3.11b}$$

The evolution equation for the two can be derived as follows: Multiplying Eq. (3.10a) by v_1^2 and then integrating over v_1, similarly multiplying Eq. (3.10b) by $v_1 v_2$ and integrating over both v_1 and v_2, yields the equations for $\Sigma_1(t)$ and $\Sigma_2(t)$ respectively. This results in a set of closed equations for $X(t) = [\Sigma_1(t), \Sigma_2(t)]^T$ with the form,

$$\frac{dX(t)}{dt} = g\big[\mathbf{R}X(t) + C\big], \tag{3.12}$$

where

$$\mathbf{R} = \begin{bmatrix} -\left(\frac{2\epsilon(1-\epsilon)(N-1)}{\tau_c} + \frac{1-r_w^2}{\tau_w}\right) & \frac{2\epsilon(1-\epsilon)(N-1)}{\tau_c} \\ \\ \frac{2\epsilon(1-\epsilon)}{\tau_c} & -\left(\frac{2\epsilon(1-\epsilon)}{\tau_c} + \frac{2(1+r_w)}{\tau_w}\right) \end{bmatrix}. \tag{3.13}$$

and $C = [\tau_w^{-1}\sigma^2, 0]^T$. Note that Eq. (3.12) is exact and no approximation is made in arriving at it from Eq. (3.10).

When $g = 1$, one can calculate the exact evolution of $X(t)$ from Eq. (3.12). However, when $g = \Sigma_1^{1/2}$, the equation becomes non-linear making the analysis difficult. The value of g changes the time dependent properties of the system as can be seen evidently in the case of a cooling system.

3.4.1. Homogeneous cooling state

From Eq. (3.12), one can obtain freely cooling behaviour of the system in the absence of driving. To do this we set $C = 0$ (i.e., $\sigma = 0$) in Eq. (3.12), which mimics a system in a static box. We first consider the linear case $g = 1$ and afterwards consider the case where $g = \Sigma_1^{1/2}$.

3.4.1.1. The linear case: $g = 1$

For $g = 1$, the equation (3.12) is linear and can be solved exactly. For $C = 0$ the solution has the form,

$$\Sigma_1(t) = \frac{\Sigma_1(0)}{\lambda_+ - \lambda_-}\left[(R_{22} - \lambda_-)e^{-\lambda_- t} + (\lambda_+ - R_{22})e^{-\lambda_+ t}\right], \tag{3.14a}$$

$$\Sigma_2(t) = \frac{R_{21}\Sigma_1(0)}{\lambda_+ - \lambda_-}\left[e^{-\lambda_- t} - e^{-\lambda_+ t}\right]. \tag{3.14b}$$

Here $R_{ij} = |\mathbf{R}_{ij}|$ denote the absolute values of the elements of the matrix $\mathbf{R}$ given by Eq. (3.13) and $-\lambda_\pm$ are the eigenvalues of the matrix $\mathbf{R}$, which can be obtained as,

$$\begin{aligned}\lambda_\pm &= \frac{1}{2}\left[(R_{11} + R_{22}) \pm \sqrt{(R_{11} + R_{22})^2 - 4(R_{11}R_{22} - R_{12}R_{21}}\right] \\ &= \frac{1}{2}\left[(R_{11} + R_{22}) \pm \sqrt{(R_{11} - R_{22})^2 + 4R_{12}R_{21}}\right].\end{aligned} \tag{3.15}$$

Note that $\lambda_\pm > 0$ for $-1 < r_w \leq 1$. In Fig. 3.1, we plot $\Sigma_{1,2}$ as a function of t, as given by Eq. (3.14).

3.4.1.2. The non-linear case: $g = \Sigma_1^{1/2}$

When $g = \Sigma_1^{1/2}$, the evolution of Σ_1 and Σ_2 is given by,

$$\frac{d\Sigma_1}{dt} = -R_{11}\Sigma_1^{3/2} + R_{12}\Sigma_1^{1/2}\Sigma_2, \tag{3.16a}$$

$$\frac{d\Sigma_2}{dt} = R_{21}\Sigma_1^{3/2} - R_{22}\Sigma_1^{1/2}\Sigma_2. \tag{3.16b}$$

The Equation (3.16b) for the evolution of Σ_2 can be solved exactly in terms of Σ_1 as

$$\Sigma_2(t) = R_{21}\int_0^t dt_1 \Sigma_1^{3/2}(t_1)\exp\left[-R_{22}\int_{t_1}^t \Sigma_1^{1/2}(t_2)\,dt_2\right], \tag{3.17}$$

where we have used the initial condition $\Sigma_2(0) = 0$. However, it is difficult to obtain an exact solution of Eq. (3.16a) for Σ_1. Nonetheless, near $t = 0$, using the initial condition $\Sigma_2(0) = 0$, we can write Eq. (3.16a) as $d\Sigma_1/dt \approx -R_{11}\Sigma_1^{3/2}$, which gives,

$$\Sigma_1(t) \approx \frac{\Sigma_1(0)}{\left(1 + \frac{1}{2}R_{11}\Sigma_1^{1/2}(0)\, t\right)^2}. \tag{3.18}$$

After substituting the above expression for $\Sigma_1(t)$ in Eq. (3.17), and performing the integration, we obtain

$$\Sigma_2(t) \approx \frac{R_{21}/R_{11}}{1-\theta}\left[\frac{\Sigma_1(0)}{\left(1 + \frac{1}{2}R_{11}\Sigma_1^{1/2}(0)\, t\right)^{2\theta}} - \Sigma_1(t)\right], \quad \text{for } \theta \neq 1, \tag{3.19}$$

where $\theta = R_{22}/R_{11}$. On the other hand for $\theta = 1$, we get

$$\Sigma_2(t) \approx \frac{2(R_{21}/R_{11})\,\Sigma_1(0)\,\ln\left(1 + \frac{1}{2}R_{11}\Sigma_1^{1/2}(0)\, t\right)}{\left(1 + \frac{1}{2}R_{11}\Sigma_1^{1/2}(0)\, t\right)^2}. \tag{3.20}$$

Therefore, for large t, we have, when $\theta \neq 1$,

$$\Sigma_2(t) \sim \begin{cases} t^{-2\theta} & \text{for } \theta < 1, \\ t^{-2} & \text{for } \theta > 1, \end{cases} \tag{3.21}$$

and for $\theta = 1$, there is a logarithmic correction

$$\Sigma_2(t) \sim (\ln t)\; t^{-2}. \tag{3.22}$$

Due to the mean field nature of the problem it is fair to assume that the rate of inter-particle collisions between a particular pair, τ_c^{-1} is inversely proportional to the of the total number of pairs [$\tau_c \propto N(N-1)/2$], while the rate of driving τ_w^{-1} is inversely proportional to the total number of particles ($\tau_w \propto N$). This is analogous to infinite-ranged spin models where one takes the coupling constant proportional to $1/N$. The assumption lets us define a parameter γ such that $\tau_c/\tau_w = \gamma(N-1)$. Thus for large N, τ_c is $O(N^{-2})$ and τ_w is $O(N^{-1})$. Consequently, one can see from Eq. (3.13) that R_{11}, R_{12} and R_{22} are $O(N^{-1})$ whereas R_{21} is $O(N^{-2})$.

Therefore, the prefactor outside the square bracket in the expression (3.19) is $O(N^{-1})$. Thus for large N, one can neglect the second term on the RHS of Eq. (3.16a) even beyond the small t region. As a result, the expression (3.18), and hence, Eq. (3.19) remain valid even for large time.

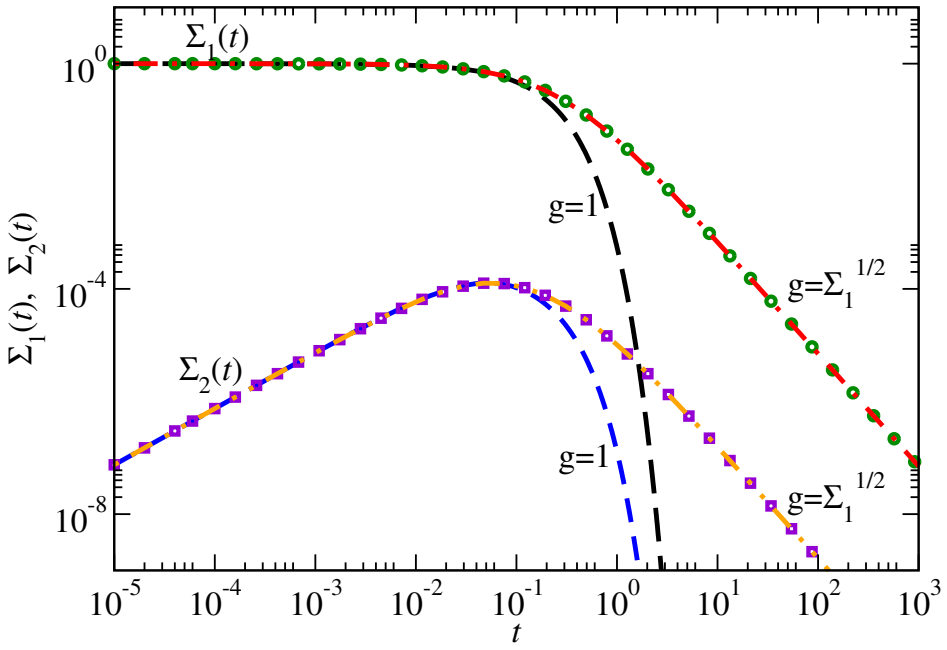

FIGURE 3.1: The variance $\Sigma_1(t)$ and the two-point correlation $\Sigma_2(t)$ of the velocities, for a cooling inelastic gas with 1000 particles in the absence of the driving (static walls), for the two cases: (1) the rate of collision is independent of the variance $g = 1$, and (2) the rate of collision is proportional to the variance $g = \Sigma_1^{1/2}(t)$. For $g = 1$, the lines plot the exact analytical expressions given by Eq. (3.14). For $g = \Sigma_1^{1/2}(t)$, the lines plot the approximate expressions given by Eqs. (3.18) and (3.19), while the points are obtained by exact numerical evaluation of the equation Eq. (3.16).

From the above analysis one finds out that for the freely cooling gas, the two-point correlation is rather not important. In the limit $N \to \infty$, the exponent θ is calculated and is given by the expression,

$$\theta = \frac{4\gamma(1 + r_w)}{1 - r^2 + 2\gamma(1 - r_w^2)}, \tag{3.23}$$

Figure 3.1 compares the expressions (3.18) and (3.19) with the exact values obtained by numerically solving Eq. (3.16).

3.4.2. Steady state dynamics

Even when the driving is present, one expects the approach to steady state to be different for the two different cases of g. The steady states, however are independent of the choice g as can be seen from Eq. (3.10) and Eq. (3.12). As one is interested in the steady state properties, it is enough to study the simpler $g = 1$ case, as in [47] which makes the Eq. (3.12) linear.

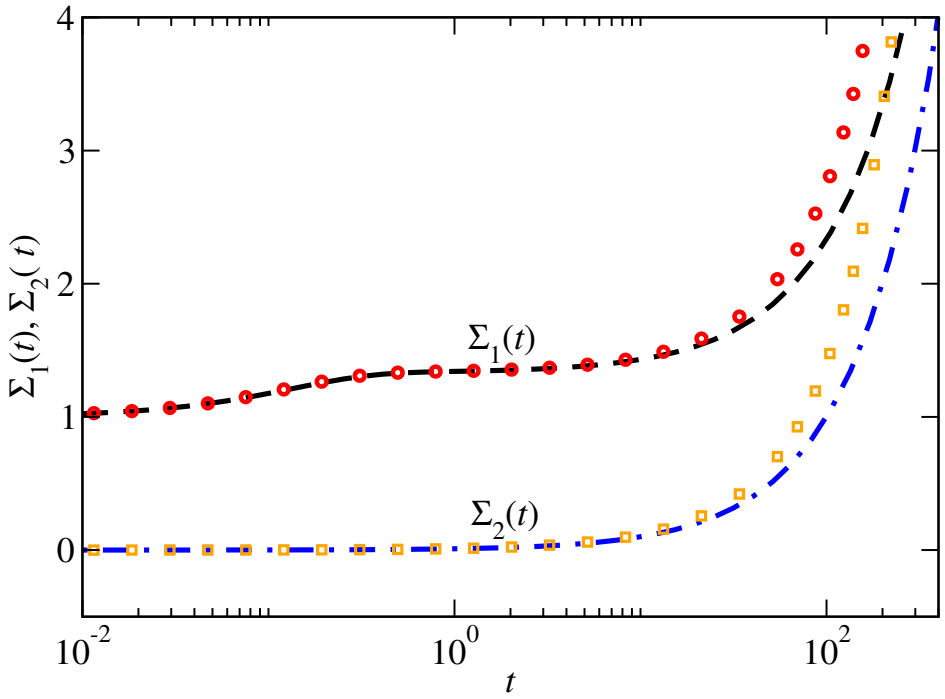

FIGURE 3.2: The variance $\Sigma_1(t)$ and the two-point correlation $\Sigma_2(t)$ of the velocities, for an inelastic gas with 1000 particles with $r = 1/2$ driven by wall collisions with $\sigma = 1$ and $r_w = -1$ for the two cases: (1) the rate of collision is independent of the variance $g = 1$, and (2) the rate of collision is proportional to the variance $g = \Sigma_1^{1/2}(t)$. For $g = 1$, the lines plot the exact analytical expressions given by Eq. (3.25). For $g = \Sigma_1^{1/2}(t)$, the points are obtained by exact numerical evaluation of the equation Eq. (3.12).

The $X(t)$ can be exactly solved for $g = 1$, as in Sec. 3.4.1 to obtain the variance $\Sigma_1(t)$ and the two-point correlation function $\Sigma_2(t)$,

$$\Sigma_1(t) = \frac{\Sigma_1(0)}{\lambda_+ - \lambda_-}\Big[(R_{22} - \lambda_-)e^{-\lambda_- t} + (\lambda_+ - R_{22})\, e^{-\lambda_+ t}\Big] + \frac{\tau_w^{-1}\sigma^2}{\lambda_+ - \lambda_-}\left[\frac{R_{22} - \lambda_-}{\lambda_-}\big(1 - e^{-\lambda_- t}\big) + \frac{\lambda_+ - R_{22}}{\lambda_+}\big(1 - e^{-\lambda_+ t}\big)\right], \tag{3.24a}$$

and

$$\Sigma_2(t) = \frac{\Sigma_1(0)R_{21}}{\lambda_+ - \lambda_-}\Big[e^{-\lambda_- t} - e^{-\lambda_+ t}\Big] + \frac{\tau_w^{-1}\sigma^2 R_{21}}{\lambda_+ - \lambda_-}\left[\frac{1}{\lambda_-}(1 - e^{-\lambda_- t}) - \frac{1}{\lambda_+}(1 - e^{-\lambda_+ t})\right], \tag{3.24b}$$

respectively, where $-\lambda_\pm$ are the eigenvalues of $\mathbf{R}$, given by Eq. (3.15), and $R_{ij} = |\mathbf{R}_{ij}|$.

Now, for the case $r_w = -1$, one of the eigenvalues of $\mathbf{R}$ becomes zero ($\lambda_- = 0$), while the other is negative ($\lambda_+ = R_{11} + R_{22} > 0$). For these particular values of $\lambda_\pm$, the above expressions become

$$\Sigma_1(t) = \frac{\Sigma_1(0)}{\lambda_+}\Big[R_{22} + R_{11}\, e^{-\lambda_+ t}\Big] + \frac{\sigma^2}{\tau_w}\frac{R_{11}}{\lambda_+^2}\Big[1 - e^{-\lambda_+ t}\Big] + \frac{\sigma^2}{\tau_w}\frac{R_{22}}{\lambda_+}\, t, \tag{3.25a}$$

$$\Sigma_2(t) = \frac{\Sigma_1(0) R_{21}}{\lambda_+}\Big[1 - e^{-\lambda_+ t}\Big] - \frac{\sigma^2}{\tau_w}\frac{R_{21}}{\lambda_+^2}\Big[1 - e^{-\lambda_+ t}\Big] + \frac{\sigma^2}{\tau_w}\frac{R_{21}}{\lambda_+}\, t. \tag{3.25b}$$

This shows that, both $\Sigma_1(t)$ and $\Sigma_2(t)$ eventually increase linearly with time and so, the system does not have a steady state for $r_w = -1$ when the driving is present ($\sigma \neq 0$).

On the other hand, when $-1 < r_w \leq 1$, both the eigenvalues of $\mathbf{R}$ are negative ($\lambda_\pm > 0$) (see Sec. 3.4.1), and hence the system reaches a steady state as shown in Fig. 3.3. The steady state values of Σ_1 and Σ_2 can be obtained by either taking the limit of $t \to \infty$ in Eq. (3.24) or setting the LHS of Eq. (3.12) to zero. Denoting the steady state values of the variance and the two-point correlation by $\Sigma_1^{\rm ss}$ and $\Sigma_2^{\rm ss}$ respectively,

$$\Sigma_1^{\rm ss} = \frac{\sigma^2\big[(1-r^2) + 4(1+r_w)(\tau_c/\tau_w)\big]}{(1-r_w^2)(1-r^2) + 2(1+r_w)\big[(1-r^2)(N-1) + 2(1-r_w^2)(\tau_c/\tau_w)\big]}\,, \tag{3.26a}$$

$$\Sigma_2^{\rm ss} = \frac{\sigma^2(1-r^2)}{(1-r_w^2)(1-r^2) + 2(1+r_w)\big[(1-r^2)(N-1) + 2(1-r_w^2)(\tau_c/\tau_w)\big]}\,. \tag{3.26b}$$

As evident from Eq. (3.26), the steady state values $\Sigma_1^{\rm ss}$ and $\Sigma_2^{\rm ss}$ depend on the relative rate at which the collisions and the driving take place. Consider that for large N, $\tau_c/\tau_w \sim N^\xi$, with ξ, a real number. From Eq. (3.26), we observe that if $\xi < 0$, both $\Sigma_1^{\rm ss}$ and $\Sigma_2^{\rm ss}$ vanish as $O(1/N)$ for large N. Also when $0 < \xi < 1$, the two quantities vanish as $\Sigma_1^{\rm ss} \sim O(1/N^{1-\xi})$ and $\Sigma_2^{\rm ss} \sim O(1/N)$, for a large enough system. But if $\xi \geq 1$, the system has non-zero steady-state variance for large N, with a value given by

$$\Sigma_1^{\rm ss} = \frac{2\sigma^2(\tau_c/\tau_w)}{N(1-r^2) + 2(1-r_w^2)(\tau_c/\tau_w)}, \tag{3.27}$$

whereas the two-point correlation function vanishes as $\Sigma_2^{\rm ss} \sim O(1/N^\xi)$.

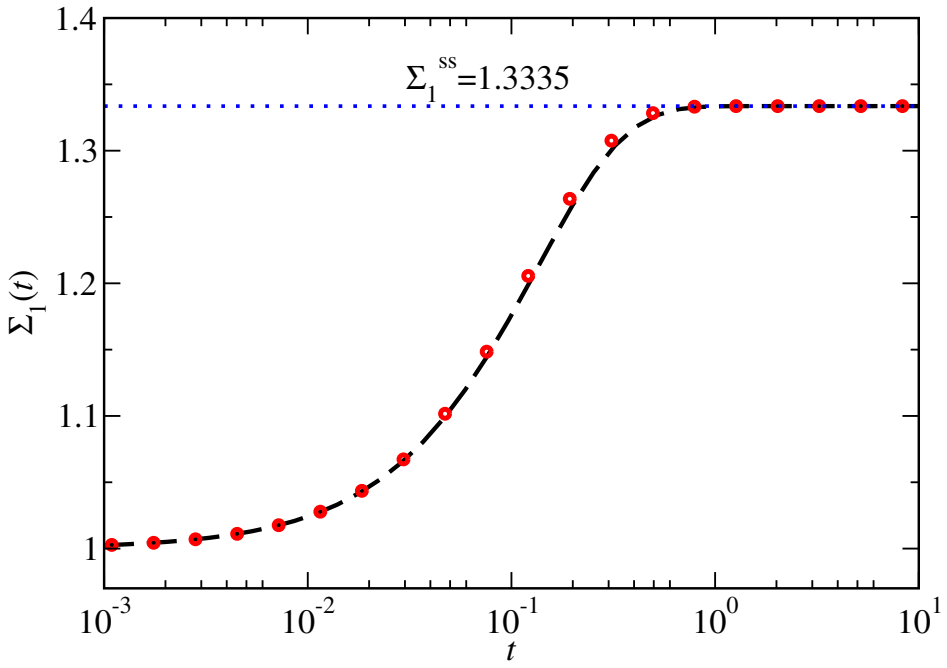

FIGURE 3.3: The variance $\Sigma_1(t)$ of the velocities, for an inelastic gas with 1000 particles with $r = 1/2$ driven by wall collisions with $\sigma = 1$ and $r_w = 1$ for the two cases: (1) the rate of collision is independent of the variance $g = 1$, and (2) the rate of collision is proportional to the variance $g = \Sigma_1^{1/2}(t)$. For $g = 1$, the line plots the exact analytical expressions given by Eq. (3.24). For $g = \Sigma_1^{1/2}(t)$, the points are obtained by exact numerical evaluation of the equation Eq. (3.12). The dotted line highlights the steady state value calculated from Eq. (3.26a).

As in Sec. 3.4.1, we consider the rates for a mean field system such that, $\tau_c \propto N(N-1)/2$, and $\tau_w \propto N$. Indeed if we set $\tau_c/\tau_w = \gamma(N-1)$, then the Eq. (3.26) become identical to those obtained for the discrete dynamics (see Eq. (3.6)). Also, in the large N limit the steady state variance becomes independent of N,

$$\Sigma_1^{ss} = \frac{2\gamma\sigma^2}{4\epsilon(1-\epsilon) + 2\gamma(1-r_w^2)}. \tag{3.28}$$

Also, as $\xi = 1$ the two-point correlation function vanishes in the limit of large N, which allows one to factorize the multi-particle distribution functions in terms of the single-particle distribution function in Eq. (3.10), e.g., $f_2(v_1, v_2) = f_1(v_1)f_1(v_2)$. Therefore, in the steady state if we multiply Eq. (3.10a) by $\exp(-\lambda v_1)$ and then integrate over v_1, we obtain the equation satisfied by the generating function $Z(\lambda)$ of the single particle PDF, $P(v) = (1/N)f_1(v)$,

$$Z(\lambda) = \frac{1}{1+\gamma} Z(\epsilon\lambda)Z([1-\epsilon]\lambda) + \frac{\gamma}{1+\gamma} Z(r_w\lambda)f(\lambda), \tag{3.29}$$

where $Z(-\lambda) = Z(\lambda)$ due to the even nature of the distribution and $f(\lambda) = \exp(\lambda^2\sigma^2/2)$. If we set $\gamma = (1-p)/2p$ as before (Sec. 3.3), then $1/(1+\gamma) = 2p/(1+p) = q$ and Eq. (3.29) becomes identical to Eq. (3.8), which we have obtained for the discrete time dynamics (Sec. 3.3). Therefore both the continuous time and the discrete time dynamics yield the same steady state.

Note that Eq. (3.8) is in fact same as Eq. (2.48) because, q of the former equation (Eq. (3.8)) and p of Eq. (2.48) are variables with the same range, $p, q \in [0, 1]$. Note that one has calculated the high energy tail of the PDF in the case of Eq. (2.48). Same analysis follows for the calculation of PDF described by Eq. (3.8) too. In particular when $r_w = 1$, we can obtain $Z(\lambda)$ as an infinite product involving simple poles by iteratively solving $Z(\lambda) = [1-(1-q)f(\lambda)]^{-1}\, qZ(\epsilon\lambda)Z([1-\epsilon]\lambda)$. Therefore, the tail of the velocity distribution is exponential

$$P(v) \sim \exp(-|v|/v^*), \tag{3.30}$$

where v^* is determined by the pole closest to the origin, coming from the prefactor $[1-(1-q)f(\lambda)]^{-1}$. Further, for $|r_w| < 1$, the reasoning used in the case of Eq. (2.48), guarantee an exact tail with the Gaussian form,

$$P(v) \approx \sqrt{\frac{1-r_w^2}{2\pi\sigma^2}}\, \exp\left[-\frac{v^2}{2\sigma^2}(1-r_w^2)\right]. \tag{3.31}$$

Figure 3.4 summarises the results for different case of r_w.

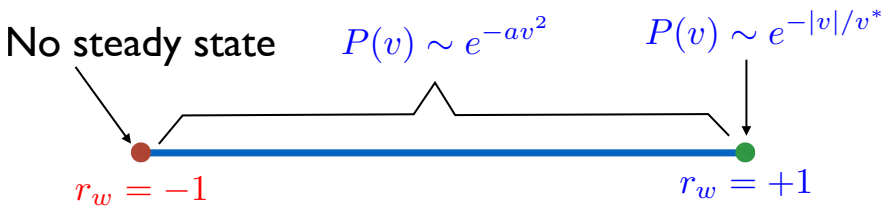

Figure 3.4: The summary of the results for the PDF of the velocity distribution for different cases of $r_w \in [-1, 1]$. For $r_w = -1$, the system does not reach a steady state, and the average energy and the two-point correlation eventually increase linearly with the time. For $r_w = 1$, the steady state PDF has an exponential tail, whereas for $-1 < r_w < 1$, the tail of the PDF for very large velocities is Gaussian.

3.5. Ornstein-Uhlenbeck driving

We observed that a system of inelastic Maxwell gas with mutual collisions and driving happening as uncorrelated events in time evolves in to a steady state, if the wall collisions have the following

characteristics. The wall collisions are either inelastic ($|r_w| < 1$) or elastic but reflecting ($r_w = 1$). In this section, we show that the mechanism of driving introduced above becomes an Ornstein-Uhlenbeck process in a special limit. Such a mechanism is usually used to model inelastic systems in dissipative environment like that of a viscous bath [4, 33, 46]. Analytical studies of these systems usually resort to perturbative calculations of the velocity distribution about the Gaussian with a variance proportional to the energy of the system. This gives the information about the PDF in the range of the variance. Our study compliments this, as we obtain the tail of PDF for a Maxwell gas driven by Ornstein-Uhlenbeck noise.

For the time being, we ignore the inter-particle collisions and also set $g = 1$. Then, Eq. (3.10a) becomes,

$$\frac{\partial f_1(v_1, t)}{\partial t} = \tau_w^{-1}\left[\int dv_1^* f_1(v_1^*, t)\langle\delta\big(v_1 - [-r_w v_1^* + \eta_1]\big)\rangle_{\eta_1} - f_1(v_1, t)\right]. \tag{3.32}$$

In terms of the characteristic function $\widetilde{f}_1(k_1, t)$, which is defined as $\widetilde{f}_1(k_1, t) \equiv \int dv_1 f_1(v_1, t)\, e^{-ik_1 v_1}$, Eq. (3.32) can be written as,

$$\frac{\partial \widetilde{f}_1(k_1, t)}{\partial t} = \tau_w^{-1}\left[\widetilde{f}_1(-k_1 r_w, t)\, e^{-k^2\sigma^2/2} - \widetilde{f}_1(k_1, t)\right]. \tag{3.33}$$

The term $\exp(-k^2\sigma^2/2)$ is the characteristic function of the Gaussian noise with variance σ^2. Let us consider the limiting case at which the frequency of the wall-particle collisions becomes very high, i.e., $\tau_w \to 0$. In order to achieve a steady state, simultaneously one has to take $\epsilon_w \equiv (1 + r_w) \to 0$ and $\sigma^2 \to 0$, while keeping appropriate ratios fixed.

Replacing r_w by $-(1 - \epsilon_w)$ in Eq. (3.33), expanding and keeping only up to the lowest order terms in the small parameters, we obtain,

$$\frac{\partial \widetilde{f}_1(k_1, t)}{\partial t} = \tau_w^{-1}\left[-\epsilon_w k_1 \frac{\partial \widetilde{f}_1(k_1, t)}{\partial k_1} - \frac{\sigma^2 k_1^2}{2}\widetilde{f}_1(k_1, t)\right]. \tag{3.34}$$

Therefore, in the limit $\tau_w \to 0$, $\epsilon_w \to 0$ and $\sigma^2 \to 0$, while keeping

$$\Gamma = \lim_{\substack{\tau_w \to 0 \\ \epsilon_w \to 0}} \frac{\epsilon_w}{\tau_w} \quad \text{and} \quad D = \lim_{\substack{\tau_w \to 0 \\ \sigma^2 \to 0}} \frac{\sigma^2}{2\tau_w} \tag{3.35}$$

fixed, Eq. (3.34) becomes,

$$\frac{\partial \widetilde{f}_1(k_1, t)}{\partial t} = -\Gamma k_1 \frac{\partial \widetilde{f}_1(k_1, t)}{\partial k_1} - D k_1^2 \widetilde{f}_1(k_1, t). \tag{3.36}$$

One can easily recognize that this is the Fokker-Planck equation of an Ornstein-Uhlenbeck process in the Fourier space. In the velocity space, the equation has the form,

$$\frac{\partial f_1(v_1,t)}{\partial t} = \Gamma \frac{\partial}{\partial v_1}\big[v_1 f_1\big] + D\frac{\partial^2 f_1}{\partial v_1^2} \ . \tag{3.37}$$

This shows that in the limit given by Eq. (3.35), the model of driving by wall collisions becomes an Ornstein-Uhlenbeck process, with the parameters defined as in Eq. (3.35).

Evolution of $\Sigma_1(t)$ and $\Sigma_2(t)$ follows Eq. (3.12), but with a modified matrix $\mathbf{R}$ and C, which is obtained from Eq. (3.10) in the above limit. The matrix $\mathbf{R}$ now has the form,

$$\mathbf{R} = \begin{bmatrix} -\left(\frac{(1-r^2)(N-1)}{2\tau_c} + 2\Gamma\right) & \frac{(1-r^2)(N-1)}{2\tau_c} \\ \\ \frac{(1-r^2)}{2\tau_c} & -\left(\frac{(1-r^2)}{2\tau_c} + 2\Gamma\right) \end{bmatrix}, \tag{3.38}$$

and $C = [2D, 0]^T$.

The eigenvalues of $\mathbf{R}$ are given by -2Γ and $-2\Gamma - N(1-r^2)/(2\tau_c)$, with the corresponding eigenvectors $[1,1]^T$ and $[1,-1/(N-1)]^T$ respectively. For $g = 1$, we can solve Eq. (3.12), by diagonalising $\mathbf{R}$. This results in two decoupled equations for the elements of $[y_1(t), y_2(t)]^T = \mathbf{S}^{-1}X$, where

$$\mathbf{S} = \begin{bmatrix} 1 & 1 \\ \\ 1 & -\frac{1}{(N-1)} \end{bmatrix} \text{ and } \mathbf{S}^{-1} = \frac{\mathrm{N}-1}{\mathrm{N}} \begin{bmatrix} \frac{1}{N-1} & 1 \\ \\ 1 & -1 \end{bmatrix}, \tag{3.39}$$

and $\mathbf{S}^{-1}\mathbf{R}\mathbf{S}$ is a diagonal matrix with the eigenvalues of $\mathbf{R}$ being the diagonal elements. It is straightforward to find the solutions as

$$y_1(t) = y_1(0)\exp\left(-2\Gamma t\right) + \frac{D}{N\Gamma}\left[1 - \exp(-2\Gamma t)\right], \tag{3.40a}$$

and

$$y_2(t) = y_2(0)\exp\left(-\left[\frac{N(1-r^2)}{2\tau_c}+2\Gamma\right]t\right) + \frac{(N-1)4D\tau_c}{N[N(1-r^2)+4\Gamma\tau_c]}\left[1-\exp\left(-\left[\frac{N(1-r^2)}{2\tau_c}+2\Gamma\right]t\right)\right]. \tag{3.40b}$$

The initial values $y_1(0)$ and $y_2(0)$ can be obtained in terms of $\Sigma_1(0)$ and $\Sigma_2(0) = 0$. Finally, one obtains the evolution of $\Sigma_1(t)$ and $\Sigma_2(t)$ by inversion to $X = \mathbf{S}[y_1(t), y_2(t)]^T$.

Thus for any non-zero values of Γ, we see from Eq. (3.40) that as $t \to \infty$, both $y_1(t)$ and $y_2(t)$, and hence, $\Sigma_1(t)$ and $\Sigma_2(t)$, approach steady state values. The steady state values are given by

$$\lim_{t\to\infty} \Sigma_1(t) = \frac{D}{\Gamma}\left(\frac{1-r^2+4\Gamma\tau_c}{N(1-r^2)+4\Gamma\tau_c}\right), \tag{3.41a}$$

$$\lim_{t\to\infty} \Sigma_2(t) = \frac{D}{\Gamma}\left(\frac{1-r^2}{N(1-r^2)+4\Gamma\tau_c}\right). \tag{3.41b}$$

Note that one can obtain this also from Eq. (3.26) by taking the limits given by Eq. (3.35).

The exact tail statistics for the system driven by an Ornstein-Uhlenbeck noise can be obtained by taking the limits as above, in Eq. (3.31), which gives

$$P(v) \approx \sqrt{\frac{\Gamma}{2\pi D}}\exp\left[-v^2\frac{\Gamma}{2D}\right], \tag{3.42}$$

which is nothing but the exact distribution of the velocity of a particle driven by an Ornstein-Uhlenbeck noise, in the absence of any particle-particle collision. Thus, as seen before, the tail statistics is determined by the driving alone and not the inter-particle collisions.

We now consider the special case, where the dissipative term $\Gamma = 0$. This represents the scenario where the driving is modelled by a Wiener process (diffusive driving), $dv_i/dt = \sqrt{2D}\,\eta_i$. In this case, one of the eigenvalues of $\mathbf{R}$ (putting $\Gamma = 0$ in the eigenvalues of $\mathbf{R}$) becomes zero, while the other is $-N(1-r^2)/(2\tau_c)$. The zero eigenvalue indicates a non-stationary state. The exact solution in the diagonal basis has a form,

$$y_1(t) = y_1(0) + \frac{2Dt}{N}, \tag{3.43a}$$

$$y_2(t) = y_2(0)\exp\left(-\frac{N(1-r^2)t}{2\tau_c}\right) + \frac{(N-1)4D\tau_c}{N^2(1-r^2)}\left[1-\exp\left(-\frac{N(1-r^2)t}{2\tau_c}\right)\right]. \tag{3.43b}$$

Inverting $y_1(t)$ and $y_2(t)$ as before we can obtain $\Sigma_1(t)$ and $\Sigma_2(t)$ exactly for any time t. In particular, the asymptotic forms for large t is obtained as:

$$\Sigma_1(t) = \frac{\Sigma_1(0)}{N} + \frac{(N-1)4D\tau_c}{N^2(1-r^2)} + \frac{2D}{N}t \ , \tag{3.44a}$$

$$\Sigma_2(t) = \frac{\Sigma_1(0)}{N} - \frac{4D\tau_c}{N^2(1-r^2)} + \frac{2D}{N}t \ . \tag{3.44b}$$

It is clear from Eq. (3.44a) and Eq. (3.44b) that both the variance $\Sigma_1(t)$ and the two-point correlation function $\Sigma_2(t)$ eventually grows linearly in time, irrespective of the timescale of collisions and the strength of the driving force. So the system does not have a steady state for the diffusive driving. Also, as the particles in the system become more and more correlated with time, the molecular chaos hypothesis remains no longer valid.

3.6. Conclusion

In this chapter we introduced a model of inelastic Maxwell gas evolving in continuous time with the inter particle collisions as well as driving – which happens through collision of the particles with the vibrating wall – being modelled as uncorrelated point processes in time. In an analytical study of the system along the lines of kinetic theory, we find that though the time evolution of the distribution functions follow an infinite hierarchy of equations, the variance and the two-point correlation function form a coupled set of equations which closes on its own. This has been observed for the discrete time model, as seen in the previous chapter. The current result makes it evident that the closure is quite general and has nothing to do with the the discrete dynamics. From the exact evolution equations for the two quantities, we see that the system reaches a steady state depending on the properties of the wall collisions; i.e the system goes to a steady state when the wall collisions are either inelastic or elastic but reflecting. We find that there is an exact mapping between the discrete and the continuous time systems, in terms of the equations satisfied by the steady state PDF of particle velocities. The exact tail of the PDF is similar to that of the discrete model for the entire range of r_w, the restitution coefficient between particle and wall. The Ornstein-Uhlenbeck driving and so the diffusive driving can be realised as a special limit of the driving by wall collision. Our calculations show that with the diffusive driving the system cannot have a steady state, as found earlier for the discrete time dynamics.

4

Inelastic gas on a one-dimensional ring

4.1. Introduction

A key observation that we made use of in the previous chapters was the fact that one can calculate the exact evolution equation for the variance and two-point correlation function of the velocity for the inelastic Maxwell gas. In this chapter, we show that the above technique can be used to understand the behaviour of spatial correlation function for a Maxwell-like gas living on a one dimensional lattice.

A distinctive feature of granular gases is the appearance of spatial correlation within the system. The inelastic collisions between particles result in their slowing down and lead to building up of density as well as velocity correlations. From non-equilibrium physics point of view it is of importance to understand the behaviour of correlations. Equilibrium systems have a generic behaviour for the correlation functions with an exponentially decaying form, when away from

the critical point. But in non-equilibrium systems the behaviour is different. Studies on non-equilibrium steady states have found spatial correlations which decay as a power-law, widely present. It will be illuminating to study specific non-equilibrium systems to have a general understanding of non-equilibrium correlations. It is useful in this direction to the characterize the behaviour of correlations in granular systems. On the other hand, the knowledge of correlation is important for the analytical studies of granular systems also. As described before, the kinetic theory studies of granular gases involve calculating the evolution equation of the distribution functions. The resulting hierarchy can be closed only if the correlations between particles are negligible.

Correlations in granular gases have been studied both for unforced [35, 52, 53] as well as forced [22, 30, 54–58] systems. We will be concentrating on the behaviour of correlations in driven systems. An inelastic gas composed of point like particles living in one dimension with periodic boundary and driven by uncorrelated white noise (diffusive noise), has been studied by Williams and Mackintosh [30]. They observed a power-law decay $\sim x^{-\alpha}$ for the density correlation function with x the spatial separation and the exponent α a function of the coefficient of restitution r. Analytical study [54] conducted for a similar system also observed power-law correlations in density. They observed that in large N limit $\alpha = 1/2$, and is independent of r.

Velocity correlations also exhibit similar features. A hydrodynamic study of inelastic hard sphere gas driven by the diffusive noise, proposes [55] long range behaviour for the velocity correlation function. It predicted logarithmic ($\ln[L/x]$ where L the system size) and power-law ($1/x$) form respectively for two and three dimensions, but matched with simulations only in the near elastic regime. Later, in an experimental study of a granular gas on an inclined plane which is driven by a vibrating wall at the bottom, Blair and Kudrolli [22] observed a power-law decay in the steady state velocity correlations. The exponent α in this case ranged from 1.2 to 2 with decreasing system size. In contrast, Prevost *et al.* [56] in their experiment on a two-dimensional granular gas driven by a rough vibrating plane, found an exponential decay in the spatial correlation of the particle velocities. The difference of the result from the previous ones was argued by the authors of Ref. [56] to be due to the different driving schemes used. Especially, in the analytical and numerical studies, the driving was modelled by the diffusive driving with the rate of change of velocity due to driving equated to uncorrelated white noise, $dv/dt = \eta(t)$. According to the

authors [56], the driving mechanism which in their case is the wall-particle collision, should also be treated as inelastic collisions.

Along similar lines, a phenomenological model was considered by Gradenigo, Puglisi and others [57, 58], where the driving involves a viscous drag term in addition to the diffusive driving, in order to account for the various dissipation that can occur while driving. They obtained an exponential form for the velocity correlation which matched with the experimental observations. Apart from the phenomenological viscous drag term in the driving, the model had the assumption of separation of timescales between the collisions and driving. In the following, we would like to consider a theoretical model of inelastic gas where one does not require this assumption, yet providing an exact result for the correlation function. Unlike the Ornstein-Uhlenbeck noise (driving with the viscous term), we consider a driving mechanism similar to that used in the experiments by Prevost *et al.* [56], which is the collision of the particles with the vibrating wall.

4.2. Outline

The system that we study is an inelastic gas in one dimension. Here the inelastic particles live in one dimension with periodic boundary and interact via inelastic collisions only to it's nearest neighbours. Unlike in hard sphere systems where the collision rate is proportional to the relative velocities, we consider a simpler model where the collisions occur with uniform rate τ_c^{-1} and is independent of the particle velocities. This can be realised by considering a set of lattice points with periodic boundary condition, with each site i carrying a scalar variable $v_i \in \mathbb{R}$, and defining an interaction between nearest neighbours, which resembles the usual inelastic collision. We are interested in the correlations in driven steady states. Suggested by the experimental studies [56], we consider the driving by wall collision which has been introduced before (Sec. 2.4). The driving acts independently at each site i with a rate τ_w^{-1}.

For the model we find an exact closure relation in terms of the variance and the two-point functions. The relation helps us to find the evolution of the quantities exactly. In chapter 3, we had obtained a similar relation for a system of Maxwell gas, where any particle can interact with any other particle. In the lattice case one has, instead of a single correlation function, a number of them which quantifies the correlation between lattice points with different separation. So the

matrix which describes the evolution in this case is a k-dimensional matrix where k is a number determined by the total number of lattice points N.

The evolution equation helps us to characterize the steady state properties. For instance, the coupled relations can be used to find out whether the system goes to a steady state or not for various values of the parameters in the driven system. We also find how the correlations vary with the site index by looking at the steady state values. One of our main result is the exact functional dependence of the steady state correlation function on the lattice separation. It has an exponential form for a large system.

Similar models have been studied for granular gases in both cooling [35] as well as driven [59] cases. The model studied by Levanony and Levine [59] considers lattice points on a line with periodic boundary. Instead of velocity, each site in the model has an 'energy' variable associated with it. The inelastic collision is represented in the model by dissipation in the energy of the lattice points, which is proportional to the sum of the energies of it with one of the neighbours. The model thus does not include the effect of correlations in the binary collisions. In our model this is taken care of by setting the rule of interaction between neighbouring lattice points to be exactly that of one-dimensional inelastic collisions.

The structure of the chapter is as follows. First, in Sec. 4.3 we introduce the model of inelastic gas on a lattice with the rules of interaction and driving. Later in Sec. 4.4 the dynamics is introduced for which we calculate the evolution equations for the velocity distribution functions. They result in a hierarchy, as seen in the kinetic theory of granular gases. Without breaking the hierarchy, an exact coupled evolution of the variance and two-point correlation functions is calculated for the system. We derive an exact formula for the steady state variance and the equal time correlation between the velocity variables at different sites. We also find the asymptotic functional form for the correlation functions. In Sec. 4.5 we conclude summarising our result. Some of the details of the analysis are given in the Appendix (A.1).

4.3. Maxwell gas on a lattice

Consider a set of N lattice points in one dimension with periodic boundary condition. Each lattice site with label i carries a scalar variable $v_i \in \mathbb{R}$ $(i = 1, 2..N)$, which we call the 'velocity'.

It needs to be kept in mind that this velocity does not correspond to any motion in the system. The interaction causes change in the velocities of the nearest neighbouring sites 'i' and '$i+1$' denoted as v_i^* and v_{i+1}^* respectively, according to the rule:

$$\begin{aligned} v_i &= \epsilon v_i^* + (1-\epsilon) v_{i+1}^*, \\ v_{i+1} &= (1-\epsilon) v_i^* + \epsilon v_{i+1}^*. \end{aligned} \tag{4.1}$$

Here, v_i and v_{i+1} are the new velocities at the lattice sites. Note that, the lattice being periodically bounded, $i+N = i = i-N$. The equations (4.1) are the same as the ones for inelastic collision between a pair of equal mass particles with velocities (v_i^*, v_{i+1}^*) resulting in the new velocities (v_i, v_{i+1}). The parameter, $\epsilon = (1-r)/2$, where r is the coefficient of restitution of inelastic collision. In real inelastic systems, r takes values between 0 and 1. As mentioned before, for a mathematical model of a dissipative gas, it is justified to consider the negative values for r such that $|r| < 1$. We thus consider the entire range of the parameter, $r \in [-1, 1]$ in our study. When $|r| < 1$, inelastic collisions take away part of the energy from the system and cause the energy of the system to decrease monotonically until all the particles have the same velocity, as that of the centre of mass.

As we know, driving is required to sustain a steady state for an inelastic system. We consider the driving to be one resembling the wall-particle collisions introduced earlier. The driving acts independently to each site i and causes a change in v_i, which follows the relation,

$$v_i = r_w v_i^* + \eta_i. \tag{4.2}$$

Here r_w is the coefficient of restitution of the wall-particle collision and quantifies the dissipation while driving. As for restitution coefficient r, the range of r_w is also taken to be such that $r_w \in [-1, 1]$. The noise η_i is taken from a Gaussian distribution with variance σ^2 and mean zero, acting on each particle independently and uncorrelated in time. The driving by wall collision is considered to be an uncorrelated point process in time. But in certain limit it becomes the viscous driving (The discussion is given in the Chapter 3). Given the above set of rules, one can ask whether there exists any exact equation or set of equations describing the temporal evolution of the system.

4.4. Dynamics

The system evolves in time t as follows. With a rate τ_c^{-1}, a pair of nearest neighbours $(i, i+1)$ which is chosen at random, interacts with each other causing their respective 'velocities' to change according to Eq. (4.1). Similarly with rate τ_w^{-1} each particle is driven according to Eq. (4.2). The evolution of the probability distribution functions for the dynamics can be calculated as follows.

Let $P_1(v_i, t)$ be the 1-site PDF for the site i to have the velocity v_i. Similarly $P_2(v_i, v_{i+d}, t)$, be the 2-site PDF for the sites $i,\ i+d$ to have velocities $v_i,\ v_{i+d}$ respectively. Similarly, one can also define the 3-site PDF, $P_3(v_{i-m}, v_i, v_{i+d})$. Here m, d are integers less than N. The evolution of the probability distributions satisfies the hierarchy of equations,

$$\begin{aligned}
\frac{\partial}{\partial t}P_1(v_i,t) =& \tau_c^{-1}\left[\int dv_{i+1}\overline{T}(v_i,v_{i+1})P_2(v_i,v_{i+1},t) + \overline{T}(v_{i-1},v_i)P_2(v_{i-1},v_i,t)\right] \\
&+\tau_w^{-1}\left[\int dv_i^* P_1(v_i^*,t)\langle\delta\left(v_i-[-r_w v_i^*+\eta_i]\right)\rangle_{\eta_i} - P_1(v_i,t)\right], \qquad (4.3a)\\
\frac{\partial}{\partial t}P_2(v_i,v_{i+d},t) =& \tau_c^{-1}\Big[\overline{T}(v_i,v_{i+d})P_2(v_i,v_{i+d},t)\delta_{d,1} + \int dv_{i-1}\overline{T}(v_{i-1},v_i)P_3(v_{i-1},v_i,v_{i+d},t) \\
&+\Big\{\int dv_{i+1}\overline{T}(v_i,v_{i+1})P_3(v_i,v_{i+1},v_{i+d},t) \\
&\quad+\int dv_{i+d-1}\overline{T}(v_{i+d-1},v_{i+d})P_3(v_i,v_{i+d-1},v_{i+d},t)\Big\}\times\ (1-\delta_{d,1}) \\
&+\int dv_{i+d+1}\overline{T}(v_{i+d},v_{i+d+1})P_3(v_i,v_{i+d},v_{i+d+1},t)]\Big] \\
&+\tau_w^{-1}\Big[\int dv_i^* P_2(v_i^*,v_{i+1},t)\langle\delta\left(v_i-[-r_w v_i^*+\eta_i]\right)\rangle_{\eta_i}+ \\
&\int dv_{i+1}^* P_2(v_i,v_{i+1}^*,t)\langle\delta\left(v_{i+1}-[-r_w v_{i+1}^*+\eta_{i+1}]\right)\rangle_{\eta_{i+1}} - 2P_2(v_i,v_{i+1},t)\Big], \qquad (4.3b)
\end{aligned}$$

and so on. $\overline{T}(v_i, v_j)$ defined as, $\overline{T}(v_i, v_j)S(v_i, v_j) = r^{-1}S(v_i^*, v_j^*) - S(v_i, v_j)$, and acts only on the two variables designated by the arguments of the $\overline{T}$ operator. The solution of these equations requires closure of the hierarchy. Motivated by our earlier observation about the closure in terms of the variance and correlation function in Maxwell gases, we proceed to see whether such a relation exist for this model also. In order to do this, we define the set of quantities from the probability distribution:

$$\Sigma(d,t) = \frac{1}{N}\sum_i^N \int dv_i dv_{i+d} v_i v_{i+d} P_2(v_i, v_{i+d}, t), \qquad (4.4)$$

which quantifies the correlation between the lattice sites as a function of their separation. The lattice separation, $d \in 0, \mathbb{Z}^+$. From the definition, $\Sigma(0,t)$ is nothing but the variance of the single particle PDF. Due to periodicity and symmetry of the system, it suffices to calculate $\Sigma(d,t)$ with d ranging from 0 to $N/2$ $[(N+1)/2]$ for even [odd] N. We calculate the evolution of the function $\Sigma(d,t)$, by multiplying Eq. (4.3) by $v_i v_{i+d}$ and integrating over v_i and v_{i+d}. This results in a closed set of equations, with $\Sigma(d,t)$ depending on $\Sigma(d-1,t)$ and $\Sigma(d+1,t)$. This leads to a tri-diagonal matrix evolution, written in compact notation as:

$$\frac{d}{dt}X(t) = \mathbf{A}X(t) + C \tag{4.5}$$

where, $X(t) = [\Sigma(0,t), \Sigma(1,t), ..\Sigma(n,t)]^T$. The tri-diagonal matrix $\mathbf{A}$ is of order $(n+1)$, with $n = N/2$ and $(N+1)/2$ respectively for N even and odd, and has the form,

$$\mathbf{A} = \begin{bmatrix} -[2\epsilon a + b(1-r_w)] & 2\epsilon a & & & & \\ \epsilon a & -[(1+\epsilon)a + 2b] & a & & \mathbf{0} & \\ & a & -2(a+b) & a & & \\ & & \ddots & \ddots & \ddots & \\ & \mathbf{0} & & a & -2(a+b) & a \\ & & & & 2a & -2(a+b) \end{bmatrix}. \tag{4.6}$$

Here, $a = 2(1-\epsilon)/\tau_c$ and $b = (1+r_w)/\tau_w$. Note that the variables $a,\ b \geq 0$ for the allowed parameter values. The column vector C is $(n+1)$ dimensional, with $C_0 = \sigma^2/\tau_w$ and all the other the elements equal to zero. The dynamics considered here has time independent rates. One can consider a more realistic situation where the rate can depend on the average kinetic energy of the system. In both the cases one obtains the same steady state. For the simpler case when the rates are time independent, $X(t)$ can be exactly calculated from Eq. (4.5). This is shown in Fig. 4.1 accompanied by results from the direct simulation.

As before, it is easy to see whether the system goes to a steady state or not, by looking at the behaviour of the eigenvalues. Consider the situation when $r_w = -1$. Now the matrix $\mathbf{A}$

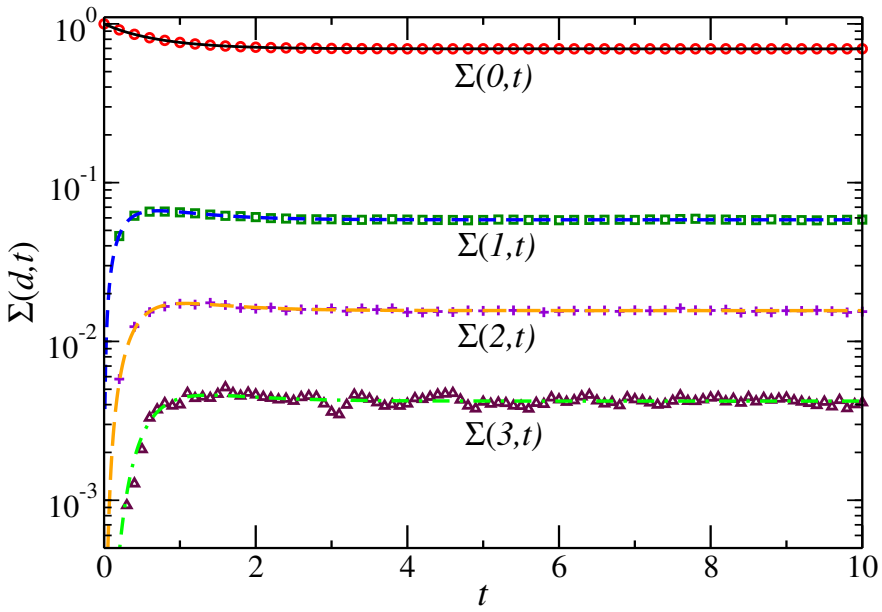

FIGURE 4.1: .The figure shows the evolution of $\Sigma(d,t)$ for $d = 0,1,2,3$ for a 10 particle system with $r = 1/2$, $r_w = 1/2$, $\sigma = 1$, $\tau_c = 1$ and $\tau_w = 1$. The lines and points represent respectively, the values obtained numerically (from Eq. (4.5)) and those from direct simulation.

has a simpler form with $b = 0$ and it can be easily shown that the determinant of A vanishes (Appendix A.1). This implies that one of the eigenvalue is zero and so, $\Sigma(d,t)$ does not have a steady state. On the other hand for $r_w \neq -1$ the eigenvalues are negative (Appendix A.1), indicating that the system goes to a steady state in this limit. In Fig. 4.1, we show the exact evolution for a 10-particle system when $r_w \neq -1$. The predicted saturation of $\Sigma(d,t)$ for different values of d is clearly visible.

The steady state values can be obtained by solving the Eq. (4.5) with the LHS equated to zero. The steady state values of $\Sigma(d,t)$, which we denote by $\Sigma_{ss}(d) = \Sigma(d, t \to \infty)$ can be obtained from the equation,

$$X_{ss} = -\mathsf{A}^{-1} C, \tag{4.7}$$

where $X_{ss} = [\Sigma_{ss}(0), \Sigma_{ss}(1), ..\Sigma_{ss}(n)]^T$.

As only the first element of the vector C is nonzero, it needs to know only the first column of the matrix A^{-1} to calculate $\Sigma_{ss}(d)$, as shown in Eq. (4.8).

$$\Sigma_{ss}(d) = -A^{-1}_{d0}\sigma^2/\tau_w. \tag{4.8}$$

Calculation of A^{-1}_{d0} is easy due to the tri-diagonal nature of A. The explicit formula for $d = 0$

follows as,

$$\begin{aligned} A_{00}^{-1} =& \frac{-\Delta_n}{\epsilon}\Big\{ [2c-(1-\epsilon)]\, c\left[(s^{n-2}+s^{-(n-2)}\right] \\ &+ [3c-(1-\epsilon)]\left[s^{[n-3]}+s^{-[n-3]}\right] \\ &+ s^{[n-4]}+s^{-[n-4]}\Big\}, \end{aligned} \tag{4.9}$$

where, $\Delta_n = -2\epsilon a^n/\det\mathbf{A}$, $c=(1+b/a)$ and $s=-(c+\sqrt{c^2-1})$. Also, $\det\mathbf{A}$ denotes the determinant of the matrix $\mathbf{A}$. Similarly one gets for $d=1,2,..n-3$:

$$A_{d0}^{-1} = (-1)^d\Delta_n\Big\{c(s^{n-(d+1)}+s^{-(n-(d+1))})+s^{[n-(d+2)]}+s^{-[n-(d+2)]}\Big\}, \tag{4.10}$$

and for $d > n-3$:

$$A_{(n-2)0}^{-1} = (-1)^{n-2}\Delta_n\Big\{c\left[s+s^{-1}+1\right]\Big\}, \tag{4.11}$$

$$A_{(n-1)0}^{-1} = (-1)^{n-1}\Delta_n c, \tag{4.12}$$

$$A_{(n)0}^{-1} = (-1)^n\Delta_n. \tag{4.13}$$

The determinant of $\mathbf{A}$, can be obtained as,

$$\det\mathbf{A} = -2a^{n+1}\Big\{K_1 c\left[s^{n-2}+s^{-(n-2)}\right]+K_2\left[s^{n-3}+s^{-(n-3)}\right]+K_3\left[s^{n-4}+s^{-(n-4)}\right]\Big\}, \tag{4.14}$$

with K_1, K_2, K_3, functions of (ϵ, c, r_w) as shown below in Eq. (4.15).

$$\begin{aligned} K_1 &= 2\epsilon(2c-1)+(1-r_w)[2(c-1)^2+(c-1)(1+\epsilon)], \\ K_2 &= 2\epsilon(3c-1)+(1-r_w)[3(c-1)^2+(c-1)(2+\epsilon)], \\ K_3 &= 2\epsilon+(1-r_w)(c-1). \end{aligned} \tag{4.15}$$

For a large system, Eq. (4.8) and Eq. (4.10) can be used to calculate the asymptotic form of the correlation function $\Sigma_{ss}(d)$, $(d=1,2,..n-3)$. To do this, rearranging Eq. (4.10) we get:

$$A_{d0}^{-1} = (-1)^d\Delta_n s^n\Big\{c(s^{-(d+1)}+s^{-(2n-(d+1))})+s^{[-(d+2)]}+s^{-[2n-(d+2)]}\Big\}. \tag{4.16}$$

As $|s|>1$, in the large n limit, Eq. (4.16) becomes,

$$A_{d0}^{-1} = (-1)^d\Delta_n s^n\Big\{cs^{-(d+1)}+s^{-(d+2)}\Big\}. \tag{4.17}$$

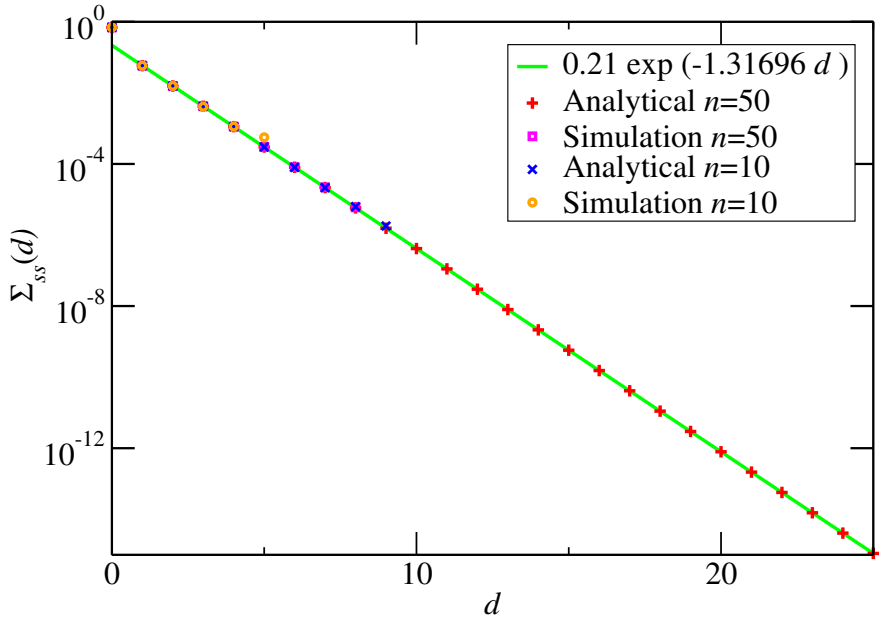

FIGURE 4.2: The figure shows the steady state values $\Sigma_{ss}(d)$, for the simulation of 10, 50 particle systems with $r = 1/2$, $r_w = 1/2$, $\sigma = 1$, $\tau_c = 1$ and $\tau_w = 1$. The rate of collision is independent of the variance ($g = 1$). The exact analytical result given by Eq. (4.10) are shown by the 'x' symbol ($n = 10$) and '+' symbol ($n = 50$). The asymptotic expression is represented by the solid line.

Similarly from Eq. (4.14), for large n, $\det \mathsf{A}$ can be shown to have the form,

$$\det \mathsf{A} = -2a^{n+1}s^n \left[K_1 c s^{-2} + K_2 s^{-3} + K_3 s^{-4}\right]. \tag{4.18}$$

Using Eq. (4.17) and Eq. (4.18) one finds that in the large n limit, $\Sigma_{ss}(d)$ goes as

$$\begin{aligned} \Sigma_{ss}(d) &= A \exp(-d \ln |s|), \\ A &= \frac{\epsilon |s|^2 [c|s| - 1]}{a\left(cK_1|s|^2 - K_2|s| + K_3\right)}. \end{aligned} \tag{4.19}$$

In other words, the system has a finite correlation length $\zeta = 1/\ln|s|$. In Fig. 4.2, we plot the asymptotic form (Eq. (4.19)) along with the result obtained from numerical calculation (Eq. (4.10)) as well as from direct simulation.

4.5. Conclusion

In the chapter, we introduced a simple model of inelastic gas in one dimension for which one can find the functional form of the spatial correlation function in its driven steady state. The

model consists of a periodically bounded lattice in one dimension with each point associated with a variable which mimics the velocity of particles in an inelastic gas. The interaction between the nearest neighbours follow the inelastic collision rules. For the model, a closed set of equations helps us to find the velocity correlation as a function of lattice separation. The correlation function is found to have an exponential form in the steady state. As the experimental observations of driven granular gases [56] find exponential decay for the spatial velocity correlation functions, simple but exact models can be useful as preliminary step in understanding real systems.

A

Appendix

A.1. Existence of steady states for various values of r_w for the inelastic gas on a 1-D lattice

A.1.1. Absence of steady state when $r_w = -1$

Here, we show that the correlation vector $X(t)$ which evolves according to Eq. (4.5), does not have a steady state when $r_w = -1$. To show this, we observe the properties of the eigenvalues of the matrix A (Eq. (4.6)). We note that when $r_w = -1$, the parameter b is equal to zero and the tri-diagonal matrix A has a simpler form (Eq. (A.1)). We denote this matrix by A($r_w = -1$).

$$\mathsf{A}(r_w=-1)= a^{n+1}\begin{bmatrix} -2\epsilon & 2\epsilon & & & & \\ \epsilon & -(1+\epsilon) & 1 & & \mathbf{0} & \\ & 1 & -2 & 1 & & \\ & & \ddots & \ddots & \ddots & \\ & \mathbf{0} & & 1 & -2 & 1 \\ & & & & 2 & -2 \end{bmatrix}. \tag{A.1}$$

The determinant of the above $(n+1)$-th order matrix denoted as $\det \mathsf{A}(r_w=-1)$, can be shown to satisfy the relation, when $n>2$:

$$\det \mathsf{A}(r_w=-1) = 2\epsilon a^{n+1}\left[\det \mathsf{A}'_{n-1} + \det \mathsf{A}'_{n-2}\right], \tag{A.2}$$

where $\det \mathsf{A}'_k$ is the determinant of A'_k, which is a matrix of order $k \in \mathbb{N}$, and has the form given below.

$$\mathsf{A}' = \begin{bmatrix} -2 & 1 & & & & \\ 1 & -2 & 1 & & \mathbf{0} & \\ & 1 & -2 & 1 & & \\ & & \ddots & \ddots & \ddots & \\ & \mathbf{0} & & 1 & -2 & 1 \\ & & & & 2 & -2 \end{bmatrix} \tag{A.3}$$

One can find $\det \mathsf{A}'_k$, as follows. Let us denote $\det \mathsf{A}'_k \equiv D'_k$. It can be shown to satisfy the relation,

$$D'_k + 2D'_{k-1} + D'_{k-2} = 0. \tag{A.4}$$

Using the boundary conditions, $D'_1 = -2$, $D'_2 = 2$, the solution of Eq. (A.4) can be easily obtained as, $D'_k = \det \mathsf{A}'_k = 2(-1)^k$. Substituting this in Eq. (A.2) we obtain the result,

$\det \mathsf{A}(r_w = -1) = 0$. This shows that at least one of the eigenvalue is zero, which implies the lack of steady state for the system.

A.1.2. Presence of steady state when $|r_w| < 1$

Consider the matrix A (Eq. (4.6)) when $r_w \neq -1$. We can use Gershgorin circle theorem [60] to predict the range of the eigenvalues of the matrix A. The theorem states that any eigenvalue λ of the matrix A should satisfy the condition:

$$|\lambda - \mathsf{A}_{ii}| \leq \sum_{j \neq i} |\mathsf{A}_{ij}| \quad , i = 0, 1, 2...n \tag{A.5}$$

From the first row of A, we find that:

$$|\lambda + [2\epsilon a + b(1 - r_w)]| \leq 2\epsilon a, \tag{A.6}$$

which says, $\lambda + b(1 - r_w) \leq 0$. Similarly for $i > 1$, using Eq. (A.5) we obtain the result, $\lambda + 2b \leq 0$. Thus all the eigenvalues are strictly less than zero as $b > 0$. This proves that when $|r_w| < 1$, the system goes to a steady state.

A.1.3. Presence of steady state when $r_w = 1$

When $r_w = 1$, Gershgorin circle theorem provides the inequalities, $\lambda \leq 0$ from the first row of $\mathsf{A}(r_w = 1)$ and $\lambda + 2b \leq 0$ from other rows of $\mathsf{A}(r_w = 1)$, to be satisfied by the eigenvalues λ of $\mathsf{A}(r_w = 1)$. This shows us that the eigenvalues of $\mathsf{A}(r_w = 1)$ should satisfy the condition $\lambda \leq 0$. But if the system goes to a steady state, the eigenvalues should be strictly negative. This is true if the determinant, $\det \mathsf{A}(r_w = 1) \neq 0$. We show this in the following.

As we are interested in the large system case, we consider a system with $n < 2$. For the system, one can show as before, that $\det \mathsf{A}(r_w = 1)$ satisfies the equation,

$$\det \mathsf{A}(r_w = 1) = 2\epsilon a^{n+1} \left[(1 + 2b/a) \ \det \mathsf{A}''_{n-1} + \det \mathsf{A}''_{n-2} \right], \tag{A.7}$$

where A''_k is a $k \times k$ matrix given by,

$$\mathsf{A}^{''} = \begin{bmatrix} -2c & 1 & & & & \\ 1 & -2c & 1 & & \mathbf{0} & \\ & 1 & -2c & 1 & & \\ & & \ddots & \ddots & \ddots & \\ & \mathbf{0} & & 1 & -2c & 1 \\ & & & & 2 & -2c \end{bmatrix}. \tag{A.8}$$

We define the determinant, $\det \mathsf{A}^{''}_k \equiv D^{''}_k$. From Eq. (A.8), one can show that $D^{''}_k$ satisfies the equation,

$$D^{''}_k + 2cD^{''}_{k-1} + D^{''}_{k-2} = 0, \ k = 3, 4.. \tag{A.9}$$

with $c = 1 + b/a$. The exact form of $D^{''}_k$ can be found by solving the difference equation using the initial conditions $D^{''}_1 = -2c$, $D^{''}_2 = 4c^2 - 2$. The general solution for Eq. (A.9) has the form,

$$D^{''}_k = As^k + Bs^{-k}, \tag{A.10}$$

with $s = -c + \sqrt{c^2 - 1}$. Using the initial conditions, the exact form of $D^{''}_k$ is found as,

$$D^{''}_k = s^k + s^{-k}. \tag{A.11}$$

Substituting $\det \mathsf{A}^{''}_k = (s^k + s^{-k})$ in Eq. (A.7), one gets:

$$\det \mathsf{A}(r_w = 1) = \ 2\epsilon a^{(n+1)} \left((1 + 2b/a) \left[s^{(n-1)} + s^{-(n-1)} \right] + \left[s^{(n-2)} + s^{-(n-2)} \right] \right). \tag{A.12}$$

Using the relations, $s = -|s|$ and $s^{-1} = -|s^{-1}|$ in Eq. (A.12),

$$\begin{aligned} \det \mathsf{A}(r_w = 1) = \ 2\epsilon a^{(n+1)} (-1)^{(n-1)} \times \Big\{ & \left[|s|^{(n-1)} - |s|^{(n-2)} + |s^{-1}|^{(n-1)} - |s^{-1}|^{(n-2)} \right] \\ & + \tfrac{2b}{a} \left[|s|^{(n-1)} + |s^{-1}|^{(n-1)} \right] \Big\}. \end{aligned} \tag{A.13}$$

Note that $c = 1 + b/a > 1$, and so the variable $|s| = \left[c + \sqrt{c^2 - 1} \right] > 1$. The first square bracket on the RHS of Eq. (A.13) can be re-written as,

$$\left[|s|^{(n-1)} - |s|^{(n-2)} + \frac{1}{|s|^{(n-1)}} - \frac{1}{|s|^{(n-2)}} \right] = \left(|s|^{2n-3} - 1 \right) \frac{|s| - 1}{|s|^{n-1}} > 0 \tag{A.14}$$

for $n \geq 2$. As the second square bracket in Eq. (A.13) is a positive definite quantity, the RHS of Eq. (A.13) will be non-zero. So the determinant of $\mathsf{A}(r_w = 1)$ is non-zero.

References

[1] M. Vergassola, B. Dubrulle, U. Frisch, and A. Noullez, Astronomy and Astrophysics **289**, 325 (1994).

[2] K. Feitosa and N. Menon, Physical review letters **88**, 198301 (2002).

[3] V. Garzó and J. Dufty, Physical Review E **60**, 5706 (1999).

[4] U. M. B. Marconi and A. Puglisi, Physical Review E **66**, 011301 (2002).

[5] K. Harth *et al.*, Physical review letters **110**, 144102 (2013).

[6] I. Aranson and J. Olafsen, Physical Review E **66**, 061302 (2002).

[7] K. Kohlstedt *et al.*, Physical review letters **95**, 068001 (2005).

[8] F. Rouyer and N. Menon, Physical review letters **85**, 3676 (2000).

[9] P. Haff, Journal of Fluid mechanics **134**, 401 (1983).

[10] T. Schwager and T. Pöschel, Physical Review E **57**, 650 (1998).

[11] I. Goldhirsch and G. Zanetti, Physical review letters **70**, 1619 (1993).

[12] E. Ben-Naim, S. Chen, G. Doolen, and S. Redner, Physical review letters **83**, 4069 (1999).

[13] M. Shinde, D. Das, and R. Rajesh, Phys. Rev. E **79**, 021303 (2009).

[14] G. Carnevale, Y. Pomeau, and W. Young, Physical review letters **64**, 2913 (1990).

[15] L. Frachebourg, Physical review letters **82**, 1502 (1999).

[16] X. Nie, E. Ben-Naim, and S. Chen, Physical review letters **89**, 204301 (2002).

[17] S. N. Pathak, Z. Jabeen, D. Das, and R. Rajesh, Physical review letters **112**, 038001 (2014).

[18] S. N. Majumdar, K. Mallick, and S. Sabhapandit, Physical Review E **79**, 021109 (2009).

[19] J. Olafsen and J. S. Urbach, Physical Review E **60**, R2468 (1999).

[20] W. Losert *et al.*, Chaos: An Interdisciplinary Journal of Nonlinear Science **9**, 682 (1999).

[21] A. Kudrolli and J. Henry, Physical Review E **62**, R1489 (2000).

[22] D. L. Blair and A. Kudrolli, Physical Review E **64**, 050301 (2001).

[23] E. Clement and J. Rajchenbach, Europhysics Letters **16**, 133 (1991).

[24] S. Warr, J. M. Huntley, and G. T. Jacques, Physical Review E **52**, 5583 (1995).

[25] T. Van Noije and M. Ernst, Granular Matter **1**, 57 (1998).

[26] S. McNamara and W. Young, Physics of Fluids A: Fluid Dynamics (1989-1993) **4**, 496 (1992).

[27] Y. Du, H. Li, and L. P. Kadanoff, Physical review letters **74**, 1268 (1995).

[28] J. Van Zon and F. MacKintosh, Physical review letters **93**, 038001 (2004).

[29] J. Van Zon and F. MacKintosh, Physical Review E **72**, 051301 (2005).

[30] D. Williams and F. MacKintosh, Physical Review E **54**, R9 (1996).

[31] S. J. Moon, M. D. Shattuck, and J. B. Swift, Phys. Rev. E **64**, 031303 (2001).

[32] J. J. Brey, J. W. Dufty, and A. Santos, Journal of statistical physics **87**, 1051 (1997).

[33] G. Costantini, U. M. B. Marconi, and A. Puglisi, Journal of Statistical Mechanics: Theory and Experiment **2007**, P08031 (2007).

[34] J. J. Brey, J. W. Dufty, C. S. Kim, and A. Santos, Physical Review E **58**, 4638 (1998).

[35] A. Baldassarri, U. M. B. Marconi, and A. Puglisi, Europhysics letters **58**, 14 (2002).

[36] S. E. Esipov and T. Pöschel, Journal of statistical physics **86**, 1385 (1997).

[37] J. M. Montanero and A. Santos, Granular Matter **2**, 53 (2000).

[38] E. Ben-Naim and P. Krapivsky, Physical Review E **66**, 011309 (2002).

[39] M. Ernst and R. Brito, EPL (Europhysics Letters) **58**, 182 (2002).

[40] M. Ernst and R. Brito, Physical Review E **65**, 040301 (2002).

[41] A. Goldshtein and M. Shapiro, Journal of Fluid Mechanics **282**, 75 (1995).

[42] J. Carrillo, C. Cercignani, and I. Gamba, Physical Review E **62**, 7700 (2000).

[43] M. H. Ernst and R. Brito, *Granular Gas Dynamics* (Springer, Berlin Heidelberg, 2003), p. 3.

[44] A. Barrat *et al.*, Journal of Physics A: Mathematical and General **35**, 463 (2002).

[45] D. Benedetto, E. Caglioti, J. A. Carrillo, and M. Pulvirenti, Journal of statistical physics **91**, 979 (1998).

[46] A. Puglisi *et al.*, Physical review letters **81**, 3848 (1998).

[47] E. Ben-Naim and P. L. Krapivsky, Physical Review E **61**, R5 (2000).

[48] T. Antal, M. Droz, and A. Lipowski, Physical Review E **66**, 062301 (2002).

[49] A. Santos and M. Ernst, Physical Review E **68**, 011305 (2003).

[50] A. Puglisi, V. Loreto, U. M. B. Marconi, and A. Vulpiani, Physical Review E **59**, 5582 (1999).

[51] J. J. Brey, M. G. de Soria, P. Maynar, and M. Ruiz-Montero, Physical Review E **70**, 011302 (2004).

[52] T. Van Noije, M. Ernst, R. Brito, and J. Orza, Physical review letters **79**, 411 (1997).

[53] M. Shinde, D. Das, and R. Rajesh, Physical review letters **99**, 234505 (2007).

[54] M. R. Swift, M. Boamfă, S. J. Cornell, and A. Maritan, Physical review letters **80**, 4410 (1998).

[55] T. Van Noije, M. Ernst, E. Trizac, and I. Pagonabarraga, Physical Review E **59**, 4326 (1999).

[56] A. Prevost, D. A. Egolf, and J. S. Urbach, Physical review letters **89**, 084301 (2002).

[57] G. Gradenigo, A. Sarracino, D. Villamaina, and A. Puglisi, Europhysics Letters **96**, 14004 (2011).

[58] A. Puglisi *et al.*, The Journal of chemical physics **136**, 014704 (2012).

[59] D. Levanony and D. Levine, Physical Review E **73**, 055102 (2006).

[60] H. E. Bell, American Mathematical Monthly 292 (1965).